DESIGN AND ENGINEERING OF 3D COLLAGEN-FIBRONECTIN SCAFFOLDS FOR WOUND HEALING APPLICATIONS

A Dissertation

Presented to the Faculty of the Graduate School

of Cornell University

In Partial Fulfillment of the Requirements for the Degree of

Master of Science

By

Junhui Ye

August 2017

DESIGN AND ENGINEERING OF 3D COLLAGEN-FIBRONECTIN SCAFFOLDS FOR WOUND HEALING APPLICATIONS

Junhui Ye
Cornell University 2017

The extracellular matrix (ECM) plays an important role in many crucial cellular processes such as gene expression, cancer progression and cell differentiation. Cells are able to sense the mechanical properties of their extracellular environment and adjust their gene expression accordingly. The ECM regulates numerous cell behaviors including cells adhesion, spreading, migration, proliferation, and death. Fibronectin, a key glycoprotein of the ECM, is critical in the early wound healing process, as it can stop bleeding and protect the tissue, facilitate cell motility and proliferation, and guide the remodeling of new ECM. Subsequently, collagen is also deposited at the wound. The resulting mature collagen-fibronectin ECM keeps the wound sterile and induces the wound closure.

Three different systems of collagen-fibronectin three-dimensional (3D) scaffolds were developed for this thesis. First, a collagen *porous* scaffold was originally fabricated using ice templating techniques and then coated with a layer of fibronectin, whose conformation was controlled via incubation temperature and monitored using Förster resonance energy transfer (FRET) spectroscopy. This platform was next utilized to investigate the effect of ECM structure and conformation on cellular invasion and viability. Second, fibronectin was assembled into 3D *fibrillar* matrix within the above-mentioned porous collagen scaffold via shearing methods, which provides a promising platform for further investigation of cell-ECM interactions. Third, collagen *fibrillar* scaffolds with tunable microarchitecture and cell content were generated via warm/cold casting techniques, which resulted in ECM platforms that closely mimic the wound physiological environment.

Collectively, our study suggests that by tuning collagen (porous vs. fibrillar) structure and fibronectin molecular conformation, we were able to control cell behaviors including cell adhesion, migration and proliferation, and thus, potentially facilitate the wound healing process. These 3D ECM-mimicking platforms offer precise control of protein microarchitecture and conformation over large volumes, i.e., for long-term cell culture, and therefore have potential applications in tissue engineering as well as regenerative medicine.

BIOGRAPHICAL SKETCH

Junhui Ye was born to Dong Ye and Shuying Zhou on April 17th, 1993 in Guangzhou, Guangdong, China. She completed her secondary education at Guangdong Experimental High School in 2011, where she got opportunities to try new things and let the experience raise her to a new level of understanding. Her natural penchant for curiosity drew her to engineering. She then continued to pursue her interest in science and engineering at South China University of Technology in Department of Material Science and Engineering. During her undergraduate study, she received many academic as well as extracurricular awards, and was honored with the top ranking National Scholarship every year. She found true pleasure in solving academic problems, and the sense of accomplishment drove her to dig into scientific research. At South China University of Technology, Junhui seized the opportunities to participate in different research projects. She joined Prof. Anqiang Zhang's research group to design and engineer the SESi film for wound healing application, and joined Prof. Shuizhu Wu's research group in *State Key Laboratory of Luminescent Materials and Devices* to study the fluorescent probe for in vivo tracking. She then finished her undergraduate research at Prof. Li Ren's group focus on antibacterial medical device in *National Engineering Research Center for Tissue Restoration and Reconstruction.* After graduation, she moved to Ithaca to continue her research in exploring materials for biomedical applications. Junhui joined Prof. Delphine Gourdon's research group in the Department of Materials Science and Engineering at Cornell University in 2015, and worked on developing biomaterials platforms to understand cell-ECM (extracellular matrix) interactions and investigate the ECM-mediated cellular process, such as wound healing. Junhui will continue pursuing her interest in biomedical materials and devote her effort to improve people's health.

DEDICATION

To my family

ACKNOWLEDGEMENTS

First and foremost, I would like to thank my research advisor and committee chair Professor Delphine Gourdon for her mentorship and support throughout my master study at Cornell University. She has been patient and inspirational in my academic research in these two years. To my committee member Professor Emmanuel Giannelis, thank you for your advice and being supportive. I would also like to acknowledge people in the Gourdon lab who made significant contributions to my work. First of all, I would like to sincerely thank Fei Wu and Weisi Chen, thank you for the training when I joined the lab, and for all the valuable suggestions. I am so grateful to our friendship that made my life more enjoyable in the lab. To my collaborator Yifan Li, thank you for your contribution, my project could not be carried out without your work. In addition, I would like to truly thank Lauren Hsu, Soyoung Min, Peter Ajayi in my group for their willingness and devotion to my projects. To wonderful facility managers and staff at Cornell, Johanna Dela Cruz (BRC), Penny Burke (NBTC).

To my family for their love and support. To my love ones Rongdi Lin, Siyu Luo, Zhiqing Wen, Kehan Chen, Sixuan Li, thank you for your unconditional love and always being on my side. To my lovely friends here, Ya Guan, Rui Yang, Wanying Li, thank you for your intellectual support and cheers.

I would also like to thank my funding sources, the National Science Foundation, the National Institutes of Health, the Cornell Center for Materials Research, the Nanobiotechnology Center, and Professor Gourdon.

TABLE OF CONTENT

LIST OF ABBREVIATIONS

Fn	Fibronectin
FRET	Förster resonance energy transfer
ECM	Extracellular matrix
PBS	Phosphate buffered saline
GdnHCl	Guanidine hydrochloride
2D	2-dimensional
3D	3-dimensional
VEGF	Vascular endothelial growth factor
bFGF	Basic fibroblast growth factor
PDMS	Polydimethylsiloxan
DI water	Deionized water
FBS	Fetal bovine serum
P/S	Penicillin/streptomycin
α-MEM	α modification of minimum essential medium
EthD-1	Ethidium homodimer
DMEM/F12	Dulbecco's Modified Eagle Medium: Nutrient Mixture F-12
PBS-X 0.05%	Triton-X in phosphate buffered saline
SEM	Scanning electron microscope
RGD	Arg-Gly-Asp amino acid sequence

Chapter 1

Introduction

Background and Motivation

The extracellular matrix (ECM) serves as structural and biochemical support to the resident cells.[1,2] It regulates the cell behaviors including cell adhesion, spreading, migration, proliferation and cell death. [3–7] The ECM has numerous functions, and is essential in many cellular processes such as growth and wound healing. It sequesters and stores various cellular growth factors, which allows the cellular functions to be activated quickly through a growth factor-mediated process responding to the physiological changes. Cells are able to sense the mechanical properties of the extracellular environment, thus, the ECM plays an important role in regulating many crucial cellular progresses such as gene expression, cancer progression, and their differentiation. [4,8,9] The ECM has a wide range of stiffnesses, as compliant as the brain tissue and stiff as the bone tissue. The stiffness and elasticity of the ECM has essential impact on numerous cell functions, which has raised new focus on research in recent decades. Cells actively detect the elasticity of their matrix and adjust their gene expression accordingly, which plays an influential role in the cells differentiation and cancer progression. [9] The understanding and control of the structure as well as composition of the ECM enables us to get insight of the complex dynamics of tumor progression and cancer metastasis, which usually involves the enzymes-induced ECM destruction such as threonine proteases, serine proteases, and matrix metalloproteinases.[10]

There are many cell types involved into the development and remodeling of the ECM, and the properties of connective tissues are determined by the local composition of the ECM. Cell adhesion to the ECM is regulated by specific integrins. Integrins are proteins on the cell

surface that bind cells to the ECM components such as fibronectin, and to the integrin on the surface of other cells. Fibronectin can facilitate cell-ECM binding process, initiate the intracellular signaling pathways, and interact with a set of adaptor molecules, such as actin, associating with the cellular cytoskeleton. [11]Fibroblasts are the most common cell type that is able to synthesize and maintain the structural framework of the ECM. They secrete the precursor molecules for the ECM, and represent the ground for the matrix development.

Collagen is the most abundant protein in mammals, making up to 35% of the body content. It provides main structural support to the resident cells in the extracellular matrix as well as various connective tissues in animal bodies. [12–14]Collagen is widely used in science research for cell culture, studying cell behaviors, the cellular interaction with their extracellular environment and tissue regeneration.[15–19] This is because collagen is a natural product, stable in vivo, with excellent properties for deposition of cells, such as fibroblasts, and the cells are able to continue to grow as normal in tissue once they invaded and adhered onto the collagen scaffolds. [20,21]

Fibronectin is a glycoprotein in the ECM that can connect the cells with the ECM structure, for example, collagen fibrils, which also enables the cells to move on the ECM. Fibronectin is initially secreted in the ECM in an inactive (soluble) form. By binding to the cell-surface integrins, fibronectin molecules unfold, forming dimers and being able to function normally. Fibronectin facilitates the cell movement via reorganizing the cell cytoskeleton when binding the integrins on cell surface with their matrix. The fibronectin molecules are dimers that contain various functional binding domains along the monomer, allowing it to assemble into fibrils and associate with cells as well as other proteins in the ECM. The fibronectin-binding domain, i.e., the sequence binding to other fibronectin molecules located on domain $I_{1-5,}$ is essential for initiating the fibronectin matrix assembly (a.k.a. fibrillogenesis). The cell

binding domains are found in modules $III_{9–10}$. The RGD sequence (Arg-Gly-Asp), found in module $III_{10,}$ provides a binding site for cells by attaching the α5β1 and αVβ3 integrins on the cell surface, while the synergy site, located on module III_9, is involved in the association with the α5β1 integrin. [22] Fibronectin also has binding domains for other proteins in the ECM, such as collagen ($I_{6–9}$), fibrin ($I_{1–5}$, $I_{10–12}$), fibulin-1 ($III_{13–14}$), heparin and syndecan ($III_{12–14}$). [23] These binding domains contribute to numerous functions of fibronectin, including cell adhesion, migration, growth and differentiation. Fibronectin assembles into a three-dimensional fibrillar matrix in the ECM, forming an insoluble network that supports the tissues of an organism and regulates the composition of the ECM.

The wound healing process mainly has four stages: hemostasis, inflammation, tissue growth, and maturation. Fibronectin plays a crucial role in the healing process, forming a blood clot that binds to platelets, forming a proper substrate that facilitates the cell movement as well as proliferation at the injured site during the development of the granulation tissue, and remodeling the new ECM. [24–27] In early wound healing stages, fibronectin is deposited at the injured tissue and forms a blood clot along with fibrin, which stops the bleeding and protects the underlying tissue.[28] Afterward, fibroblasts move to the wound and begin to remodel the area, repairing the injured tissue. The exposure of the cell binding domains on fibronectin molecules can facilitate this cellular process. Meanwhile the proteins in the provisional blood clot will be replaced by the newly deposited ECM, which is more similar to normal,healthy tissue. The fragmentation of fibronectin induced by fibroblasts secreted proteases can promote wound contraction, which is considered critical in the wound healing process. This fibronectin fragments further expose the α4β1 integrin binding site and thus enhance its binding to the cells that express α4β1 integrins, so that the cells can use them to adhere to and apply contracting forces to the extracellular matrix.[28] In later wound healing stages,

fibronectin will assemble into a three-dimensional (3D) fibrillar matrix on the cell surface, which is vital for establishing and maintaining the tissue architecture, regulating the cellular processes, such as cell adhesion, spreading, proliferation, and migration, and determining the deposition of other extracellular proteins and hence the composition of the ECM. The significant role of fibronectin in the mechanism of wound healing *in vivo* has been continually studied in the past decades.[29] As a key natural content in body, collagen can also benefit the wound healing process.[30] Because of its natural role against infection, collagen can keep the wound sterile, which is vital in the healing process. The wound closure can occur when collagen is deposited in the wound bed. Also, collagen can provide space for fibroblasts to attach and accelerate the development of the healthy tissue, which aids the healing process.[31] Collagen serves several function in the wound healing stages, such as interacting with blood platelets to make a hemostatic plug, attracting and guiding the fibroblasts to migrate along the matrix, and guiding new collagen matrix deposition and capillary growth.

To better mimic the physiological ECM and understand the role of collagen as well as fibronectin in regulating cellular processes, especially wound healing, three different models of collagen-fibronectin three-dimensional (3D) scaffolds were designed and fabricated in this thesis. In the first model, porous scaffolds were fabricated using the ice-templating technique, with allowed for control of pore size and mechanical properties. Then, a fibronectin layer was coated on the 3D collagen substrate. The conformation of fibronectin was monitored and studied by using external forces (as in previous studies), however, they were hard to reproduce and could hardly be applied on the 3D platform. Therefore, to control fibronectin conformation, as quantified by Förster resonance energy transfer (FRET) spectroscopy, we first utilized the effect of fibronectin molecular density and coating temperature, and we next

investigated its corresponding impact on cellular adhesion, viability and proliferation. In the second model, we tried to directly assemble fibronectin molecules into fibers (to better mimic the ECM) within above 3D porous collagen template. It is known that the conformation and function of fibronectin differs after assembly into fibers, which has not been fully understood yet. Several force-based methods have been used in this thesis including stirring, shaking, manually pulling and blowing, to develop the fibrous fibronectin network within the 3D collagen scaffold, which provides a promising ECM mimicking platform for further investigation on ECM regulating cellular behavior. In the third model, fibrillar collagen scaffolds with tunable microarchitecture were fabricated using a warm/cold casting technique, which can be better mimic the *in vivo* collagen matrix and the wound physiological extracellular environment.

Experimental design

Source of type I collagen

Two types of collagen were used for this thesis: fibrillar bovine type I collagen and soluble rat-tail type I collagen.

In vivo, collagen exists in the tissues in various stiffnesses, such rigid (bone), compliant (tendon), or has a gradient from rigid to compliant (cartilage), depending on the degree of mineralization. Type I collagen, in the form of elongated fibrils, is mostly found in fibrous tissues such as tendons and skin. As the most abundant collagen in human body, it is also found in artery walls, cornea, fibrocartilage, the organic part of bones, and the endomysium surrounding muscle fibers. When tissues heal by repair, collagen is also present in the scar tissues. The collagen is known to possess a triple helix structure, composed of two identical α1chains and an additional α2 chain.[32] To assemble into matrix,

tropocollagen is first formed by procollagen peptidase, then tropocollagen molecules are covalent cross-linked by aldol reaction to form collagen fibrils, and finally multiple collagen fibrils bundle up into collagen fibers.

The fabrication and characterization of synthetic pore-structure collagen scaffolds and fibrillar collagen scaffolds will be discussed in Chapter 1 and Chapter 4, respectively.

Source of fibronectin

In vivo, two types of fibronectin, plasma Fn and cellular Fn, are present in a soluble molecular form in body fluids (300 μg/mL in plasma, less in other fluids) and in a insoluble fibrillar form in the tissue ECM. These two types of fibronectin have very similar structures and properties, besides cellular Fn specifically contains variable amounts of ED-A and ED-B alternative splicing regions.[33] While fibroblasts and endothelial cells produce cellular Fn, plasma Fn can be found in hepatocytes in the liver.[34] In this study, human plasma Fn, obtained from Invitrogen (Thermo Fisher Scientific) was used and stored at -80 ˚C in 1 mg/mL stock solution reconstituted with DI water. The fibronectin stock solution was then diluted with 1x phosphate buffered saline (PBS) before use based on desired concentrations. Fibronectin solutions were used either to coat on the Labtek^{TM} chambers and on the collagen scaffolds for studying the role of fibronectin molecules conformation (described in Chapter 2), or to deposit fibronectin fibers within the 3D collagen structure via several cell-free techniques (described in Chapter 3).

Source of cells

MC3T3-L1 cells were used in this thesis. 3T3-L1 cell line, derived from mouse 3T3 cells, is a continuous strain of 3T3 developed through clonal isolation and is widely used in biological research. The 3T3-L1 cells have a fibroblast-like morphology. Fibroblasts play a major role

in wound healing by adhering to fibrin, which requires fibronectin. The cells are not inhibited contact. Thus, the MC3T3-L1 cell line is a good model for studying *in vitro* fibroblasts adhesion, proliferation, migration, and the corresponding effects on wound healing, particularly under the ECM signaling. Their behavior are similar to fibroblasts.

It needs to be noted that these cell lines may not fully reflect the *in vivo* response due to genetic modifications as compared with primary cells that are harvested directly from the tissue of interest.

Requirements for cell culture platform

The cell behavior studies in this thesis were performed under standard cell culture conditions. Basic environmental conditions, including temperature, humidity, osmolality, pH and appropriate growth medium, were taken into account during cells culture. Typical culture medium contains amino acids, inorganic salts, vitamins, glucose, and serum as a source of growth factors, hormones, and attachment factors for cells, and should be optimized based on cell type.[35] In this thesis, cells were incubated in αMEM (Sigma Aldrich) supplemented with 10% fetal bovine serum (FBS, Atlanta Biologicals) and 1% penicillin/streptomycin (P/S, Quality Biological) under 37 ˚C and 5% CO_2. αMEM is the α modification of Minimum Essential Medium (MEM), which contains amino acids, salts, vitamins and so on. FBS contains many growth factors that support embryonic growth, bovine serum albumin, glucose, as well as other defined and undefined components. The addition of P/S prevents bacterial contamination of cell cultures. The cell culture platforms developed in this thesis were all tested for good cell viability before cell function studies were performed, as described in Chapter 2, Chapter 3 and Chapter 4.

Conclusion

The scope of this thesis was to develop cell culture platforms with tunable protein conformation and mechanics to investigate the role of collagen microstructure and fibronectin conformation in regulating cellular behavior during wound healing. Three different 3D platforms were designed and engineered in order to control the protein properties. To control the collagen mechanical properties, we used two strategies. The first strategy utilized the ice-templating technique to fabricate *porous* collagen structures and control their pore size, pore connectivity, as well as scaffold stiffness by altering the collagen concentration and freeze-drying rate. In the second strategy, the warm/cold casting technique was used to develop a more closely ECM mimicking *fibrillar* collagen scaffold with tunable microarchitecture. The conformation of the Fn molecules coated on the collagen scaffold was altered via thermal treatment and analyzed using FRET spectroscopy. Later, the Fn molecules were induced to assemble into Fn fibers within the 3D collagen structure by using several cell-free methods. Then, these dual protein scaffolds were used for studying altered cellular behaviors to establish a correlation with differential collagen structures and Fn conformation.

In this thesis, a combination of material science and biochemical approached was developed to (i) control the morphology and mechanics of 3D collagen scaffolds, (ii) alter the conformation of Fn layers within the collagen scaffolds, (iii) induce Fn fibrillogenesis within the 3D collagen structure. Overall, insights gained by these structural and mechanical studies not only increase our understanding of the role of collagen and fibronectin in wound healing, but also have important implications for the design of large volume cell culture platforms for tissue regeneration applications.

Reference:

1. Michel, G., Tonon, T., Scornet, D., Cock, J. M. & Kloareg, B. The cell wall polysaccharide metabolism of the brown alga Ectocarpus siliculosus. Insights into the evolution of extracellular matrix polysaccharides in Eukaryotes. *New Phytol.* **188,** 82–97 (2010).
2. Alberich-Bayarri, A. *et al.* Microcomputed tomography and microfinite element modeling for evaluating polymer scaffolds architecture and their mechanical properties. *J. Biomed. Mater. Res. - Part B Appl. Biomater.* **91,** 191–202 (2009).
3. Lo, C. M., Wang, H. B., Dembo, M., Wang, Y. L. & Jacobson, K. Cell movement is guided by the rigidity of the substrate. *Biophys. J.* **79,** 144–52 (2000).
4. Engler, A. J., Sen, S., Sweeney, H. L. & Discher, D. E. Matrix Elasticity Directs Stem Cell Lineage Specification. *Cell* **126,** 677–689 (2006).
5. Discher, D. E., Janmey, P. & Wang, Y.-L. Tissue cells feel and respond to the stiffness of their substrate. *Science* **310,** 1139–43 (2005).
6. Hadjipanayi, E., Mudera, V. & Brown, R. A. Close dependence of fibroblast proliferation on collagen scaffold matrix stiffness. *J. Tissue Eng. Regen. Med.* **3,** 77–84 (2009).
7. Wang, H. B., Dembo, M. & Wang, Y. L. Substrate flexibility regulates growth and apoptosis of normal but not transformed cells. *Am. J. Physiol. Cell Physiol.* **279,** C1345-50 (2000).
8. Wang, J. H.-C., Thampatty, B. P., Lin, J.-S. & Im, H.-J. Mechanoregulation of gene expression in fibroblasts. *Gene* **391,** 1–15 (2007).
9. Provenzano, P. P., Inman, D. R., Eliceiri, K. W. & Keely, P. J. Matrix density-induced mechanoregulation of breast cell phenotype, signaling and gene expression through a FAK-ERK linkage. *Oncogene* **28,** 4326–43 (2009).

10. Liotta, L. A. *et al.* Metastatic potential correlates with enzymatic degradation of basement membrane collagen. *Nature* **284,** 67–68 (1980).

11. Barabási, A.-L. & Oltvai, Z. N. Network biology: understanding the cell's functional organization. *Nat. Rev. Genet.* **5,** 101–113 (2004).

12. Di Lullo, G. A., Sweeney, S. M., Korkko, J., Ala-Kokko, L. & San Antonio, J. D. Mapping the ligand-binding sites and disease-associated mutations on the most abundant protein in the human, type I collagen. *J. Biol. Chem.* **277,** 4223–31 (2002).

13. Karsenty, G. & Park, R.-W. Regulation of Type I Collagen Genes Expression. *Int. Rev. Immunol.* **12,** 177–185 (1995).

14. Kern, B., Shen, J., Starbuck, M. & Karsenty, G. Cbfa1 contributes to the osteoblast-specific expression of type I collagen genes. *J. Biol. Chem.* **276,** 7101–7 (2001).

15. Cross, V. L. *et al.* Dense type I collagen matrices that support cellular remodeling and microfabrication for studies of tumor angiogenesis and vasculogenesis in vitro. *Biomaterials* **31,** 8596–8607 (2010).

16. Van Susante, J. L. C. *et al.* Linkage of chondroitin-sulfate to type I collagen scaffolds stimulates the bioactivity of seeded chondrocytes in vitro. *Biomaterials* **22,** 2359–2369 (2001).

17. Zhang, Q., Lu, H., Kawazoe, N. & Chen, G. Pore size effect of collagen scaffolds on cartilage regeneration. *Acta Biomater.* **10,** 2005–2013 (2014).

18. Madaghiele, M., Sannino, A., Yannas, I. V & Spector, M. Collagen-based matrices with axially oriented pores. (2007). doi:10.1002/jbm.a.31517

19. Murphy, C. M. & O'Brien, F. J. Understanding the effect of mean pore size on cell activity in collagen-glycosaminoglycan scaffolds. *Cell Adhes. Migr.* **4,** 377–381 (2010).

20. Oliveira, S. M. *et al.* An improved collagen scaffold for skeletal regeneration. *J. Biomed. Mater. Res. A* **94,** 371–9 (2010).

21. Singh, O. *et al.* Collagen dressing versus conventional dressings in burn and chronic wounds: a retrospective study. *J. Cutan. Aesthet. Surg.* **4,** 12–6 (2011).

22. Sechler, J. L., Corbett, S. A. & Schwarzbauer, J. E. Modulatory roles for integrin activation and the synergy site of fibronectin during matrix assembly. *Mol. Biol. Cell* **8,** 2563–73 (1997).

23. Mao, Y. & Schwarzbauer, J. E. Fibronectin fibrillogenesis, a cell-mediated matrix assembly process. *Matrix Biology* **24,** 389–399 (2005).

24. Grinnell, F. Fibronectin and wound healing. *J. Cell. Biochem.* **26,** 107–116 (1984).

25. Wasserman, J. K. *et al.* Phosphaturic Mesenchymal Tumor Involving the Head and Neck: A Report of Five Cases with FGFR1 Fluorescence In Situ Hybridization Analysis. *Head Neck Pathol.* **10,** 279–285 (2016).

26. Bachman, H., Nicosia, J., Dysart, M. & Barker, T. H. Utilizing Fibronectin Integrin-Binding Specificity to Control Cellular Responses. *Adv. wound care* **4,** 501–511 (2015).

27. Midwood, K. S., Mao, Y., Hsia, H. C., Valenick, L. V & Schwarzbauer, J. E. Modulation of cell-fibronectin matrix interactions during tissue repair. *J. Investig. Dermatology Symp. Proc.* **11,** 73–78 (2006).

28. Valenick, L. V., Hsia, H. C. & Schwarzbauer, J. E. Fibronectin fragmentation promotes α4β1 integrin-mediated contraction of a fibrin–fibronectin provisional matrix. *Exp. Cell Res.* **309,** 48–55 (2005).

29. Grinnell, F., Billingham, R. E. & Burgess, L. Distribution of fibronectin during wound healing in vivo. *J. Invest. Dermatol.* **76,** 181–9 (1981).

30. Gould, L. J. Topical Collagen-Based Biomaterials for Chronic Wounds: Rationale and Clinical Application. *Adv. wound care* **5,** 19–31 (2016).

31. Birbrair, A. *et al.* Type-1 pericytes accumulate after tissue injury and produce collagen

in an organ-dependent manner. *Stem Cell Res. Ther.* **5,** 122 (2014).

32. Blow, N. Cell culture: building a better matrix. *Nat. Methods* **6,** 619–622 (2009).

33. Hynes, R. O. & Yamada, K. M. Fibronectins: multifunctional modular glycoproteins. *J. Cell Biol.* **95,** 369–77 (1982).

34. Magnusson, M. K. & Mosher, D. F. Fibronectin. *Arterioscler. Thromb. Vasc. Biol.* **18,** (1998).

35. Arora, M. Cell culture media: A review. *Mater methods* (2013).

Chapter 2

Engineering 3D tunable porous collagen scaffolds for machanobiology study: pore structure, stiffness, cell invasion

In collaboration with Yifan Li

Contributors: Junhui Ye, Yifan Li, Baoquan Guo, Peter Ajayi, Emmanuel Giannelis and Delphine Gourdon

Abstract

In this study, ice-templating was used to fabricate three-dimensional (3D) scaffolds from type I bovine collagen. 3D platforms with suitable microstructure and mechanical property are crucial for tissue engineering applications. As a natural product, collagen is one of the most promising materials for supporting 3D cell culture. The synthesis and characterization of porous collagen scaffolds with tunable morphological and mechanical properties is reported. The microstructure, especially porosity, of the scaffolds is essential for cell invasion, controllable biodegradability, and for tuning mechanical properties. These 3D matrix-mimicking platforms offer precise control of collagen pore structure and hence provide physical supports as well as coarsely regulate major cell functions, such as cell infiltration, over large volumes and long-term cell cultures. These 3D collagen porous scaffolds have many potential applications in tissue engineering and regenerative medicine, and lay a groundwork for future study in this thesis.

Introduction

Biomedical scaffolds, which provide support for cell culture and proliferation, are used to replace or regenerate *in vivo* tissues.[1] Ever since the cells were successfully grown on two-dimensional substrates, such as petri dish, within the *in vitro* environment, tremendous effort has been placed to better mimic the complexity of living tissues, for instance, a three-dimensional biocompatible cell culture platform.[2] It was shown by previous studies that the cellular behaviors are significant different between two-dimensional (2D) and three-dimensional (3D) platforms, which might be due to the complex and inherent micro-environmental properties in three-dimension platforms.[2–5] Therefore, a specific 3D structure, which resembles the extracellular matrix (ECM) of living tissue, would have great potential applications for the regeneration of damaged living tissues.[6,7] Research on how to better replicate and control the microstructure of ECM has long been the focus of intensive study.[8,9] Collagen, a natural polymeric material, has a wide range of correct properties for such 3D cell culture platform for tissue regeneration, i.e. excellent biocompatibility, permeability, low antigenicity, and appropriate mechanical properties. [10] Collagen scaffolds have frequently been used for cell culture, studying cell behavior, and the cellular interactions with their matrix.

In previous study, several methods have been reported to fabricate the 3D scaffolds with various morphologies and mechanical properties.[4,7] However, many of those methods are based on overheating or use of harsh chemicals, for example, injection molding, porogen leaching, solvent evaporation and wire heating.[11–13] These methods may be able to apply on the fabrication of 3D scaffolds based on artificial polymers but they can not satisfy the demand for synthesizing protein-based scaffolds, since proteins are easily denatured by tough

environmental conditions and loose their biological properties.[12] In this thesis, we used a technique called ice-templating, which could overcome these shortcomings and be utilized in the formation of collagen 3D scaffolds.[4] In this technique, the suspension of water-soluble materials, such as collagen, is frozen under a freezing temperature, creating ice crystals in the solute. These solute particles are then sublimated by reducing the chamber pressure, which eventually forms an interconnected porous 3D scaffold. Studies have shown that an isotropic pore arrangement could be obtained in the lyophilized matrices under uniform conditions thorough the sample during freezing drying process.[14]

Here, a polytetrafluoroethylene (Teflon) mold was designed to improve the homogeneity of the resulting structure. The conventional ice-templating technique was modified, and a more uniform interface between the collagen suspension and the freezing shelf was created. This new mold enables the fabricated collagen porous structure to keep the same morphology thorough the entire 3D system with uniform control on the growth of the ice crystals produced during freezing within the scaffold. At the same time, the cooling rate of the collagen suspension was slowed down to produce more homogeneous freezing conditions during the process of ice crystals formation. [15,16]To control the topography and porosity of the scaffold, we adjusted the freeze drying conditions and solvent concentration.[14,13]

In this work, we report the fabrication of 3D collagen scaffolds with controlled morphology and mechanics via the ice-templating technique. Later cell experiments were performed on the collagen templates to assess if these 3D platforms were capable of supporting 3D cell cultures. The potential applications of this synthetic type I collagen 3D scaffold with tunable properties are especially advantageous for future study of the ECM-mediated cell behavior, cell-ECM interaction, and could be used in the biomedical and therapeutic applications.[17]

Materials and Methods

Fabrication of 3D Type I Collagen Scaffolds

The porous collagen scaffolds were fabricated using an ice templating technique named freeze-drying, in which we controlled the collagen concentration, freeze casting rate/temperature, and crosslinking duration to alter the collagen scaffold monoliths with different pore sizes and stiffness. Briefly, scaffolds were fabricated from a suspension of the insoluble microfibrillar type I collagen, which was derived from bovine Achilles tendon (Advanced BioMatrix). The type I collagen powder was dissolved in 0.05 M acetic acid solution (Sigma-Aldrich) at a concentration from 0.5 wt.% to 1.25 wt.%, and the pH was adjusted to 2.0 with hydrochloric acid (VWR International). The collagen suspension was then put in a cold water bath and blended via an overhead homogenizer (T 10 BASIC S001) for 30 min. After mixing, the collagen suspension was centrifuged at 2500 rpm for 15 min to remove air bubbles. Before put into the freeze-dryer, the prepared collagen solution was casted into the designed rectangular Teflon molds, $10 \times 7 \times 2$ mm^3 in size. The samples were then placed in a freeze-dryer (VirTis Advantage Plus ES; SP Scientific; PA, USA) at a controlled freeze casting rate. To generate 3D collagen scaffolds with varied properties, we applied the "Controlled Nucleation Temperature Method". Collagen solutions in various concentrations were frozen at a constant temperature (-10°C) for 5 hours, and dried at the same temperature under 10 mTorr for 24 hours.

Chemical Crosslinking Treatment

To enhance the structural stability of the collagen scaffolds, the lyophilized samples were crosslinked with a water soluble carbodiimide. The fabricated collagen scaffolds were immersed in a 95% ethanol solution containing 33 mM 1-ethyl-3-(3-dimethylamino propyl)-

carbodiimide hydrochloride (EDC) (Sigma-Aldrich, UK) and 6 mM N-hydroxysuccinimide (NHS) (Sigma-Aldrich, UK) for 4 h at 25 ℃. Afterward, the scaffolds were washed thoroughly with distilled water for 5 times (5 min each time) and were subsequently refrozen and re-lyophilized using the same controlled freezing temperature method detailed above.

Scanning electron microscopy (SEM)

After freeze-drying, the structure of collagen scaffolds was characterized by scanning electron microscopy (SEM) and Hg intrusion porosimetry. SEM (Mira3 FESEM, Tescan) was used to visualize the microstructure of the collagen scaffold. Before imaging, the samples were sputtered with a layer of Au/Pd to improve the image quality. The SEM images were obtained at 15 keV.

Mercury (Hg) intrusion porosimetry

Hg intrusion porosimetry (Autopore IV 9500; Micromeritics) was used for quantification of the collagen structure created by freeze-casting and was performed to probe pore sizes and pore area. Briefly, ten pieces of collagen scaffolds were placed in a glass penetrometer whose weight and volume had already been measured, then, the penetrometer was inserted into the instrument. Analysis were performed under an automatic procedure, which first evacuated the sample to 50 μm Hg and then filled with Hg at 0.2 psi. Pressure applied to the column of Hg was ramped stepwise to 48 psi, in order to probe pores whose diameters were greater than 4 μm.

Dynamic mechanical analyzer (DMA)

The mechanical properties of the freeze-casting collagen scaffold were characterized using the dynamic mechanical analyzer (DMA Q800; TA Instruments). Collagen scaffolds were

incubated in cell culture medium (αMEM, Sigma-Aldrich) at room temperature overnight prior to testing. The measurements were performed on wet samples under compressive loads during a single loading cycle, with an initial contact force of 0.05N and a ramp rate of 0.005 N/min to 0.075N. Elastic modulus was calculated as the slope of the stress-strain curve over the 1-2% strain regime.

Cell culture experiments

1 mm thick scaffolds were prepared for cell culture experiments by being placed under UV light for 30min for disinfection, and then rinsed 3 times with sterile PBS (Life Technologies). Cell adhesion was assessed with 3T3-L1 cells (ATCC #CL-173), an adipogenic subtype of mouse fibroblasts. These cells were incubated in αMEM (Sigma-Aldrich) containing 10 vol% fetal bovine serum (FBS, Tissue Culture Biologicals) and 1 vol% penicillin/streptomycin (pen/strep) (Life Technologies) prior to seeding. The cells were seeded in 10 μL suspensions (containing 30 thousand cells) into scaffolds and were allowed to adhere for 1 hour. Then, fresh media containing 1 vol% fetal bovine serum (FBS, Tissue Culture Biologicals) was added to the wells with the scaffolds, and they were cultured in the incubator at 37 °C (5% CO2) for 24 hours. Afterward, cell-seeded scaffolds were soaked in 3.7% ice-cold paraformaldehyde for chemical fixation and stained with 4′,6-diamidino-2-phenylindole (DAPI) (Life Technologies), in order to evaluate cell viability and infiltration within the scaffolds through fluorescence microscopy.

Results and Discussion

Impact of collagen concentration on pore morphology and mechanical properties of freeze-casting scaffolds

The internal microstructure of collagen scaffolds generated via ice-templating in different collagen concentrations was assessed by SEM (Fig. 2.1). The freeze casting temperature was controlled at -10 °C for all the samples, and as the images show, the pore sizes of the collagen scaffold could be tune by varying the concentration of collagen solution under such

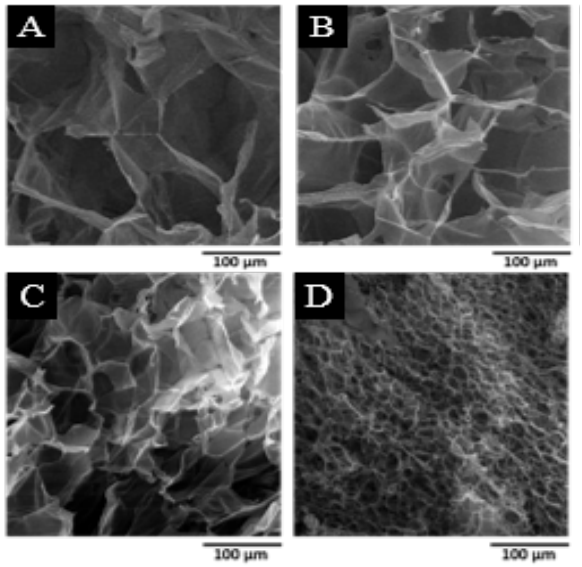

Fig. 2.1 SEM micrographs of collagen scaffold fabricated via ice-templating at -10 °C in different collagen concentration (A) 0.5 wt.%; (B) 0.75 wt.%; (C) 1.0 wt.%; (D) 1.25 wt.% .

constant freezing rate. Our results (Fig. 2.2) suggest that the pore sizes of the collagen scaffolds decreased significantly as the collagen concentration increased. Also, the distribution of the pore sizes (Fig. 2.2 C) appeared to be more uniform in the lower collagen concentration. The smallest pore size was found in the 1.25% collagen scaffolds (35µm) along with a largest pore area (2.013 m^2/g), while the largest pore size was found in the 0.5% collagen scaffold (214µm) along with a smallest pore area (0.676 m^2/g).

Table 2.1 Macroporosity of collagen scaffolds as determined by Hg intrusion porosimetry

Collagen Concentration (wt.%)	Average Pore Diameter (μm)	Total Intrusion Volume (mL/g)	Total Pore Area (m^2/g)
0.5	214.4279	36.2309	0.676
0.75	147.1496	31.7798	0.864
1.0	74.0197	21.9908	1.188

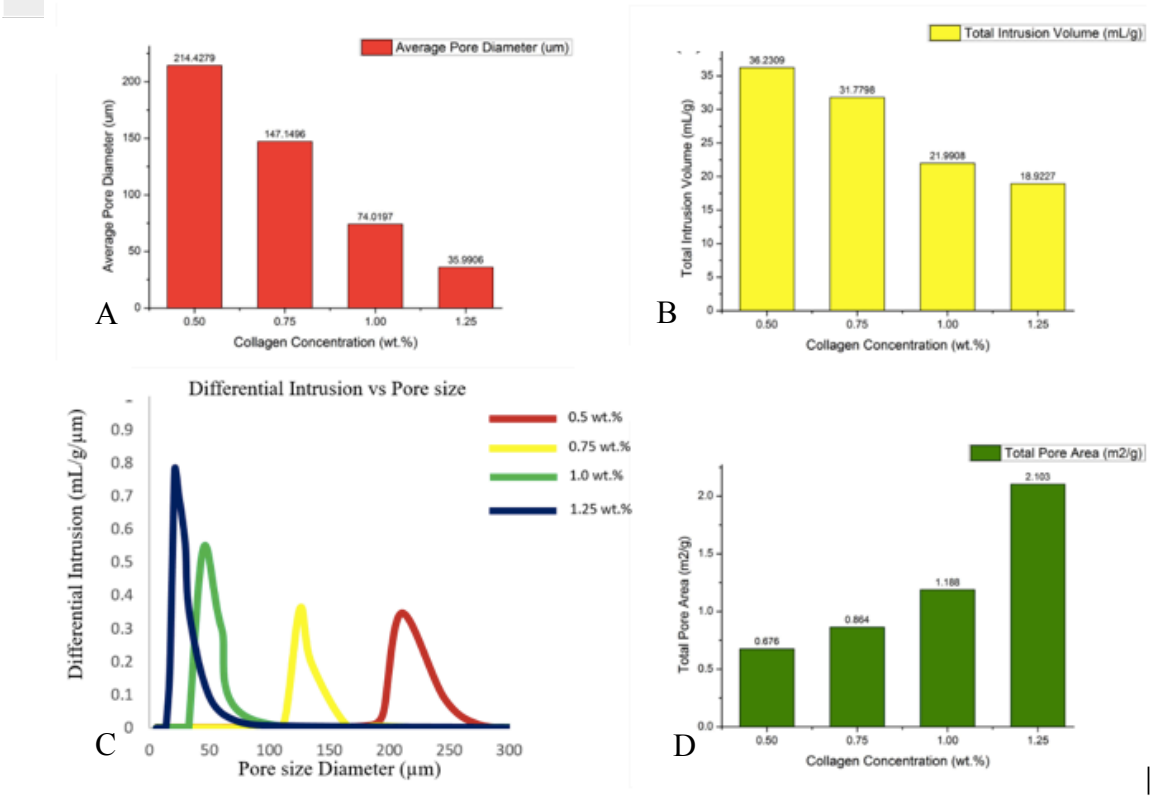

Fig. 2.2 The structure of the collagen scaffold was quantified by the Hg porosimetry. (A) Average pore diameters of the type I collagen scaffolds with four different concentrations. The pore sizes of the scaffolds decrease as a function of collagen concentration. (B) Total intrusion volume of the type I collagen scaffolds with four different concentrations. The intrusion volume decreases as a function of collagen concentration. (C) Pore size distribution of the type I collagen scaffolds with four different concentrations. Red: 0.5 wt.%, Yellow: 0.75 wt.%, Green: 1.0 wt.%, Blue: 1.25 wt.%. (D) Total pore area of the type I collagen scaffolds with four different concentrations. The total pore area increases as a function of collagen concentration.

Additionally, the mechanical properties of the collagen scaffold were tested by DMA in an

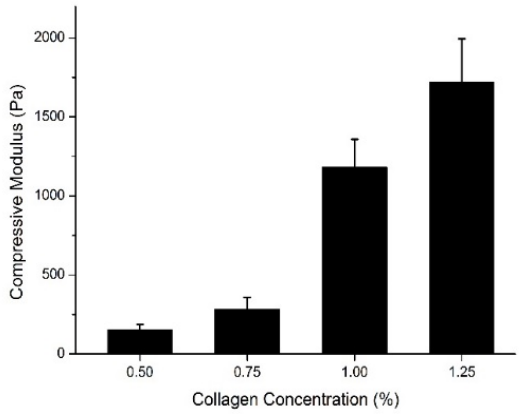

Fig. 2.3 The mechanical properties of the collagen scaffold was quantified by the DMA in aqueous environment. Average compressive modulus of the type I collagen scaffolds with four different concentrations. The compressive modulus of the scaffolds increased as a function of collagen concentration.

aqueous environment (Fig. 2.3). The compressive modulus of the collagen scaffolds increased as the collagen concentration varied from 0.5 wt.%. to 1.25 wt.%. The 1.25 wt.% collagen scaffold showed the highest stiffness, measured as 1720 ± 300 Pa, which is a 11-fold increase compared to 0.5 wt.% collagen.

Cell Invasion

To evaluate the use of these collagen scaffolds for cell culture experiments, we first seeded them with 3T3-L1 mouse preadipocyte cells (representative of stromal cells). Briefly, the scaffolds were cut into 1mm width from central part and individually placed into the wells of Labtek^{TM} chambers. With the cross section of the scaffolds faced upside, cells were pipetted on top of the scaffolds in 1% FBS αMEM. The scaffolds were incubated for an hour to allow the cells to adhere, after which fresh media was added to the wells. The scaffolds were then placed in an incubator for 24 hours.

The scaffold-bound cell populations were characterized after 24 hours of culture. (Fig. 2.4) Then, a fluorescent live-dead assay of fixed scaffolds showed that the majority of the cells

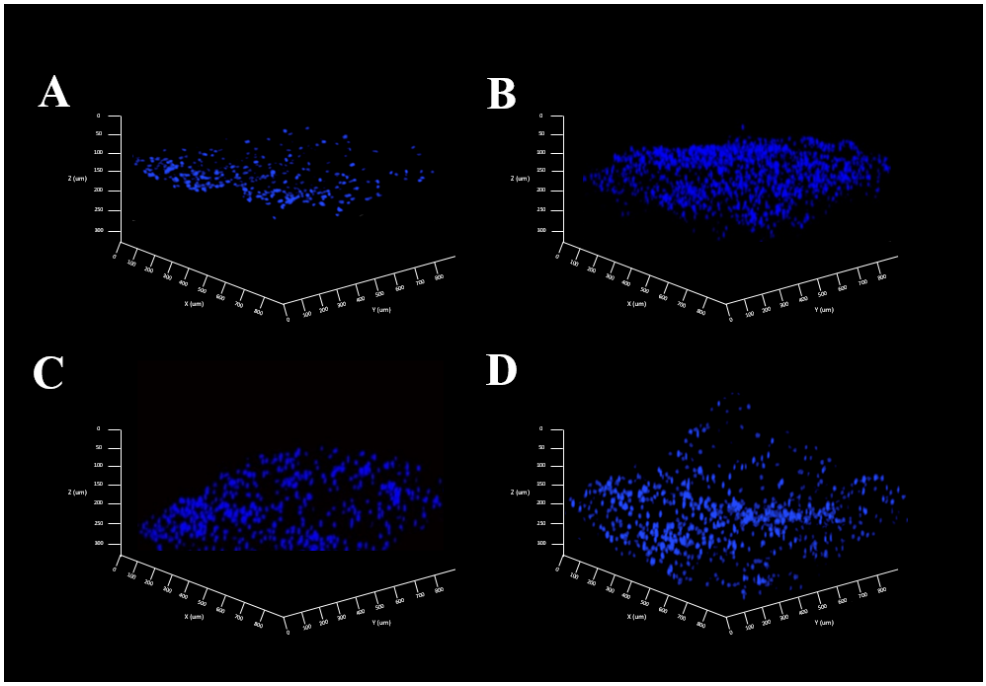

Fig. 2.4 Fluorescence micrograph of collagen scaffolds, with cell nuclei are stained with DAPI (blue) after 24 hours of 3T3-L1 culture. Z-stacks were taken from the top of the scaffolds. A) 0.5wt% collagen scaffold B) 0.75wt% collagen scaffold C) 1wt% collagen scaffold D) 1.25wt% collagen scaffold.

showed different viabilities in collagen scaffolds with different pore sizes and stiffness after short-term (24 hours) culture. Our cell invasion data indicated that cells showed better viability in the scaffolds with higher concentration of collagen, which also had smaller pore sizes. In 0.5% and 0.75% collagen scaffolds, the majority of cells adhered on the top of the scaffolds, while 0.75% collagen scaffolds showed higher cells number. In 1% and 1.25% collagen scaffolds, cells seemed to invade through the scaffolds. Further, we collected more data by investigating the cell adhesion on the top, middle and bottom of the scaffolds.

Interestingly, our results indicated that (Fig. 2.5), although cells invaded both 1% and 1.25% scaffolds, there were fewer cells adhering on the middle of the 1% collagen scaffolds, from

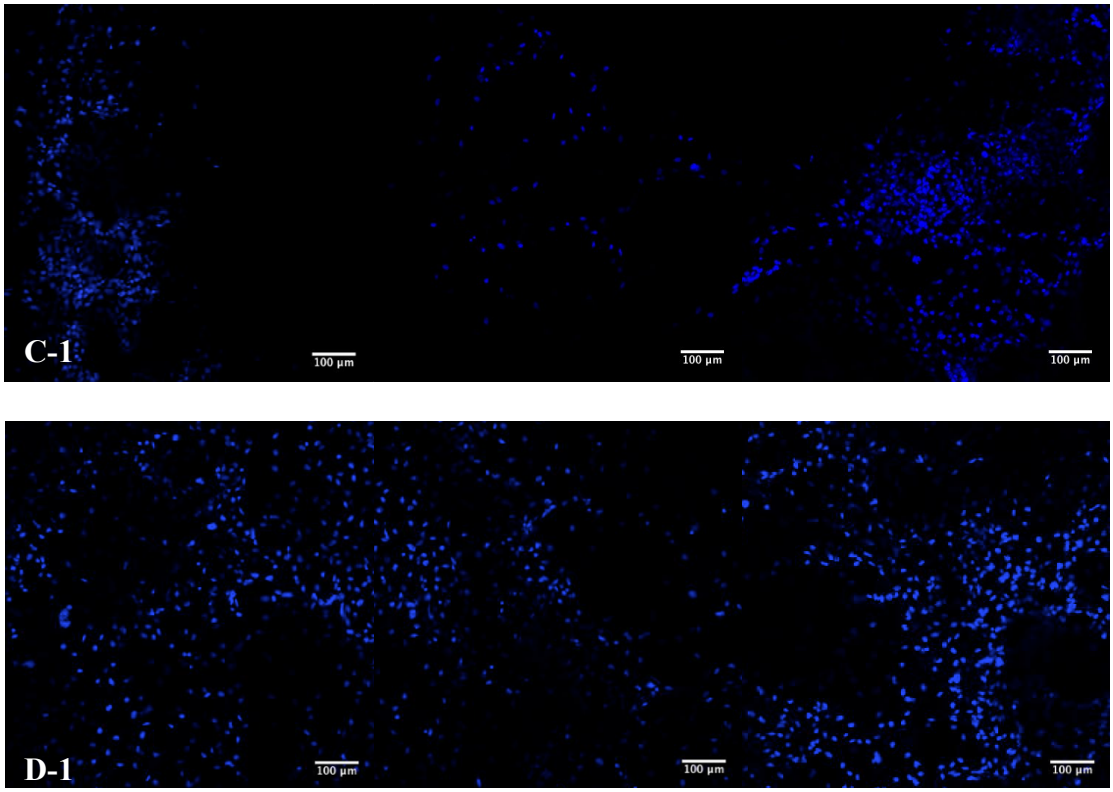

Fig. 2.5 Fluorescence micrograph of collagen scaffolds, with cell nuclei are stained with DAPI (blue) after 24 hours of 3T3-L1 culture. From left to right were images taken on the bottom, middle and top of the scaffolds, respectively. C-1) 1wt% collagen scaffold D-1) 1.25wt% collagen scaffold

which we inferred that the pore size in the middle of the scaffolds might be larger than normal(some pores were not interconnected). The pore size distribution curve (Fig. 2.2C) showed that the 1.25% collagen scaffold had a higher uniformity in pore sizes, suggesting that there were less abnormal large pores, which supported our hypothesis. These findings indicated that the 1.25% collagen scaffolds provide a suitable 3D environment for fibroblasts to attach and grow, which represent essential criteria for the development of a physiologically relevant 3D cell-culture platform based on collagen.

Conclusion

Tunable type I collagen scaffolds were fabricated via ice-templating using collagen concentration of 0.5 wt.%, 0.75 wt.%, 1.0 wt.% and 1.25 wt.%. These samples were then crosslinked by EDC and NHS to increase their mechanical stability after freeze drying. The pore size of the collagen scaffold was controlled by the freeze drying rate, which turned to control the rate of ice nucleation in the cooling process as well as the consequent sublimation of the ice crystals.[18,19] Our results suggest that the 1.25 wt.% collagen scaffold had the smallest mean pore diameter at 36μm with the largest pore area and the highest stiffness. In general, the pore size of the collagen scaffold was proved to be varying as a function of collagen concentration at a constant freeze drying rate. The increased collagen content would occupy more space within the Teflon mold, which resulted in smaller area for ice crystals formation, explaining the decrease in pore size (which mirrors ice crystal volume).

Scaffolds for tissue engineering must have suitable properties that are able to facilitate cellular adhesion, migration and tissue formation. This required sufficient, interconnected pore structure to allow cell migration into the center of scaffold, adequate diffusion of nutrients in and waste products out of the scaffold. Also, appropriate mechanical stability is essential for providing the scaffold functionality *in vitro*.[20,21] Our work suggests that the 1.25 wt.% collagen scaffold displaying the smallest pore size of 35.9μm and the highest compressive modulus of 1720 ± 300 Pa showed the best cell invasion among all collagen scaffolds tested. This collagen scaffold lays a groundwork for future study in this thesis and could serve as a promising physiological and pathological relevant 3D platform usable for long-term and large volume cells assays.

Reference:

1. Davidenko, N. *et al.* Acta Biomaterialia Biomimetic collagen scaffolds with anisotropic pore architecture. *Acta Biomater.* **8,** 667–676 (2012).

2. Wan, A. M. *et al.* 3D conducting polymer platforms for electrical functions †. 5040–5048 (2015). doi:10.1039/c5tb00390c

3. Madaghiele, M., Sannino, A., Yannas, I. V & Spector, M. Collagen-based matrices with axially oriented pores. (2007). doi:10.1002/jbm.a.31517

4. Mallick, K. K. Freeze Casting of Porous Bioactive Glass and Bioceramics. **94,** 85–94 (2009).

5. Murphy, C. M., Haugh, M. G. & Brien, F. J. O. Biomaterials The effect of mean pore size on cell attachment , proliferation and migration in collagen – glycosaminoglycan scaffolds for bone tissue engineering. *Biomaterials* **31,** 461–466 (2010).

6. Schwegman, J. J., Carpenter, J. F. & Nail, S. L. Evidence of Partial Unfolding of Proteins at the Ice / Freeze-Concentrate Interface by Infrared Microscopy. **98,** 3239–3246 (2009).

7. Porter, M. M., Imperio, R., Wen, M., Meyers, M. A. & Mckittrick, J. Bioinspired Scaffolds with Varying Pore Architectures and Mechanical Properties. 1978–1987 (2014). doi:10.1002/adfm.201302958

8. Oh, H. H., Ko, Y. G., Lu, H., Kawazoe, N. & Chen, G. Preparation of Porous Collagen scaffolds with micropatterned structures. *Adv. Mater.* **24,** 4311–4316 (2012).

9. Pawelec, K. M., Husmann, A., Best, S. M. & Cameron, R. E. Understanding anisotropy and architecture in ice-templated biopolymer scaffolds. *Mater. Sci. Eng. C* **37,** 141–147 (2014).

10. Van Susante, J. L. C. *et al.* Linkage of chondroitin-sulfate to type I collagen scaffolds stimulates the bioactivity of seeded chondrocytes in vitro. *Biomaterials* **22,** 2359–2369 (2001).

11. Haugh, M. G., Jaasma, M. J. & O'Brien, F. J. The effect of dehydrothermal treatment on the mechanical and structural properties of collagen- GAG scaffolds. *J. Biomed. Mater. Res. A* **89,** 363–369 (2009).

12. Lungu, A. *et al.* Superporous collagen-sericin scaffolds. *J. Appl. Polym. Sci.* **127,** 2269–2279 (2013).

13. Haugh, M. G., Murphy, C. M. & O'Brien, F. J. Novel freeze-drying methods to produce a range of collagen-glycosaminoglycan scaffolds with tailored mean pore sizes. *Tissue Eng. Part C. Methods* **16,** 887–94 (2010).

14. Tierney, C. M. *et al.* The effects of collagen concentration and crosslink density on the biological, structural and mechanical properties of collagen-GAG scaffolds for bone tissue engineering. *J. Mech. Behav. Biomed. Mater.* **2,** 202–209 (2009).

15. Ko, Y. G., Grice, S., Kawazoe, N., Tateishi, T. & Chen, G. Preparation of collagen-glycosaminoglycan sponges with open surface porous structures using ice particulate template method. *Macromol. Biosci.* **10,** 860–871 (2010).

16. Deville, S. Freeze-casting of porous biomaterials: Structure, properties and opportunities. *Materials (Basel)*. **3,** 1913–1927 (2010).

17. Badylak, S. F. The extracellular matrix as a biologic scaffold material. *Biomaterials* **28,** 3587–3593 (2007).

18. Wegst, U. G. K., Schecter, M., Donius, A. E. & Hunger, P. M. Biomaterials by freeze casting. *Philos. Trans. A. Math. Phys. Eng. Sci.* **368,** 2099–2121 (2010).

19. Deville, S. *et al.* Metastable and unstable cellular solidification of colloidal suspensions. *Nat. Mater.* **8,** 966–72 (2009).

20. Karageorgiou, V. & Kaplan, D. Porosity of 3D biomaterial scaffolds and osteogenesis. *Biomaterials* **26,** 5474–5491 (2005).

21. Gao, J., Crapo, P. M. & Wang, Y. Macroporous elastomeric scaffolds with extensive micropores for soft tissue engineering. *Tissue Eng.* **12,** 917–25 (2006).

Chapter 3

Thermally Controlled Scaffold-adsorbed Fibronectin Conformation: Effect on Cell Adhesion, Viability and Proliferation

Contributor: Junhui Ye, Soyoung Min, Fei Wu, Weisi Chen, Lauren Hsu and Delphine Gourdon

Abstract

In this study, bioactive three-dimensional (3D) collagen scaffolds coated with a layer of fibronectin is reported. In the extracellular environment, cells actively detect the mechanical properties and adjust the cellular processes accordingly. Therefore, the extracellular matrix (ECM) plays an important role in regulating cell behaviors including cell adhesion, migration and proliferation. Fibronectin is a key ECM protein that connects the cells with their matrix and is crucial in the cell-ECM bio-signaling. By studying the effect of fibronectin molecule density and incubating temperature on its conformation, we successfully controlled the fibronectin conformation, which was assessed by Förster resonance energy transfer (FRET) spectroscopy, as a function of coating/incubation temperature. This fibronectin layer with tunable conformation adsorbed onto the 3D collagen substrate in turn regulated the cell behaviors. The fibronectin-collagen scaffolds, especially with fibronectin in a more compact conformation, proved to facilitate the growth of mouse fibroblasts (3T3-L1) and improve cell viability, which indicates its excellent performance in the early stage of wound healing.

Introduction

By creating porosity in the collagen structure as described in Chapter 2, a suitable substrate was constructed for protein adsorption, Fn specifically, and hence served as an extracellular matrix mimicking 3D platform to host cells. This 3D structure provides us with a promising platform to study and hence control the cell-matrix interactions by altering the properties of the substrate, such as protein conformation. Cells are known to sense and respond to the topography, structure, and mechanical properties of their substrates. [1–5] The difference in rigidity and microscale physical features of the matrix is correlated with a large amount of effects including cell adhesion, proliferation, and their morphology as well as secretion. [4,6–10]

Fibronectin (Fn) has proved to be involved in almost all stages of wound healing, from platelet aggregation, haemostasis, to cell migration and angiogenesis. [11] The cell-matrix adhesion and consequently migration are assumed to be mediated by Fn signaling. Fn serves as a mechanochemical signal convertor. It was first indicated in the single-molecule force-spectroscopy experiments and high-resolution structural models were used to study the relationship between unfolding of FnIII modules and altered Fn functions.[12–15] Fn can be unfolded by cell tractions and sequentially cause a partial loss of the secondary structure of the Fn domains.[16,17]. These varying Fn conformations can be detected by fluorescence resonance energy transfer (FRET) under confocal microscopy.[16–18] Yet, the prospective methods of altering the protein structure and underlying functions, a change in the spatial exposure of binding sites, remain unclear. The mechanism of protein unfolding relates to the fundamental question of the structural biology. [19,20] External forces, such as atomic force microscopy and laser tweezers, have been used to unfold individual protein molecules, which

gives us a chance to obtain important information on the behavior of the protein molecules.[13,21–26] The unfolding process of a protein can be correlated with its folding pattern and its secondary structure stability. Nevertheless, the reported stretching-simulated Fn unfolding methods have limitations as they can hardly apply on 3D substrates. Variation of temperature has been used in previous research to unfold Fn molecules in soluble solution, and its effect has been studied by calibration using denaturalizing solution. [27,28]

In this study, we first assessed the capability of the porous collagen scaffolds to support 3D cell culture including cell infiltration, adhesion, viability, proliferation and functionality. Afterward, we investigated the effect Fn and its conformation by thermally controlling Fn conformation within the 3D collagen template. Then, 3T3-L1 cells, representing fibroblasts were seeded on these 3D collagen-fibronectin platforms with precisely tuned protein conformation to study how fibronectin, and its conformation regulated the cellular behavior, which potentially monitor the wound healing process.

Materials and Methods

Fabrication of 3D Type I Collagen Scaffolds

The 3D collagen scaffolds were fabricated by my co-worker Yifan Li. By use of the techniques of freeze-drying various collagen scaffold monoliths with different pore sizes were produced. Briefly, scaffolds were fabricated from a suspension of an insoluble type I microfibrillar collagen (bovine Achilles tendon, Advanced BioMatrix) in concentration of 1.25 wt.%. The suspension was prepared in 0.05 M acetic acid solution (Sigma-Aldrich), with pH adjusted to 2.0 with hydrochloric acid (VWR International), and was blended by an overhead homogenizer (T 10 BASIC S001) for 30 min at cold water bath then centrifuged at 2500 rpm for 15 min to remove the air bubbles. The type I collagen suspension was poured. The samples were then placed in a freeze-dryer (VirTis Advantage Plus ES; SP Scientific; PA, USA) within a rectangular Teflon molds, 10 × 7 × 2 mm^3 in size. The 3D collagen scaffolds generated at a constant temperature (-10°C) for 5 hours, and dried at the same temperature under 10 mTorr for 24 hours. After that, the lyophilized samples were crosslinked with 95% ethanol solution containing 33 mM 1-ethyl-3-(3-dimethylamino propyl)-carbodiimide hydrochloride (EDC) (Sigma-Aldrich, UK) and 6 mM N-hydroxysuccinimide (NHS) (Sigma-Aldrich, UK) for 4 h at 25 ℃., to enhance the structural stability. Following, the scaffolds were washed thoroughly with distilled water and were subsequently refrozen and re-lyophilized using the controlled freezing temperature method as above.

Scanning electron microscopy (SEM) imaging

After freeze-drying, the structure of collagen scaffolds was characterized by scanning electron microscopy (SEM, Mira3 FESEM, Tescan). The samples were mounted on the conductive carbon adhesive tab (Electron Microscopy Sciences), and then coated with gold/palladium alloy in sputter coater (Denton Vacuum, Desk II).

For SEM analysis of the 3T3s-embedded collagen scaffolds microarchitecture, the 3T3s-embedded collagen scaffolds were cultured for 24 hours and briefly fixed by 2.5% glutaraldehyde in 0.05M cacodylate buffer. The fixed scaffolds were sequentially dehydrated by a series of ethanol solution (25%, 50%, 75%, 95%, and 100%) and dried by a treatment with hexamethyldisilazane (Electron Microscopy Sciences). The dehydrated samples were mounted on the conductive carbon adhesive tab (Electron Microscopy Sciences), and then coated with gold/palladium alloy in sputter coater (Denton Vacuum, Desk II).

Cell culture experiments

1 mm thick scaffolds, cut from the center part of the collagen scaffold, were prepared for cell culture experiments by being placed under UV light for 1 hour for disinfection, and then rinsed 3 times with sterile PBS (Life Technologies). Cell adhesion was assessed with 3T3-L1 cells (ATCC #CL-173), an adipogenic subtype of mouse fibroblasts. These cells were incubated in αMEM (Sigma-Aldrich) containing 10 vol% fetal bovine serum (FBS, Tissue Culture Biologicals) and 1 vol% penicillin/streptomycin (pen/strep) (Life Technologies) prior to seeding. The cells were seeded in 10 μL suspensions (containing 15 thousand cells) into scaffolds and were allowed to adhere for 1 hour. Then, fresh media containing 1 vol% fetal bovine serum (FBS, Tissue Culture Biologicals) was added to the wells with the scaffolds, and they were cultured in the incubator at 37 °C (5% CO2) for 24 hours. Afterward, cell-seeded scaffolds were soaked in 3.7% ice-cold paraformaldehyde for chemical fixation and stained with 4′,6-diamidino-2-phenylindole (DAPI), calcein AM, and propidium iodide (PI) (all from Life Technologies), in order to evaluate cell viability and infiltration into the scaffolds through fluorescence microscopy.

Fibronectin and FRET labeling

Fibronectin (Fn) was acquired from Life Technologies, NY. AlexaFluor 633 succinimidyl ester were used to randomly single-label Fn. AlexaFluor 488 succinimidyl ester and AlexaFluor 546 maleimide (Invitrogen, CA) were used to dual-label Fn for intramolecular FRET (traces amount) as previously described by Smith et al. [17] Labeling ratios and Fn concentrations were obtained using a DU®730 UV/Vis spectrophotometer (Beckman, IN) at 280 nm, 495 nm, and 556 nm. Calibration of FRET-labeled Fn was performed in guanidine hydrochloride (GdnHCl) solution at concentrations of 0 M, 2 M, and 4 M to calculate FRET ratios, defined as acceptor/donor intensity ratios (IA/ID), and as a function of protein denaturation.

The collagen scaffolds were gently rinsed with PBS and then coated with 50μg/ml either 15% single-labeled Fn or 10% traces amount FRET-labeled Fn for 24h under different conditions. After incubation, the samples were washed with PBS and kept in PBS before cell seeding.

FRET data acquisition and analysis

FRET-Fn adsorbed substrates were imaged with a Zeiss 710 confocal microscope (Zeiss, Munich, Germany). Z-stack images are obtained in 16-bit using the C-Apochromat water-immersion 40×/1.2 objective, with the pinhole of 1 AU, 488 nm laser with 5% laser power, pixel dwell time of 6.3 μs, PMT1 and PMT2 gains of 500 V, and z-step size of 1 μm. FRET-labeled Fn is excited with a 488 nm laser line; emissions from donor and acceptor fluorophores are simultaneously collected in the PMT1 channel (514–526 nm) and the PMT2 channel (566–578 nm), respectively. These z-stack images are analyzed with user-defined Matlab code to calculate the FRET ratio (IA/ID) images as well as the mean FRET ratios for

the z-stacks. 6 different spots per sample, and three samples per condition are analyzed to calculate the mean and standard deviation of the FRET intensities, and the histogram figures are generated with FRET intensity at each representative location.

FRET calibration

The Fn conformation as a function of concentration and coating temperature was first studied on 2D substrades using LabTek^{TM} chambers. The Fn solution was made into 5µg/ml, 25µg/ml, 50µg/ml and 100µg/ml using 10% FRET-labeled Fn, unlabled Fn and PBS. Afterward, 125µl Fn solutions of different concentrations were added separately in the wells in a LabTek^{TM} chamber. These chambers containing the Fn concentration sets were placed either under 4°C for 1 hour, room temperature for 1 hour, or heated at 55°C for 5min/25min, respectively. Finally, the FRET ratio on each condition was acquired as previously described.

Statistical analysis

One-way ANOVA with Tukey's posttest and Student's t-test were used to determine statistical significance between conditions in GraphPad Prism (GraphPad Software, California USA). In all cases, $p < 0.05$ is indicated by a single star (*), $p < 0.01$ by a double star (**), and $p < 0.0001$ by four stars (****).

Results and Discussion

Morphological and mechanical characterization

The collagen scaffolds that were prepared in this work via ice-templating by collaborator Yifan Li, exhibited a typical total pore area of 2.103 m^2/g and a median pore diameter of 36 mm, as measured by mercury porosimetry. The elastic modulus measured in an aqueous environment was 1720 $\pm$ 300 Pa, indicating a good stiffness match with a variety of tissues *in vivo*. The detailed morphology and macroporous structure of the scaffolds can be seen by SEM (Fig. 3.1A), which clearly reveals an interconnected network of open macropores that should enable efficient cell invasion and mass transport. While immersing the scaffolds in an aqueous environment certainly causes some swelling of the polymer, the presence of the cross-linker aids substantially in preserving the structure of the scaffolds. Indeed, SEM images of scaffolds that were soaked in cell culture media for several days showed that their microstructure remained unchanged from as-fabricated scaffolds.

Cell Invasion

To evaluate the use of collagen scaffolds for cell culture experiments, we first seeded them with 3T3-L1 mouse fibroblast cells, which represent fibroblasts that are essential in wound healing. Due to the distinct external and internal microstructures of the scaffolds, the scaffolds were cut into 1mm width from central part, according to previous experimental proof that it would be better for cell infiltration. Briefly, with the cross section of the scaffolds faced upside, the collagen scaffold slices were individually placed into the wells of a LabTek^{TM}, then cells were pipetted onto the top of the scaffolds in 1% FBS αMEM. The scaffolds were incubated for an hour to allow the cells to adhere, after which fresh media was added to the wells. The scaffolds were then cultured in the incubator for 24 hours.

The scaffold-bound cell distributions and populations were characterized after 24 hours of culture with a fluorescent assay. The 3D reconstructed cell invasion data indicated that cells

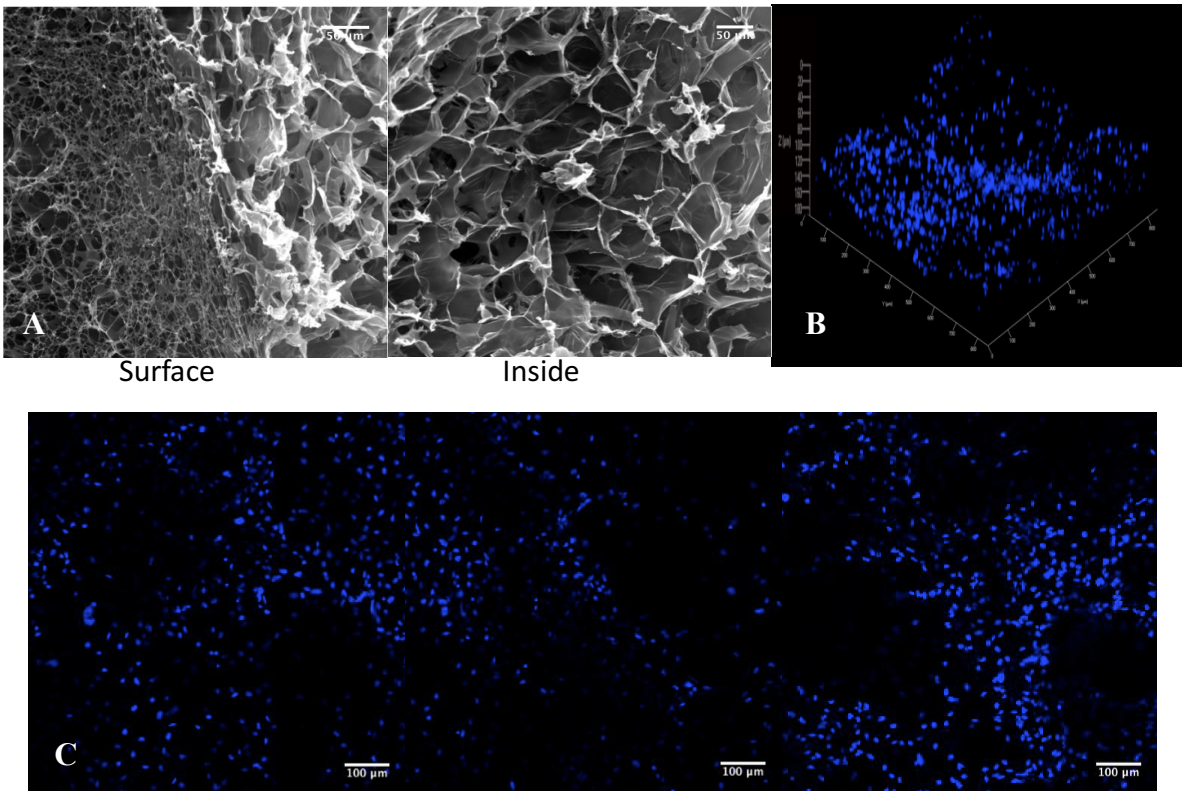

Fig. 3.1 (A) SEM image of the 1.25% collagen scaffold, showing the different microstructure between the surface and the intersection of the collagen scaffold fabricated by ice-templating technique. (B) 3D reconstruction of fluorescence micrographs of collagen scaffolds, with cell nuclei are stained with DAPI (blue) after 24 hours of 3T3-L1 culture. Z-stacks were taken from the top of the scaffolds. (C) Fluorescence micrograph of collagen scaffolds, with cell nuclei are stained with DAPI (blue) after 24 hours of 3T3-L1 culture. From left to right were images taken on the bottom, middle and top of the scaffolds, respectively. Scale bars = 100µm

showed good adhesion in the collagen scaffolds. Further fluorescent images taken on the bottom, middle and top of the collagen scaffolds proved that cells invaded through and

adhered well on the collagen scaffold after short-term (24 hours) culture.

Cell viability and matrix deposition

We next tested cell viability and cell capability of its own matrix deposition. The fluorescent viability assay of unfixed collagen scaffolds confirmed that the majority of the cells were viable in the 3D collagen structure after both short-term (24 hours) and long-term (6 days)

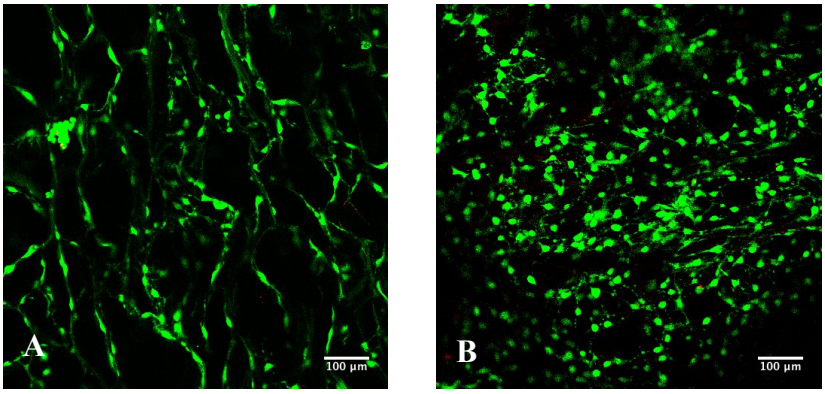

Fig 3.2 (A) Fluorescence micrograph of collagen scaffold after 24h of 3T3-L1 culture. (B) Fluorescence micrograph of collagen scaffold after 6 days of 3T3-L1 culture, showing very high cell viability. Live cells are stained with calcein (green), and dead cells are stained with propidium iodide (red).

culture (Fig. 3.2). To assess whether the 3T3-L1s functioned regularly, for instance, being able to assemble extracellular matrix (ECM), we utilized traces amounts of fluorescently-labeled Fn to visualize cell-deposited Fn fibers. As shown in the image, Fn not only decorated the surfaces of the scaffold, but was also assembled into thin fibrils (with higher brightness) around the periphery of cells (Fig. 3.3), proving the ability of the cells to polymerize Fn molecules into Fn fibers, i.e., to perform fibrillogenesis, a key process in tissue regeneration. These findings suggested that the 1.25% collagen scaffolds provide a satisfying 3D environment for fibroblasts to attach, grow, and function normally, which

fulfilled the essential criteria for an *in-vivo* mimicking of 3D cell-culture platform based on collagen.

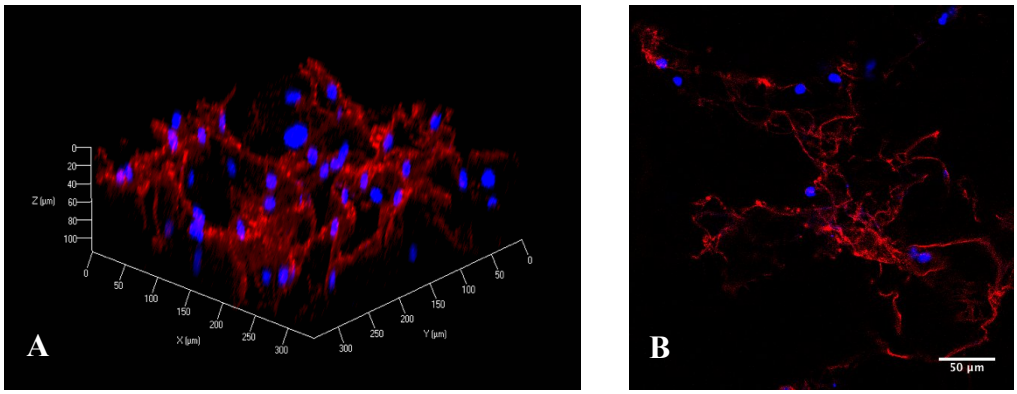

Fig 3.3 (A) 3D reconstruction of fluorescence micrographs of collagen scaffold after seeding 3T3-L1 cells and incubated with media containing labeled Fn. (B) Fluorescence micrograph of collagen scaffold after seeding 3T3-L1 cells and incubated with media containing labeled Fn. Cell-deposited fibronectin fibers (red) after 24 hours of 3T3-L1 culture. Cell nuclei are stained with DAPI (blue). Scale bar = 50µm.

Control of fibronectin conformation

Fibronectin(Fn) was diluted into a series of concentrations at 5µg/ml, 25µg/ml 50µg/ml and 100µg/ml, then was coated on a labtek under different conditions. Briefly, 10% FRET labeled fibronectin was added into a labtek, and the labteks were then i) placed under room temperature for 24 hours, ii) first placed at room temperature for 1 hour, then heated in an oven for 5 minutes., iii) first placed at room temperature for 1 hour, then heated in an oven for 25 minutes. After that, we assessed Fn conformation with intramolecular Förster Resonance Energy Transfer (FRET) imaging, using Fn molecules that were dual-labeled for FRET, as previously described, with imaging on a confocal microscope. Our FRET data

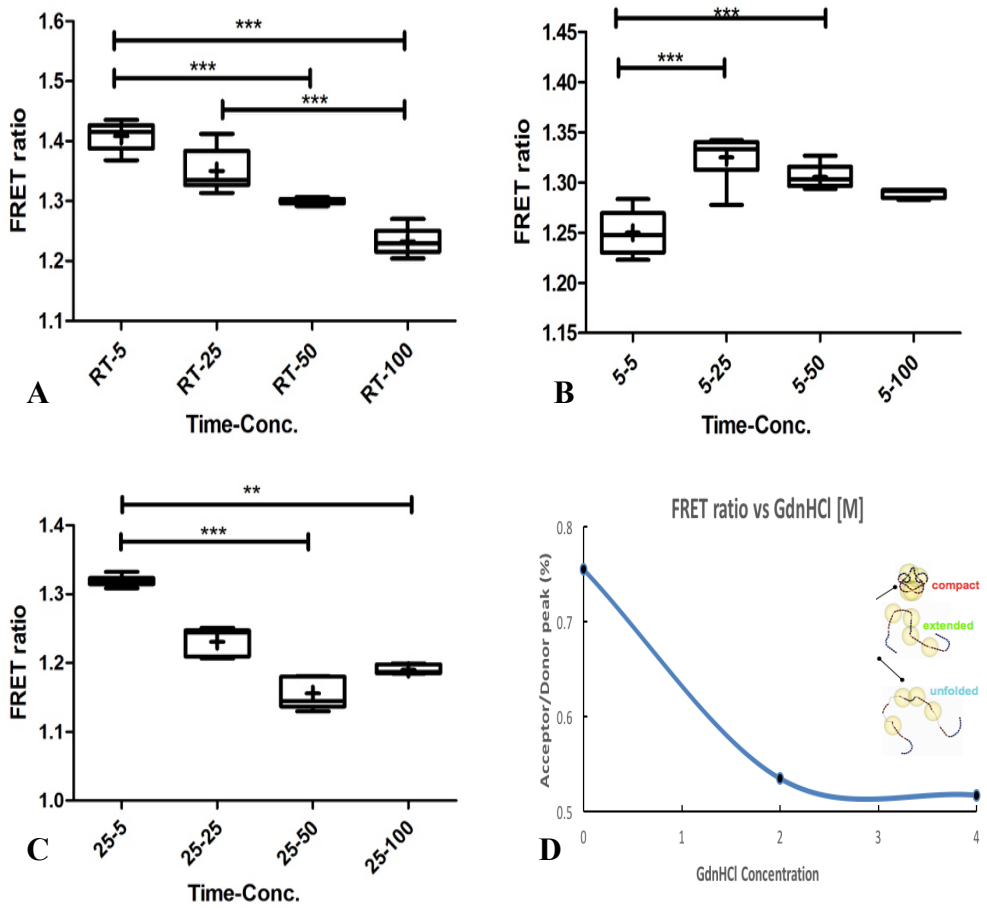

Fig 3.4 FRET intensity ratio for labtek-adsorbed Fn in concentrations of 5µg/ml, 25µg/ml 50µg/ml and 100µg/ml under different coating conditions. (A) Labtek-adsorbed Fn placed under room temperature for 24 hours, (B) Labtek-adsorbed Fn first placed at room temperature for 1 hour, then heated in an oven for 5 minutes., (C) Labtek-adsorbed Fn first placed at room temperature for 1 hour, then heated in an oven for 25 minutes. In all cases, *** indicates $p < 0.001$, with 8 to 12 measurements per condition. (D) FRET ratio calibration curve

(combined with the FRET intensity ratio calibration shown in Fig. 3.4D) indicate that the Fn showed different conformations as a function of Fn concentrations (Fig. 3.4) and coating conditions (Fig. 3.5). As the results show, FRET ratio decreased, indicating the Fn was more

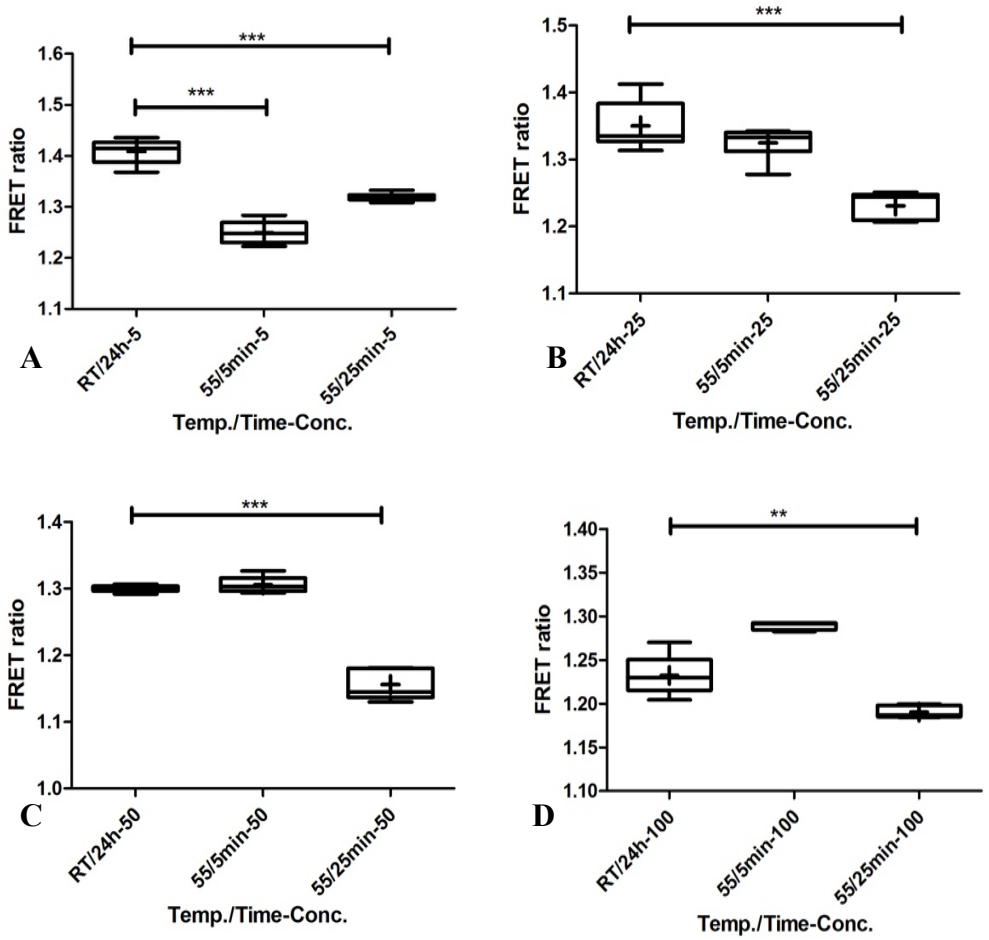

Fig. 3.5 FRET intensity ratio for labtek-adsorbed Fn under different coating conditions: i) placed under room temperature for 24 hours, ii) first placed at room temperature for 1 hour, then heated in an oven for 5 minutes., iii) first placed at room temperature for 1 hour, then heated in an oven for 25 minutes. (A) Labtek-adsorbed Fn in concentration of 5μg/ml. (B) Labtek-adsorbed Fn in concentration of 25μg/ml. (C) Labtek-adsorbed Fn in concentration of 50μg/ml. (D) Labtek-adsorbed Fn in concentration of 100μg/ml. In all cases, *** indicates $p < 0.001$, with 8 to 12 measurements per condition.

unfolded, as the Fn concentrations increased under room temperature. *We assumed that in higher concentration, the density of the Fn molecules increased, and hence increased Fn-Fn interactions which lead to partially unfolding of the Fn molecules.* We also notice that low Fn

concentrations seemed to be more sensitive to short-time thermally unfolding, from which *we hypothesized that such low Fn density gave more space for unfolding under short-period heating*. While Fn was thermally unfolded by heated under 55°C in all the concentrations, the effect on Fn in high concentration seemed to be mitigated *assumedly by the dual-effect that the space is limited for Fn unfolding due to the high molecules density.* Moreover, it is reported that some of the Fn molecules were able to refold when cooled down at room

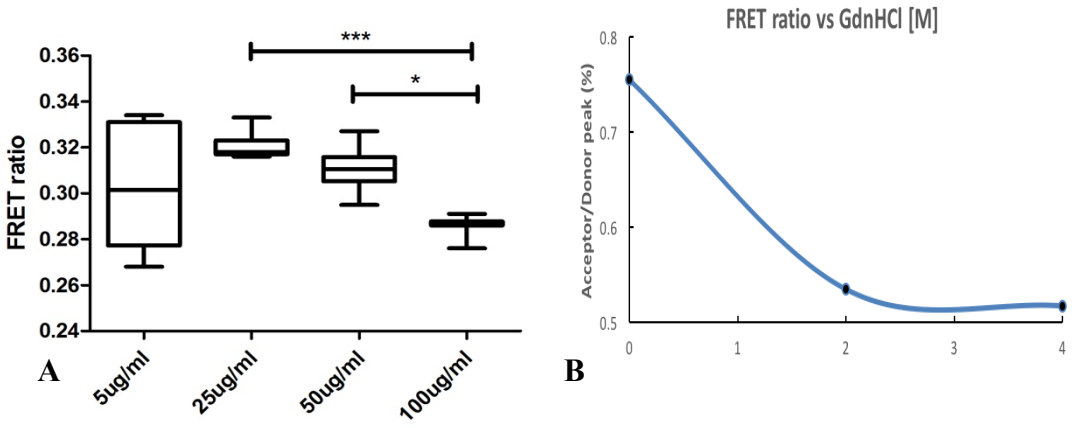

Fig. 3.6 (A) Labtek-adsorbed Fn coated under 4°C for 24h in concentration of 5, 25, 50, 100 µg/ml. (B) FRET ratio calibration curve

temperature after heating under high temperature [28], which inferred that the thermally-induced unfolding by heating under high temperature was unstable. Additionally, to avoid denaturation, Fn could only heated under temperature lower than 65°C and normally less than 1 hour in the range of 50°C to 65°C. [27,28] That means we were not able to keep the time scale, which affects Fn-adsorbed quantity, in consistence between the samples coated under RT and by heating.

Thus, we further investigated the labtek-adsorbed Fn conformations under lower temperature and more gentle heating conditions. This also enables us to coat the Fn in a same duration, 24 h, which will affect the amount of Fn that adsorbed by the substrate. We first confirmed the

trend of the conformations of Fn in different concentrations at low temperature was in consistence of previous research (Fig. 3.6), by coating Fn on a labtek under 4°C for 24 hours.

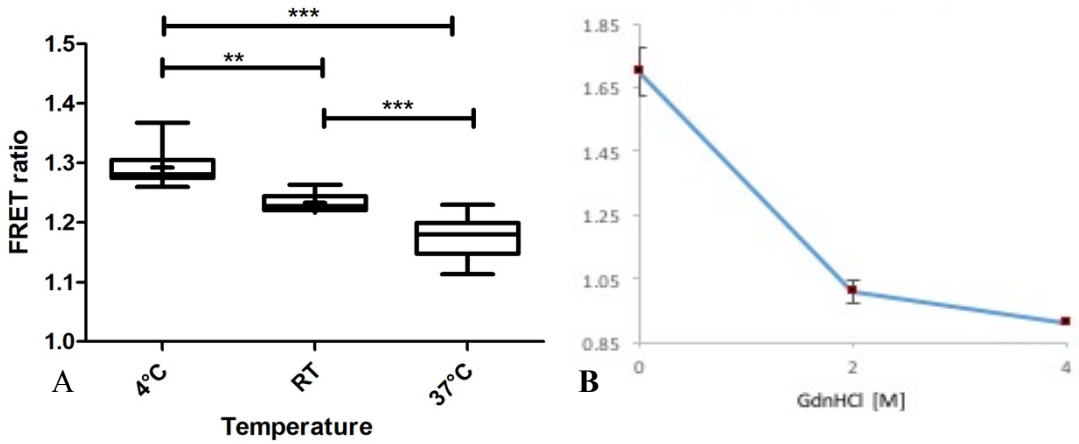

Fig. 3.7 (A) Labtek-adsorbed Fn in selected concentration of 50µg/ml coated under i) 4°C ii) room temperature iii) 37°C for 24 h (B) FRET ratio calibration curve

Then, as higher concentration of Fn benefits further cell culture, we designed the coating condition using 50µg/ml Fn solution, which previously showed more uniform results. The collagen scaffold which was immersed in FRET labeled Fn solution was then i) placed in the 4°C fridge for 24 hours, ii) placed under room temperature for 24 hours, iii) placed in the 37°C incubator for 24 hours. Our data (Fig. 3.7) indicates that we were able to control the adsorbed-Fn conformations by applying different thermal conditions, more specifically, by controlling the coating temperature during the Fn incubation. The Fn molecules adsorbed on the 2D substrate were more unfolding as the coating temperature increased.

Control of fibronectin conformation on Fn-coated collagen scaffolds

We already knew that the conformation of fibronectin varied with temperature as described above. Fn molecules assumed more compact conformations (high FRET ratios) at low temperature, and more extended conformations (low FRET ratios) at high temperature (Fig. 3.7). While the porous 3D form of collagen represents an excellent scaffold material to

support cell culture, we further tried to control the Fn conformation on the collagen scaffold, by absorbing Fn under different temperatures, which may further affect the adhesion of cells and their subsequent secretion behavior. We assessed Fn conformation with intramolecular Förster Resonance Energy Transfer (FRET) imaging, using traces amounts of Fn molecules

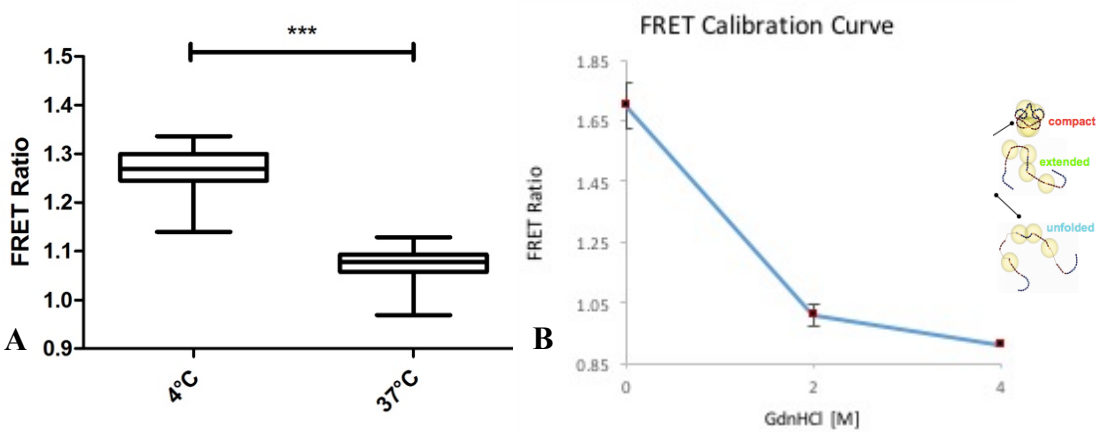

Fig. 3.8 (A) Measured FRET intensity ratio for scaffold-adsorbed Fn, on low-temperature-coated (1.28 ± 0.05),and high-temperature-coated (1.09 ± 0.05) collagen scaffolds. The FRET ratios of Fn on 4°C-coated scaffolds were 20% higher than those on 37°C-coated scaffolds, indicating more compact Fn conformations in low-temperature coating, and more unfolded Fn conformations in high-temperature coating. In all cases, *** indicates $p < 0.001$, with 8 to 12 measurements per condition. (B) FRET ratio calibration

that were dual-labeled for FRET, as previously described. The scaffolds were rinsed in PBS for 3 times after disinfection, then 10% FRET labeled fibronectin was added into the wells to submerge the scaffolds (only 10% was labeled for FRET, to avoid spurious intermolecular FRET). After that, one batch of scaffolds were put into 4°C fridge for 24 hours while another batch of scaffolds were incubated in 37°C for 24 hours. After coating Fn under different conditions, the scaffolds were rinsed thoroughly in PBS, and imaged on a confocal microscope. Our FRET data (combined with the FRET intensity ratio calibration shown in Fig. 3.8) indicate that the scaffold-adsorbed Fn showed different conformation in different

coated temperatures, with Fn molecules assuming more compact conformations (high FRET ratios) in the low-temperature-coated collagen scaffolds, and more extended conformations (low FRET ratios) in the high-temperature-coated collagen scaffolds. These findings are in agreement with previous results on the pre-condition experiments which demonstrated Fn conformations varied with temperatures and concentrations. We chose an optimal concentration of Fn and a range of temperature that was large enough (4°C and 37°C), to further enable the range of conformational changes of Fn molecules adsorbed on the collagen scaffold.

Effect of Fn conformation on cell adhesion and viability

We next tested whether the difference in Fn conformation on the collagen scaffold further affected cell adhesion and their subsequent viability. Considering Fn conformation plays an important role on guiding numerous cell functions, we investigated whether Fn coated on the collagen scaffolds under different temperature would affect the cells adhesion and their viability. Two batches of scaffolds were biased at Fn coating temperature (as described above for the FRET experiment), with control sample immersed in PBS at room temperature for 24 hours. Afterward, as fibroblasts, which migrate to the wound area and assemble ECM proteins to contract and organize the new matrix[29–32], together with fibronectin are crucial in the wound healing process, 3T3-L1 cells (to represent fibroblasts) were seeded onto the top of scaffolds, and fresh media was added after 1 hour of culture. Cell culture was performed in the absence of applied bias for 12 hours and 24 hours respectively, and subsequently, the total number of cells adhere on the Fn-adsorbed collagen scaffolds (Fig. 3.9A,B) was quantified on ImageJ with the fluorescent imaging. Interestingly, by comparing results of short-term culture (12h) and long-term culture (24h), we noticed that cells were not likely to proliferate on the collagen scaffolds without coating Fn (~30k at 12h and almost the same at 24h), whereas

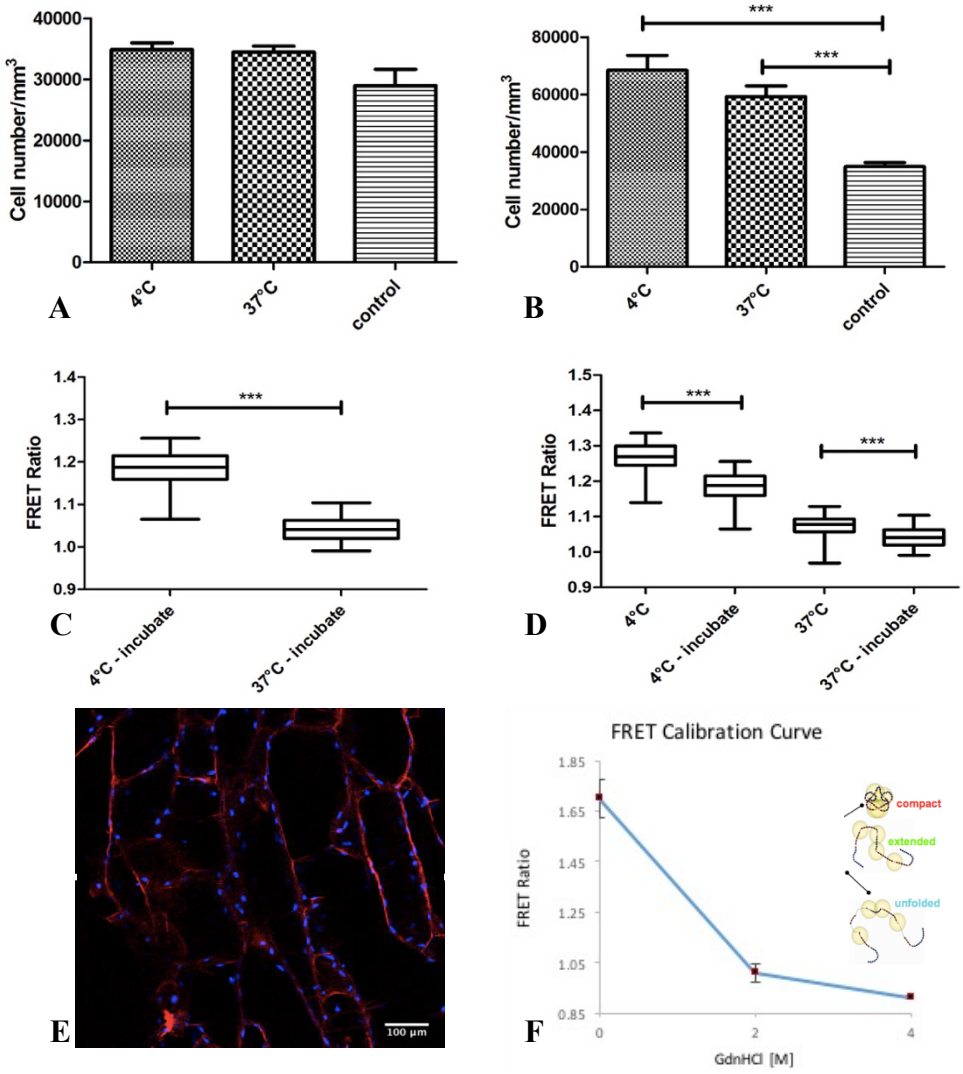

Fig. 3.9 3T3-L1 cells adhesion after initial seeding for (A)12 h and (B) 24 h as quantify by cell number per volume via fluorescent assay. (C) Measured FRET intensity ratio for scaffold-adsorbed Fn on low-temperature-coated (1.19±0.05),and high-temperature-coated (1.03±0.05) collagen scaffolds, after incubating in cell culture media for 24h. (D) Comparison of the FRET intensity ratio for scaffold-adsorbed Fn before and after incubating in the cell culture media. In all cases, *** indicates $p < 0.001$, with 8 to 12 measurements per condition. (E) Cells (blue, staining nuclei with DAPI) adhere on the collagen scaffold with adsorbed-Fn. Scaffolds were incubated in 15% Alexa633 labeled Fn for 24h before seeding cells. (F) FRET ratio calibration

cells did proliferate on the Fn-coated collagen scaffolds (~35k at 12h and ~65k, almost twice,

at 24h). The long-term culture results show that the cells adhesion on Fn-coated collagen scaffolds is significantly higher than the control sample, which without coating Fn, and cells prefer 4°C-coated Fn with high FRET ratio (Fig. 3.9C). This is consistent with our previous work showing that cells prefer compact Fn rather that unfolded Fn to adhere to, as they can use alpha5beta1 integrins (the most common type of integrins) to adhere to the substrate, which requires the concomitant engagement of both the FnIII9 (synergy site) and FnIII10 (RGD loop). This 'double' engagement is not allowed/possible when Fn is extended or unfolded so cells have to use other types of integrins that engage only the RGD loop (for example alphaVbeta3 integrin), which are less common and often associated with a pathological behavior.

It is known that pH, ions, and temperature would affect Fn conformations. Therefore, we further investigated if the incubation in cell culture media under 37°C would alter the initial-coated Fn conformations on the collagen scaffolds. Briefly, after adsorbed 10% FRET-labeled Fn on the collagen scaffolds either under 4°C or 37°C, all of the samples were incubated in 300µl 1%FBS media for 24 hours (exactly the same as cell seeding procedure). Afterward, the collagen scaffold was thoroughly rinsed by PBS for three times, and FRET data was acquired as previously described. By comparing the FRET ratios before and after incubation in the cell culture media, we found that the Fn molecules were more extended during the culture process, which should be due the the thermal effect (incubated under 37°C), and probably affected by the salt in the media. However, our data (Fig. 3.9D) suggests that the FRET intensity ratio still had significant difference on the low-temperature-coated scaffolds and the high-temperature-coated scaffolds, which indicates the Fn conformations remained distinct during the cell culture process. Therefore, such collagen-adsorbed Fn (in different conformations) 3D scaffolds could serve as an exellent platform to study the matrix-

interacted cellular behaviors.

The viability of 3T3-L1 fibroblasts cells in these three samples was assessed via Live/Dead Assay (Fig. 3.10). The live cells (green) and dead cells (red) were quantified by fluorescent imaging and counted via ImageJ. Our data suggests that the samples coated with Fn showed

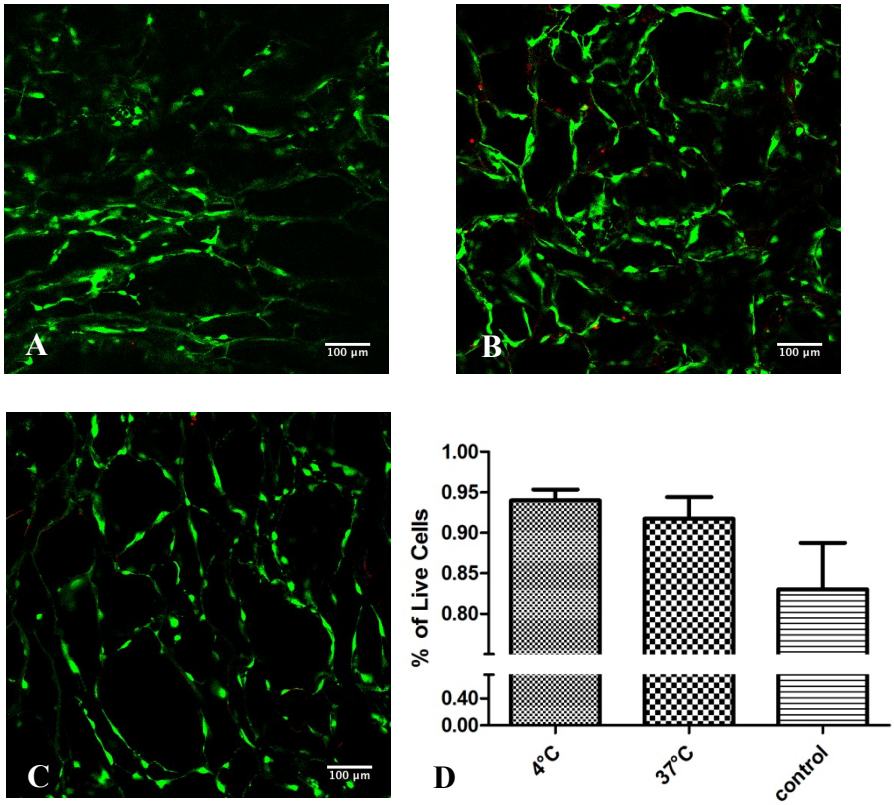

Fig 3.10 (A) Fluorescence micrograh of control sample after 24h of 3T3-L1 culture. (B) Fluorescence micrograph of low-temperature-coated collagen scaffold after 24h of 3T3-L1 culture. (C) Fluorescence micrograph of high-temperature-coated collagen scaffold after 24h of 3T3-L1 culture. All shows very high cell viability. Live cells are stained with calcein (green), and dead cells are stained with propidium iodide (red). (D) 3T3-L1 cell viability after initial seeding for 24h as quantify by cell number per volume via Live/Dead assay.

relatively high cell viability compared to the control collagen scaffold, while there are no significant differences between the two Fn-coated scaffolds on cell viability (both above 93%) though the compact-Fn-coated scaffold had slightly higher percentage of live cells.

Conclusion

In summary, our work suggests that the 1.25 wt.% collagen scaffold, with an average pore size of 36μm and a compressive modulus of 1720 ± 300 Pa, could serve as a promising cell culture platform as 3T3-L1 mouse fibroblast cells were able to migrate through the scaffold, function normally and remain viable after short-term as well as long-term culture. The presence of fibronectin improved the cell viability and significantly enhanced the cell adhesion and proliferation on the collagen scaffold. Collectively, our findings indicate that the collagen scaffold-adsorbed Fn could be thermally unfolded, and this thermally-altered Fn conformation was able to regulate the cell adhesion, viability and proliferation, which could potentially coordinate cell behaviors in wound healing. Fn, which is the major early component of the fibrin clot in the ECM of regenerating tissues, is crucial in the early wound healing stage, when the fibroblasts migrate, adhere and proliferate on the wound area. These controlled-conformation Fn-coated collagen scaffolds are able to provide a promising physiological and pathological relevant 3D platform that can monitor cell functions and function for long-term cell cultures in large volume assays.

Reference:

1. Discher, D. E., Janmey, P. & Wang, Y.-L. Tissue cells feel and respond to the stiffness of their substrate. *Science* **310,** 1139–43 (2005).

2. Ingber, D. E. Cellular mechanotransduction: putting all the pieces together again. *FASEB J.* **20,** 27 (2006).

3. Vogel, V. & Sheetz, M. Local force and geometry sensing regulate cell functions. *Nat. Rev. Mol. Cell Biol.* **7,** 265–75 (2006).

4. Dalby, M. J. *et al.* Attempted endocytosis of nano-environment produced by colloidal lithography by human fibroblasts. *Exp. Cell Res.* **295,** 387–394 (2004).

5. Dalby, M. J., Riehle, M. O., Sutherland, D. S., Agheli, H. & Curtis, A. S. G. Morphological and microarray analysis of human fibroblasts cultured on nanocolumns produced by colloidal lithography. *Eur. Cells Mater.* **9,** 1–8 (2005).

6. Engler, A. J., Sen, S., Sweeney, H. L. & Discher, D. E. Matrix Elasticity Directs Stem Cell Lineage Specification. *Cell* **126,** 677–689 (2006).

7. Galbraith, C. G., Yamada, K. M. & Sheetz, M. P. The relationship between force and focal complex development. *J. Cell Biol.* **159,** 695–705 (2002).

8. Giannone, G. & Sheetz, M. P. Substrate rigidity and force define form through tyrosine phosphatase and kinase pathways. *Trends in Cell Biology* **16,** 213–223 (2006).

9. Kostic, A. & Sheetz, M. P. Fibronectin rigidity response through Fyn and p130Cas recruitment to the leading edge. *Mol. Biol. Cell* **17,** 2684–95 (2006).

10. Yeung, T. *et al.* Effects of substrate stiffness on cell morphology, cytoskeletal structure, and adhesion. *Cell Motil. Cytoskeleton* **60,** 24–34 (2005).

11. Boccafoschi, F., Habermehl, J., Vesentini, S. & Mantovani, D. Biological performances of collagen-based scaffolds for vascular tissue engineering. *Biomaterials* **26,** 7410–7417 (2005).

12. Craig, R. & Beavis, R. TANDEM: matching proteins with tandem mass spectra. *Bioinformatics* (2004).

13. To, W. S. *et al.* Plasma and cellular fibronectin: distinct and independent functions during tissue repair. *Fibrogenesis Tissue Repair* **4,** 21 (2011).

14. Antia, M., Islas, L. D., Boness, D. A., Baneyx, G. & Vogel, V. Single molecule fluorescence studies of surface-adsorbed fibronectin. *Biomaterials* **27,** 679–690 (2006).

15. Reilly, G. C. *et al.* Intrinsic extracellular matrix properties regulate stem cell differentiation. *J. Biomech.* **43,** 55–62 (2010).

16. Baneyx, G., Baugh, L. & Vogel, V. Fibronectin extension and unfolding within cell matrix fibrils controlled by cytoskeletal tension. *Proc. Natl. Acad. Sci. U. S. A.* **99,** 5139–5143 (2002).

17. Smith, M. L. *et al.* Force-induced unfolding of fibronectin in the extracellular matrix of living cells. *PLoS Biol.* **5,** 2243–2254 (2007).

18. Barker, T. H. *et al.* SPARC regulates extracellular matrix organization through its modulation of integrin-linked kinase activity. *J. Biol. Chem.* **280,** 36483–36493 (2005).

19. Larsen, M., Artym, V. V, Green, J. A. & Yamada, K. M. The matrix reorganized: extracellular matrix remodeling and integrin signaling. *Curr. Opin. Cell Biol.* **18,** 463–471 (2006).

20. Vakonakis, I. & Campbell, I. D. Extracellular matrix: from atomic resolution to ultrastructure. *Curr. Opin. Cell Biol.* **19,** 578–583 (2007).

21. Singh, P., Carraher, C. & Schwarzbauer, J. E. Assembly of fibronectin extracellular matrix. *Annu. Rev. Cell Dev. Biol.* **26,** 397–419 (2010).

22. Mains, P. E., Sulston, I. A. & Wood, W. B. Dominant maternal-effect mutations causing embryonic lethality in Caenorhabditis elegans. *Genetics* **125,** 351–369 (1990).

23. George, E. L., Georges-Labouesse, E. N., Patel-King, R. S., Rayburn, H. & Hynes, R. O. Defects in mesoderm, neural tube and vascular development in mouse embryos lacking fibronectin. *Development* **119,** (1993).

24. Fontana, L. *et al.* Fibronectin is required for integrin alphavbeta6-mediated activation of latent TGF-beta complexes containing LTBP-1. *FASEB J.* **19,** 1798–808 (2005).

25. Oberhauser, A. F., Badilla-Fernandez, C., Carrion-Vazquez, M. & Fernandez, J. M. The mechanical hierarchies of fibronectin observed with single-molecule AFM. *J. Mol. Biol.* **319,** 433–447 (2002).

26. Samorì, B., Zuccheri, G. & Baschieri, P. Protein unfolding and refolding under force: Methodologies for nanomechanics. *ChemPhysChem* **6,** 29–34 (2005).

27. Ingham, K. C., Brew, S. a, Broekelmann, T. J. & McDonald, J. a. Thermal stability of human plasma fibronectin and its constituent domains. *J. Biol. Chem.* **259,** 11901–11907 (1984).

28. Paci, E. & Karplus, M. Unfolding proteins by external forces and temperature: the importance of topology and energetics. *Proc. Natl. Acad. Sci.* **97,** 6521–6526 (2000).

29. Brito, T. N. de S., Rocha, L. R. M. da, Jatobá, C. A. N., Sales, M. P. & Medeiros, A. da C. Effect of topical application of fibronectin in duodenal wound healing in rats. *Acta Cir. Bras.* **18,** 97–101 (2003).

30. Zhu, Q. L., Denefle, J. P. & Lechaire, J. P. Fibronectin (FN) localizations in early

wound healing of cultured frog skins. *Biol. cell* **57,** 161–7 (1986).

31. Bachman, H., Nicosia, J., Dysart, M. & Barker, T. H. Utilizing Fibronectin Integrin-Binding Specificity to Control Cellular Responses. *Adv. wound care* **4,** 501–511 (2015).

32. Midwood, K. S., Mao, Y., Hsia, H. C., Valenick, L. V & Schwarzbauer, J. E. Modulation of cell-fibronectin matrix interactions during tissue repair. *J. Investig. Dermatology Symp. Proc.* **11,** 73–78 (2006).

Chapter 4

3D Fibronectin-Collagen Dual Protein Scaffold with Fibrillar Fibronectin Matrix

Contributor: Junhui Ye, Soyoung Min and Delphine Gourdon

Abstract

In this study, several techniques have been used to introduce fibronectin (Fn) fibers into the three-dimensional (3D) porous collagen platform. The Fn fibrillogenesis under a cell-free process has long been a challenge, especially in a 3D platform. We modified the previous force-based methods that created Fn fibers on the 2D substrate, and designed new techniques to induce Fn *fibers* (rather than a monomolecular *film* of Fn molecules as in Chapter 3) within the 3D collagen template, including stirring, shaking, manually pulling and blowing. Short Fn fibrils were produced by the shaking technique under precisely defined conditions. Longer and thicker Fn fibers were generated by the manually pulling technique, while air flow applied on the system was able to increase the quantity of the Fn fibers and improve the fibers distribution within the system. This fibronectin-collagen dual-protein scaffold could be customized in designated forms of Fn and tunable collagen microstructure based on the need of future study. This dual-protein scaffold would better mimic the ECM that comprises a fibrous Fn network in various length, thickness and conformation. It would, in turn, be able to support large volume cell culture and hence providing a platform to investigate the cell-ECM interaction. As the key component in wound healing environment, the fibronectin-collagen scaffold could potentially facilitate the wound healing process and be used in application for regeneration medicine.

Introduction

In recent decades, the need for an *in vitro* mimicking model of extracellular matrix (ECM) has been raising extensive research interest to investigate the structural, mechanical and functional properties of the fibrillar ECM. [1–6] Collagen and fibronectin (Fn) are the most abundant proteins constituents of the ECM, which is essential in regulating cellular behaviors. *In vitro*, cells assemble Fn molecules into nanoscale fibrils through the integrin-binding-dependent force-induced mechanism. [5,7–9] Fibronectin fibrils are able to stretch up to several times their length *in vivo*, during which the Fn molecule is unfolding, indicating this protein would be very likely to alter mechanochemical signaling in such process.[1,10,11] However, few studies were able to develop artificial Fn fibrillar substrates, especially in a three dimensional platform which was essential on investigating the cellular responses entirely caused by the correlation between cells and Fn fibrils. Cell-free Fn fibrillogenesis is based on the unfolding of Fn molecules from their globular/compact conformation, which enables Fn-Fn interaction, and further leads to Fn polymerization and fibrils formation. As previously reported, the methods used in cell-free Fn fibrillogenesis are: 1) reduction or oxidation agents, 2) denaturing, cationic or anionic compounds, 3) peptidic Fn fragments, 4) force-based assembly, including mechanical tension and shear force, 5) surface-initiated assembly.[12–27] In this study, we focus on the force-induced methods that do not introduce any impurities into the system. The manually pulling technique to produce single fibrils from a high concentration drop of Fn has proved to yield Fn fibrils with diameters in a range of 0.5um to 5um. [1,28,29] The unidirectional stirring technique in an ultrafiltration cell was described to produce artificially oriented fibrous Fn mat based on the tendency of Fn to form insoluble aggregates from concentrated solutions. [21] The drawbacks of the reported approaches are that they can only yield few individual fibrils on a 2D substrate, or in a 3D platform but whose fibrils alignment are highly oriented, both of which are not suitable to imitating the *in vivo*

micro-environment. Fn plays a critical role in the process of wound healing.[5,15,30–36] The fibrillogenesis of soluble Fn molecules are highly regulated. [8,37] It has been known that the assembly into fibers needs i) Fn-Fn interactions, and ii) air-solution interface. This 440kD dimeric protein contains multiple exposed molecular recognition sites and cryptic binding sites buried in the folded structure, which are able to regulate the fibrillogenesis, interaction of other ECM proteins, and the cell adhesion as well as proteolytic activity. [5,8,23,38,39] 70-kDa fragments, for instance, are essential for N-terminal assembly as well as containing collagen binding sites.

In this study, we designed several force-based methods to create Fn fibers in the 3D collagen template under cell-free process, including (i) stirring that generated the shear flow by a stir bar, (ii) shaking on a rocking platform shaker and (iii) manually pulling of the structure from droplets of concentrated Fn solution. The Fn fibers were then characterized to visualize the deposition and quantify their conformation. Afterward, 3T3-L1 cells, representing fibroblasts, were seeded on the dual-protein scaffold to confirm cell invasion and adhesion. These engineered dual-protein 3D templates have a broad potential in many biological applications, including tissue engineering, diagnostics, actuation, and drug delivery systems.

Materials and Methods

Fibronectin Fibrillogenesis in 3D collagen template

We first tried to produce orientated Fn matrix within the collagen scaffold under continuous unidirectional shear.[21] Briefly, the pore-structure collagen scaffold was clipped on a cross shape stir bar then placed in the well of the Labtek chamber. Fn labeled with 15% Alexa633 was diluted in PBS for a concentration of 300µg/ml, then was added into the well. Afterward, the Labtek chamber was placed in a desiccator and stirred under a speed of 800 for 6 hours. Second, we applied random shear force on the Fn-submerged collagen scaffold by putting it

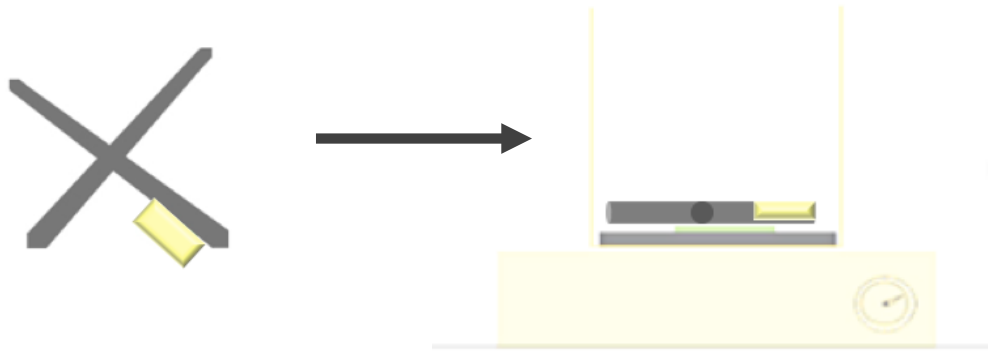

Fig. 4.1 Scheme of the stirring technique for Fn fibrillogenesis. On the left is a collagen scaffold (yellow) being clipped on a cross shape stir bar (black). The structure were then placed in a well and stirred on the machine as described on the right.

on a shaker, and provided an air-solution interface during shaking by precisely controlling the volume of the Fn solution. The collagen scaffold was immersed in unlabeled Fn for 1 hour at room temperature, then 15% Alexa633 Fn solution at a concentration of 300µg/ml was added in the chamber. Subsequently, the sample was put on a shaker overnight at a speed of 6. It should be emphasized that the speed and the shaking angle of the machine highly impact on the liquid flow, and hence the shear forces applied on the system. Therefore, it should be carefully monitored as it plays an essential role on the fiber initiation.

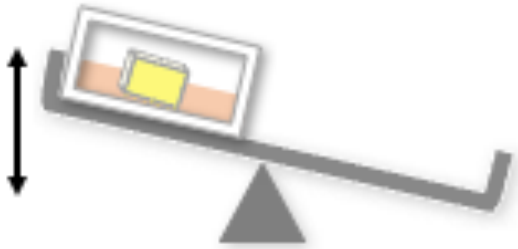

Fig. 4.2 Scheme of the shaking technique for Fn fibrillogenesis. The collagen scaffold (yellow) in place in a suitable volume of fluorescent labeled Fn solution (red). The structure were then placed on the shaker and treated under a controlled speed.

Deposition of Fn fibers on the collagen scaffold by manually pulling was following a modified procedure as previously described (Ejim et al., 1993). Briefly, after sterilization under the UV light for 1 hour, the collagen scaffold was cut into a 1mm thick and dipped into a 0.3 mg/mL 15% Alexa633 labeled/10% FRET labeled Fn droplet and gently drawn toward the air to initiate Fn polymerization. Once in contact with the collagen substrates, the fibers were able to attach on the collagen, which was later confirmed by SEM. Further, we created an air flow using the nitrogen gun in the interim during the multiple pulling to induce higher quantity of the Fn fibrils and introduce Fn fibrils into deeper layer of the collagen scaffold. After fibronectin fibrillogenesis, samples were left in PBS at room temperature no longer than 1 day before use.

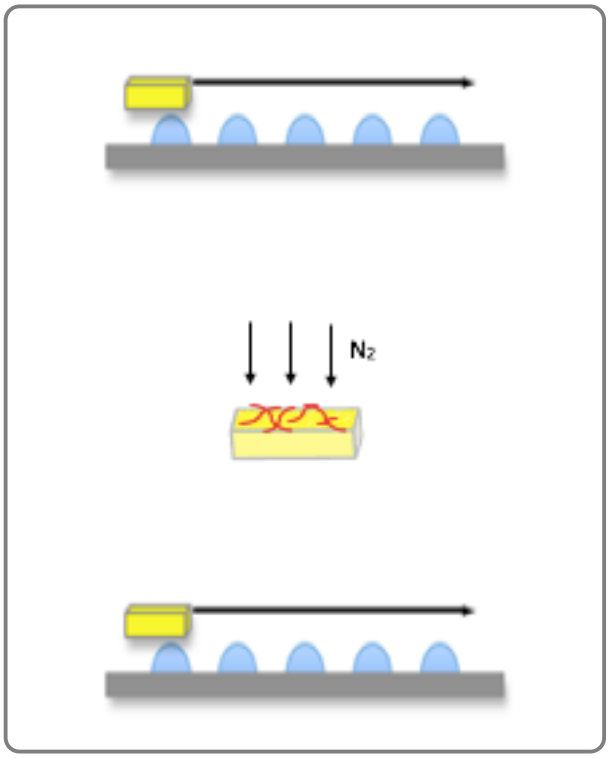

Fig. 4.3 Scheme of the combined technique of manually pulling and blowing for Fn fibrillogenesis. The collagen scaffold (yellow) was pulled over the droplets of concentrated fluorescently-labeled Fn solution (blue). In further study, the structure was then placed under the nitrogen air flow during each interim of the pulling. (The manually deposited Fn fibers by pulling technique were indicated in the scheme as the red lines on the collagen scaffold.)

Fibronectin and FRET labeling

Fibronectin (Fn) was acquired from Life Technologies, NY. AlexaFluor 633 succinimidyl ester were used to randomly single-label Fn. AlexaFluor 488 succinimidyl ester and AlexaFluor 546 maleimide (Invitrogen, CA) were used to dual-label Fn for intramolecular FRET as previously described by Smith et al. [40] Labeling ratios and Fn concentrations were obtained using a DU®730 UV/Vis spectrophotometer (Beckman, IN) at 280 nm, 495 nm, and

556 nm. Calibration of FRET-labeled Fn was performed in guanidine hydrochloride (GdnHCl) solution at concentrations of 0 M, 2 M, and 4 M to calculate FRET ratios, defined as acceptor/donor intensity ratios (IA/ID), and as a function of protein denaturation.

FRET data analysis

Fn-adsorbed scaffolds were imaged with a Zeiss 710 confocal microscope (Zeiss, Munich, Germany). Z-stack images were obtained in 16-bit using the C-Apochromat water-immersion 40×/1.2 objective, with the pinhole of 1 AU, 488 nm laser with 5% laser power, pixel dwell time of 6.3 μs, PMT1 and PMT2 gains of 500 V, and z-step size of 1 μm. FRET-labeled Fn was excited with a 488 nm laser line; emissions from donor and acceptor fluorophores were simultaneously collected in the PMT1 channel (514–526 nm) and the PMT2 channel (566–578 nm), respectively. These z-stack images were analyzed with user-defined Matlab code to calculate the FRET ratio (IA/ID) images as well as the mean FRET ratios for the z-stacks. 6 different spots per sample, and three samples per condition were analyzed to calculate the mean and standard deviation of the FRET intensities, and the histogram figures were generated with FRET intensity at each representative location.

Cell culture experiments

1 mm thick scaffolds were prepared for cell culture experiments by being placed under UV light for 30min for disinfection, and then rinsed 3 times with sterile PBS (Life Technologies). Cell adhesion was assessed with 3T3-L1 cells (ATCC #CL-173), an adipogenic subtype of mouse fibroblasts. These cells were incubated in αMEM (Sigma-Aldrich) containing 10 vol% fetal bovine serum (FBS, Tissue Culture Biologicals) and 1 vol% penicillin/streptomycin (pen/strep) (Life Technologies) prior to seeding. The cells were seeded in 10 μL suspensions (containing 15 thousand cells) on the top of the prepared scaffolds and were allowed to

adhere for 1 hour. Then, fresh media containing 1 vol% fetal bovine serum (FBS, Tissue Culture Biologicals) was added to the wells with the scaffolds, and they were cultured in the incubator at 37 °C (5% CO_2) for 24 hours.

After culture, the cell-seeded scaffolds were rinsed in PBS for twice and soaked in 3.7% ice-cold paraformaldehyde for chemical fixation. To assess cell infiltration and adhesion into the scaffolds, the samples were stained with 4′,6-diamidino-2-phenylindole (DAPI), calcein AM, and propidium iodide (PI) (all from Life Technologies), and imaged via fluorescent confocal microscope (Zeiss710, Zeiss, Munich, Germany) using a 10X/0.25 objective. And the number of cells were quantified via ImageJ on 6 different spots of each samples.

Results and Discussion

Effect of different techniques on fibronectin fibrillogenesis

By clipping the collagen scaffold in a shear flow of Fn solution created by stirring (Fig. 4.4), we observed a lot of Fn aggregation within the collagen template though there were some Fn nanofibrils.

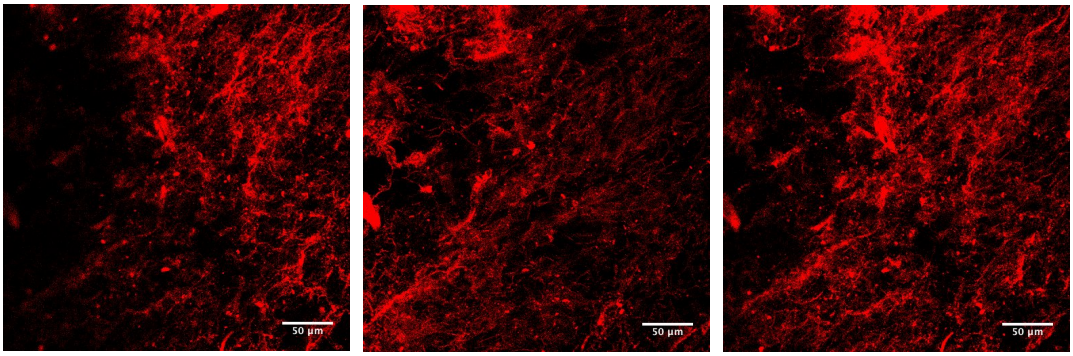

Fig. 4.4 After stirring, the fibronectin fibrillogenesis effect was evaluated on confocal microscope. Fn was single-labeled with Alexa633 (red). (Scale bars = 50µm)

While by shaking the Fn-immersed collagen scaffold for 24 hours, we had a collagen scaffold well-decorated by Fn molecules, and induced thin, short Fn fibrils simultaneously (Fig. 4.5).

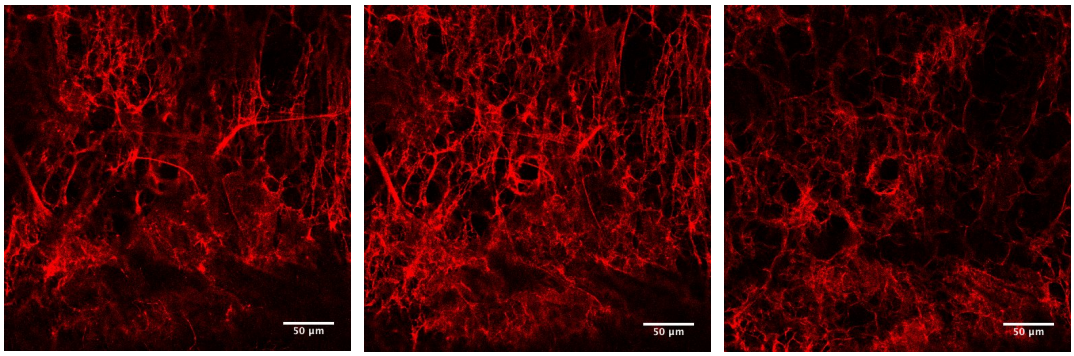

Fig. 4.5 After placing on the shaker overnight, the fibronectin fibrillogenesis effect on Fn-immersed collagen scaffold was evaluated on confocal microscope. Fn was single-labeled with Alexa633 (red). (Scale bars = 50µm)

Fn fibers were successfully deposited on the collagen scaffolds by manually pulling the structure through a high concentration of Fn solution droplet. (Fig. 4.6) It has been reported previously that manually deposited Fn fibers on 2D surface pulled from concentrated

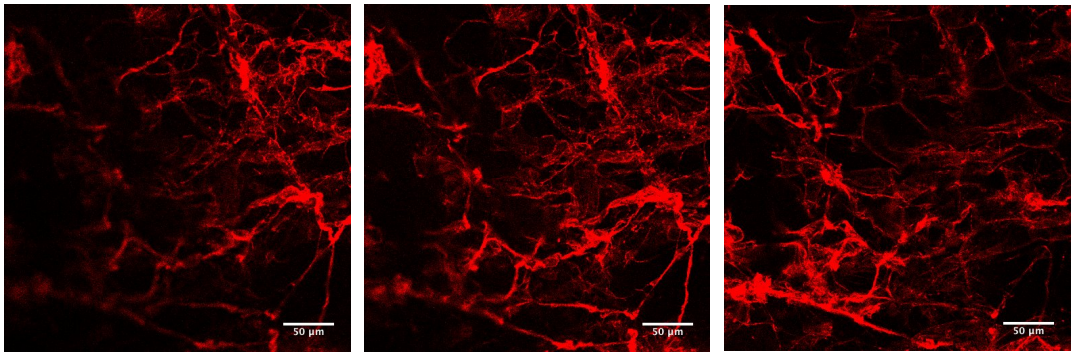

Fig. 4.6 After manually pulling, the fibronectin fibrillogenesis effect was evaluated on confocal microscope. Fn was single-labeled with Alexa633 (red). (Scale bars = 50µm)

solutions of soluble Fn resembled *in vivo* Fn fibers in diameter.[20] To simply characterize the morphology of the deposited fibers, the diameter was calculated from the fluorescent images using ImageJ. The results suggested that the average diameter (1±0.5 µm) of our Fn fibers deposited from a 0.3 mg/mL Fn solution on the collagen scaffold, as observed via fluorescence confocal microscopy, is similar to that of the thickest fibers and branching areas found in cell-deposited matrices.[41] The thickness of the fiber can be moderately adjusted during the pulling procedure.

Fibronectin fibrillogenesis via mechanical pulling

We further investigated whether altering the manually pulling technique could control the morphology of the deposited Fn fibers. We already knew that pulling force and speed affect the deposited Fn fibers thickness and length, as previously described. [28,29] We had half of the samples pulled through a concentrated labeled-Fn solution once, defined as ‘single-pulling’,

while other half of the samples were pulled through the labeled-Fn droplet for five times, defined as 'multiple-pulling'. According to the fluorescent images (Fig.4.7) of the manually deposited fibers on the collagen scaffold, we observed average thicker and longer Fn fibers in the multiple-pulling sample, compared to single-pulling. The thicker and longer Fn fibers

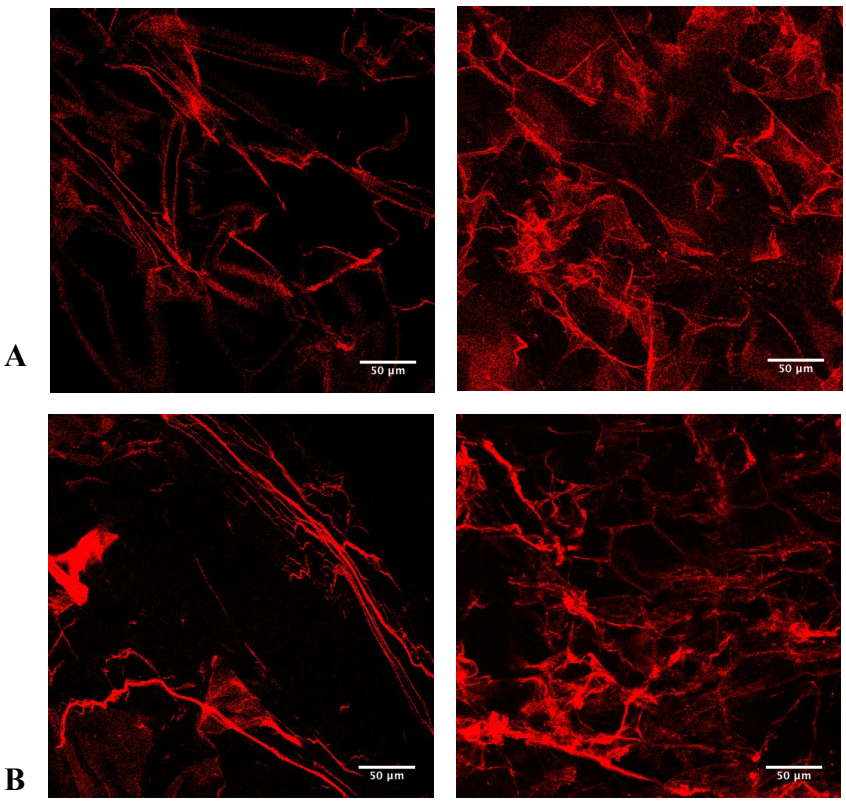

Fig. 4.7 Fluorescent images of manually pulling deposited Fn fibers on the collagen scaffold. Fn was labeled with Alexa 633 (red). (A) single-pulling deposited Fn fibers (B) multiple-pulling deposited Fn fibers. (Scale bars = 50µm)

deposited by multiple-pulling might be due to submicron fibril produced in each pulling bundle together to form larger bundles of fibrils in agreement with previously published images of such artificial Fn fibers [20,21]. Indeed, cryo-scanning electron microscopic images

suggest that Fn fibers exist as bundles comprising individual fibrous strands of ~5– 15 nm in diameter and larger, [24,25,42,43] which are proposed to be held together by hydrogen bonds,

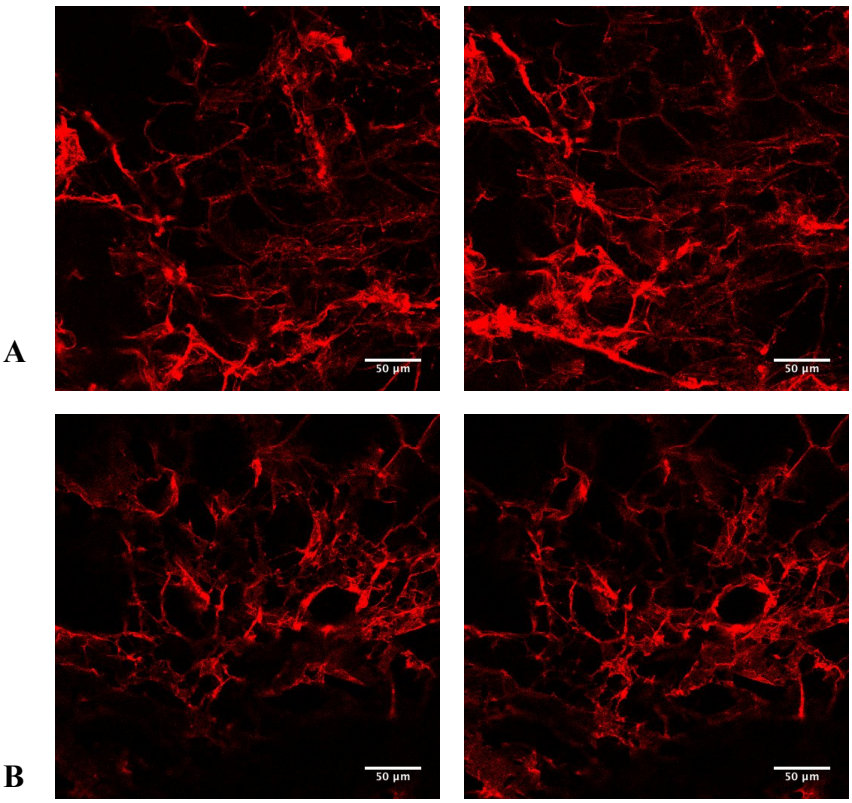

Fig. 4.8 Fluorescent images of manually pulling deposited Fn fibers on the collagen scaffold. Fn was labeled with Alexa 633 (red). (A) multiple-pulling deposited Fn fibers on originally dry scaffold (B) multiple-pulling deposited Fn fibers on collagen scaffold immerse in PBS for 2h. (Scale bars = 50µm)

intermolecular beta-strand swapping,[44,45] disulfide bonds which are potentially formed by cryptic disulfide isomerase activity,[46] and other weak electrostatic interactions.[47,48]

To assess if the surface moisture of the collagen scaffold affected the initial polymerization of Fn fibril, we used two different samples for the pulling. Half of the collagen scaffolds were immersed in PBS for 2h before pulling, while the rest maintained dry before pulling. As the result shows (Fig. 4.8), Fn was more likely to decorate on the wet collagen scaffold surface

and forming short fibrils on it, whereas Fn was able to assemble into longer and thicker fibrils on the dry collagen surface. Then, we hypothesized that the polymerization of Fn fibrils was easier initiated on the dry surface of the scaffold.

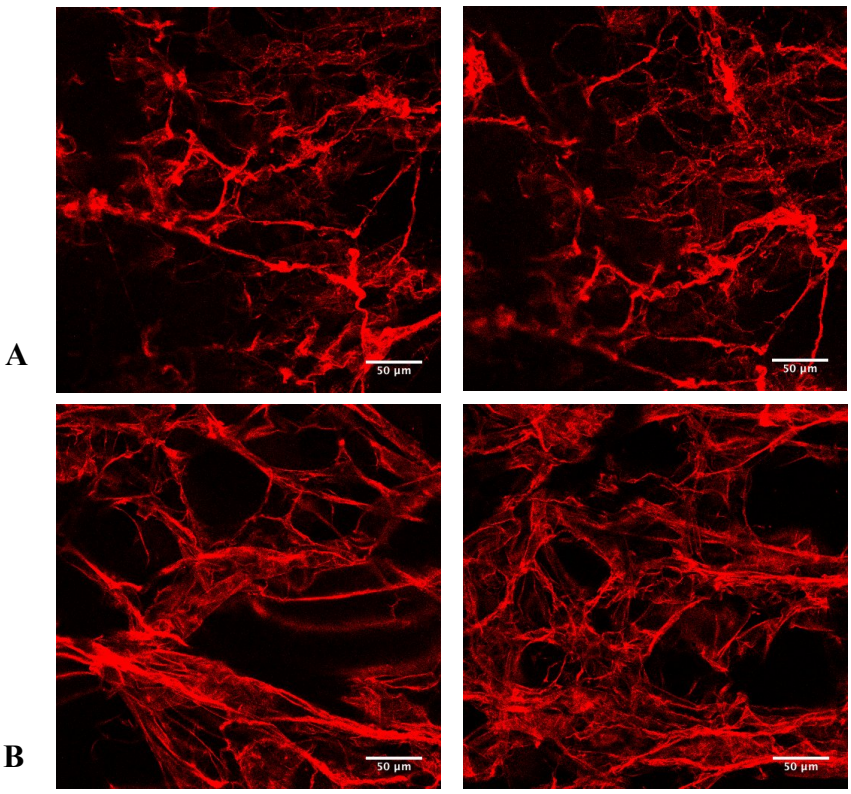

Fig. 4.9 Fluorescent images of manually pulling deposited Fn fibers on the collagen scaffold. Fn was labeled with Alexa 633 (red). (A) multiple-pulling deposited Fn fibers (B) multiple-pulling with blowing deposited Fn fibers. (Scale bars = 50µm)

Therefore, we created an air flow in the interim of each multiple pulling to improve the Fn fibrillogenesis effect within the collagen scaffold. Briefly, an air flow created by nitrogen gun was applied on the collagen scaffold after three times manually pulling, and repeat for five times on each side. Our images show that (Fig. 4.9), by applying an air flow, we were able to obtain higher quantity and thicker Fn fibrils inside the scaffold. Thus, we were able to verify our hypothesis that the Fn fibrils were better initiate on the dry collagen scaffold surface and

bundle up to form thicker and longer fibers. With the air flow, the Fn fibrils reached as deep as 200μm inside the collagen scaffold. By this technique, we developed a collagen-fibronectin dual protein scaffold that provided a promising platform for mimcking the ECM to study cell behavior. Further, Fn is an excellent ECM protein that intricately involved in cell behavior and plays a key role in cell adhesion, migration and differentiation. With binding sites for integrins, other ECM proteins, such as collagen in this case, and growth factors, Fn in this dual-protein matrix could serve as a mediator in many cellular interactions with the ECM.

Characterization of COL-Fn scaffold

To evaluate the conformation of the manually deposited Fn fibrils in the collagen scaffold as described above, we replaced the 15% single-labeled Fn solution with the 10% FRET-labeled Fn solution for the pulling. Briefly, trace amount (10%) FRET-labeled Fn was used for the concentrated droplet for manually pulling. The collagen scaffold was pulled over the droplet for three times after which an air flow was applied while the whole process repeated five times. Subsequently, FRET data was analyzed using a customized MatLab code. From the analyzed images (Fig. 4.10) we found that the conformation of the manually-deposited Fn fibrils varied among different fibrils within the collagen scaffold. Some of the fibrils were more compact, while others were more unfold, which was similar as the fibronectin fibrils deposited in vivo. Interestingly, we also noticed that the longer and thicker fibrils showed more compact conformation (which are green on the analyzed images, indicating low FRET ratio) than the short fibrils. It has been suggested that binding sites in native III_2 and a cryptic site in III_1 which is exposed in unfolded protein are domains for the Fn assembly. [49,50] This knowledge, together with the fact that mechanical stretch elongated the Fn fibrils and enhances binding of 70 kDa, explains our results that the longer and bundle up fibrils within

the 3D scaffolds, which need more Fn-Fn interaction, were more unfolded in their conformations. [51]

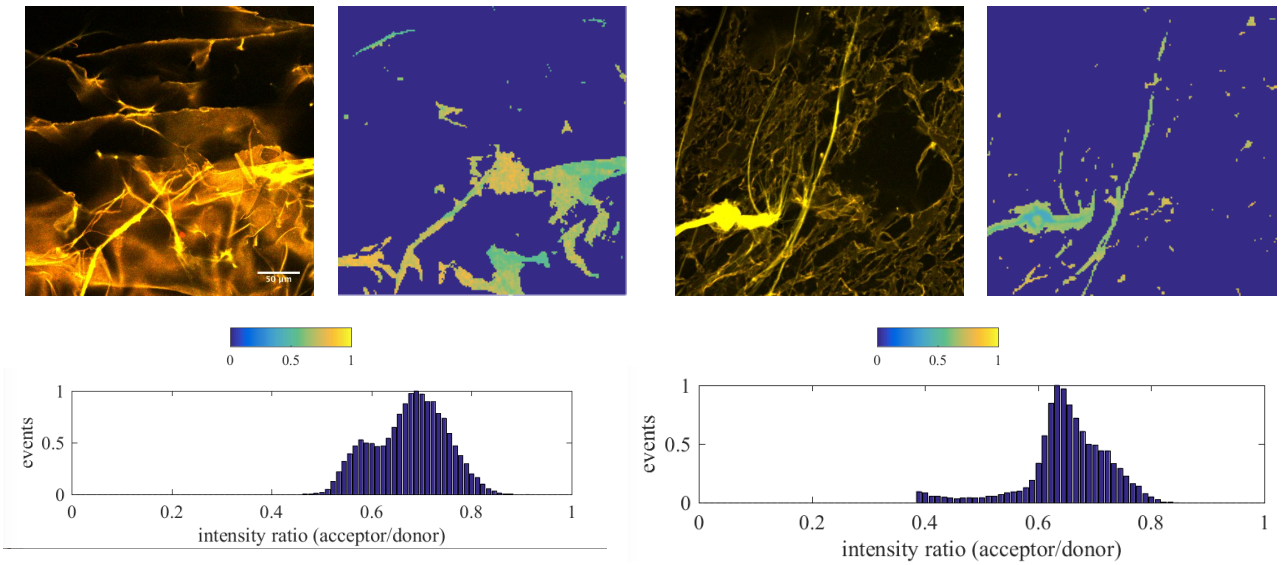

Fig. 4.10 Measured FRET intensity ratio for Fn fibrils deposited within the 3D collagen template by the manually pulling and blowing technique. A range of Fn conformations were gained after the pulling, where the FRET ratio of long Fn fibrils were lower than those on short Fn fibrils, indicating Fn conformations in long fibrils were more compact, while more unfolded Fn conformations in short fibrils.

The morphology of the collagen-fibronectin scaffold was observed by SEM (Fig. 4.11). Briefly, the collagen scaffold was cut in the center after the pulling procedure, and the interior cross-section was exposed to Au sputter before putting into the microscope. In the SEM images, we are able to see Fn molecules decorating on the collagen scaffold surface, Fn fibrils deposited on the collagen scaffold by manually pulling and some Fn aggregation, which might be due to the contraction of the pulling Fn fibrils.

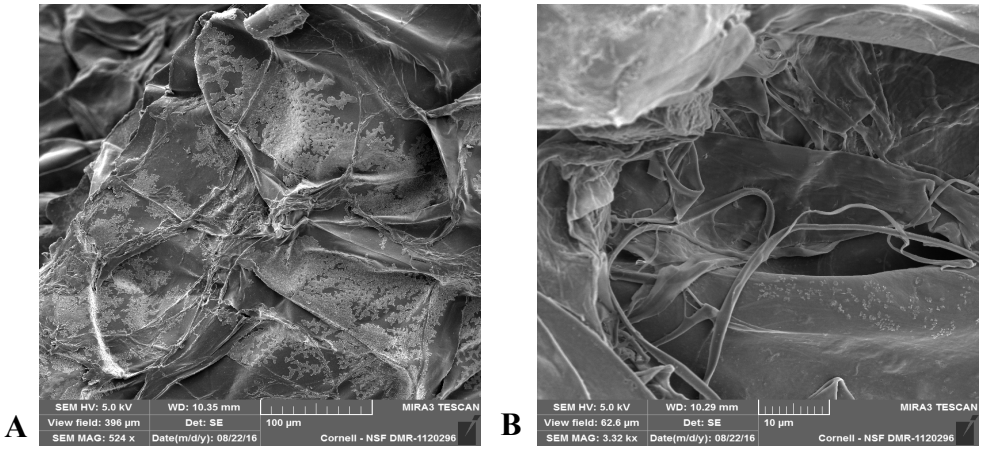

Fig. 4.11 SEM images of collagen-fibronectin scaffold after manually pulling technique. (A) Fn molecules decorating on the surface of the collagen scaffold and polymerizing into fibrils. Scale bar = 100µm (B) Fn fibrils on the collagen scaffold were clearly observed in the zoom-in images and were able to be analyzed using ImageJ. Fn aggregation could also be seen on the upper left of the image. Scale bar = 10µm

Cell invasion and adhesion on the dual-protein scaffold

To assess the cells invasion and adhesion in the collagen scaffold with Fn fibrils deposited by the combined technique of manually pulling and blowing, we seeded 3T3-L1, representing fibroblasts, on top of the dual-protein scaffold and incubated them for 24h before imaging. Briefly, the collagen scaffold was cut into 1mm and pulled on the cross-section over a drop of concentrated Fn solution which was 15% labeled with Alexa633. Then, an air flow was applied on the pulled scaffold after 3 times of manually pulling on the Fn droplet, while the pulling-blowing process repeat 5 times. Afterward, cells were pipetted onto the top of the scaffolds in 1% FBS αMEM. The scaffolds were incubated for an hour to allow cells to adhere, after which fresh media was added to the wells. The scaffolds were then cultured in the incubator for 24 hours. The cell distribution and adhesion within the dual-protein scaffold was then evaluated by a fluorescent assay. Our images (Fig. 4.12) indicate that, the majority of cells adhered on the Fn fibrils instead of the collagen substrates, from which we could

infer that cells were able to make use of the Fn fibrils to stretch, migrate, and proliferate, as well as assembly and remodeling the new ECM. Those exposed β1 binding sites on Fn

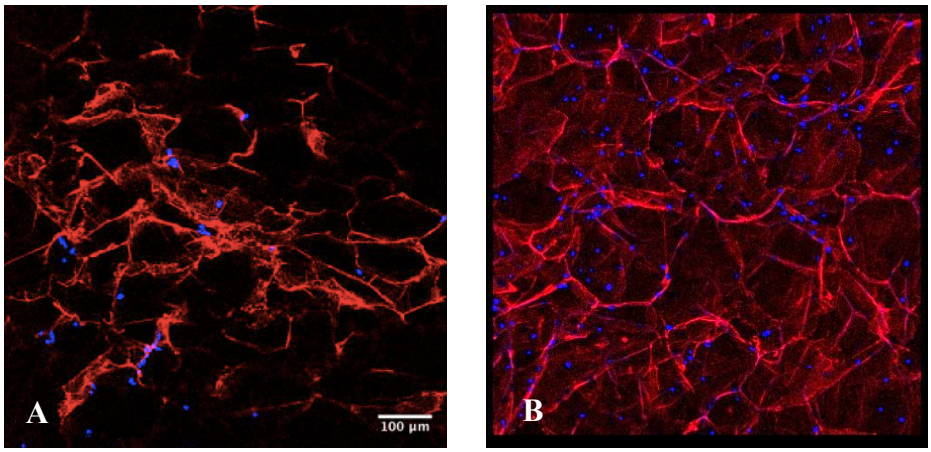

Fig. 4.12 (A) Fluorescent image of 3T3-L1 cells adhered on the Fn fibrils in the collagen scaffold. Scale bar = 100µm (B) Z projection of the z-stack slices. Cells nuclei were staining with DAPI (blue) after 24h of incubation, and Fn fibrils were deposited by pulling and blowing technique using concentrated Fn solution labeled with Alexa633 (red).

provided the mimicking matrix to engage β1 integrin on cells which is critical for wound closure and ECM deposition.

Conclusion

In summary, we used different techniques to assemble fibronectin in different forms based on the collagen scaffolds in this study. In previous chapter we focused on the cellular responses towards the structure of Fn molecules assembled in a 2D *film* decorating the porous structure of collagen, whereas in this chapter we have provided a three-dimensional platform of Fn in a form of fibrils for further cells behaviors study. It is known that Fn, which is capable for various cell-binding (integrin) sites, functions distinctly in molecules and after assembly into fibers. Short Fn fibrils were introduced into the 3D porous collagen system under a shaking treatment. By using a combined technique of manually pulling and blowing, we were able to develop a dual-protein 3D scaffold comprises of porous collagen and fibrous Fn, which contains longer and thicker Fn fibers. The Fn fibers in this dual protein scaffold were present in high quantity and even distribution, whose conformation, quantifying by FRET, varied among fibers and was more unfolded in longer fibers. This 3D template comprising collagen and fibrous fibronectin can better mimic the extracellular matrix, and lays a groundwork for studying the cell-ECM interaction. Even, the Fn fibers could be customized in different forms based on the need of future study.

Hence this ECM structure mimicking three-dimensional template could be used to mechanical support cells culture and further form the basis of tissue engineering. Fn plays a key role in cell behavior, including cells adhesion, migration and differentiation, and coordinates tissue behaviors such as morphogenesis and wound healing. A previous reported diabetic mouse wound model has shown that the Fn matrix mimetics were able to promote wound healing, though the impact of integrin specificity was uncertain.[36]

Reference:

1. Little, W. C., Smith, M. L., Ebneter, U. & Vogel, V. Assay to mechanically tune and optically probe fibrillar fibronectin conformations from fully relaxed to breakage. *Matrix Biol.* **27,** 451–461 (2008).
2. Larsen, M., Artym, V. V, Green, J. A. & Yamada, K. M. The matrix reorganized: extracellular matrix remodeling and integrin signaling. *Curr. Opin. Cell Biol.* **18,** 463–471 (2006).
3. Reilly, G. C. *et al.* Intrinsic extracellular matrix properties regulate stem cell differentiation. *J. Biomech.* **43,** 55–62 (2010).
4. Badylak, S. F. The extracellular matrix as a biologic scaffold material. *Biomaterials* **28,** 3587–3593 (2007).
5. Cukierman, E., Pankov, R. & Yamada, K. M. Cell interactions with three-dimensional matrices. *Current Opinion in Cell Biology* **14,** 633–639 (2002).
6. Yeung, T. *et al.* Effects of substrate stiffness on cell morphology, cytoskeletal structure, and adhesion. *Cell Motil. Cytoskeleton* **60,** 24–34 (2005).
7. Singh, P., Carraher, C. & Schwarzbauer, J. E. Assembly of fibronectin extracellular matrix. *Annu. Rev. Cell Dev. Biol.* **26,** 397–419 (2010).
8. Mao, Y. & Schwarzbauer, J. E. Fibronectin fibrillogenesis, a cell-mediated matrix assembly process. *Matrix Biology* **24,** 389–399 (2005).
9. Ohashi, T., Kiehart, D. P. & Erickson, H. P. Dynamics and elasticity of the fibronectin matrix in living cell culture visualized by fibronectin-green fluorescent protein. *Proc. Natl. Acad. Sci. U. S. A.* **96,** 2153–2158 (1999).
10. Paci, E. & Karplus, M. Force Unfolding of Fibronectin Type 3 Modules: An Analysis by Biased Molecular Dynamics Simulations. *J. Mol. Biol.* **288,** 441–459 (1999).
11. Baneyx, G., Baugh, L. & Vogel, V. Fibronectin extension and unfolding within cell

matrix fibrils controlled by cytoskeletal tension. *Proc. Natl. Acad. Sci. U. S. A.* **99,** 5139–5143 (2002).

12. Salmerón-Sánchez, M. *et al.* Role of material-driven fibronectin fibrillogenesis in cell differentiation. *Biomaterials* **32,** 2099–2105 (2011).
13. Klotzsch, E. *et al.* Fibronectin forms the most extensible biological fibers displaying switchable force-exposed cryptic binding sites. *Proc. Natl. Acad. Sci.* **106,** 18267–18272 (2009).
14. Ahmed, Z., Underwood, S. & Brown, R. A. Nerve Guide Material Made from Fibronectin: Assessment of in Vitro Properties. *Tissue Eng.* **9,** 219–231 (2003).
15. Underwood, S., Afoke, A. & Brown, R. A. Wet extrusion of fibronectin-fibrinogen cables for application in tissue engineering. *Biotechnol. Bioeng.* **73,** 295–305 (2001).
16. Harding, S. I., Underwood, S., Brown, R. A. & Dunnill, P. Assessment of cell alignment by fibronectin multi-fibre cables capable of large scale production. *Bioprocess Eng.* **22,** 159–164 (2000).
17. Underwood, S., Afoke, A., Brown, R. A., MacLeod, A. J. & Dunnill, P. The physical properties of a fibrillar fibronectin-fibrinogen material with potential use in tissue engineering. *Bioprocess Eng.* **20,** 239–248 (1999).
18. Ahmed, Z. & Brown, R. A. Adhesion, alignment, and migration of cultured Schwann cells on ultrathin fibronectin fibres. *Cell Motil. Cytoskeleton* **42,** 331–343 (1999).
19. Ahmed, Z., Idowu, B. D. & Brown, R. A. Stabilization of fibronectin mats with micromolar concentrations of copper. *Biomaterials* **20,** 201–209 (1999).
20. Wòjciak-Stothard, B., Denyer, M., Mishra, M. & Brown, R. a. Adhesion, orientation, and movement of cells cultured on ultrathin fibronectin fibers. *In Vitro Cell. Dev. Biol. Anim.* **33,** 110–7 (1997).
21. Ejim, O. S., Blunn, G. W. & Brown, R. A. Production of artificial-oriented mats and

strands from plasma fibronectin: a morphological study. *Biomaterials* **14,** 743–748 (1993).

22. Garikipati, K. & Arruda, E. M. *IUTAM Symposium on Cellular, Molecular and Tissue Mechanics*. **16,** (2010).

23. Zhong, C. *et al.* Rho-mediated contractility exposes a cryptic site in fibronectin and induces fibronectin matrix assembly. *J. Cell Biol.* **141,** 539–551 (1998).

24. Peters, D., Chen, Y., Zardi, L. & Brummel, S. Conformation of Fibronectin Fibrils Varies: Discrete Globular Domains of Type III Repeats Detected. *Microsc. Microanal.* **4,** 385–396 (1998).

25. Chen, Y., Zardi, L. & Peters, D. M. High-resolution cryo-scanning electron microscopy study of the macromolecular structure of fibronectin fibrils. *Scanning* **19,** 349–355 (1997).

26. Mosher, D. F. 4,705,751. (1987).

27. Vartio, T. Disulfide-bonded polymerization of plasma fibronectin in the presence of metal ions. *J. Biol. Chem.* **261,** 9433–9437 (1986).

28. Lu, H., Isralewitz, B., Krammer, a, Vogel, V. & Schulten, K. Unfolding of titin immunoglobulin domains by steered molecular dynamics simulation. *Biophys. J.* **75,** 662–71 (1998).

29. Rief, M., Gautel, M., Oesterhelt, F., Fernandez, J. M. & Gaub, H. E. Reversible Unfolgind of Individual Titin Immunoglobulin Domains by AFM. *Science (80-.).* **276,** 1109–1112 (1997).

30. Guan, J.-L. & Hynes, R. O. Lymphoid cells recognize an alternatively spliced segment of fibronectin via the integrin receptor α4β1. *Cell* **60,** 53–61 (1990).

31. Midwood, K. S., Mao, Y., Hsia, H. C., Valenick, L. V & Schwarzbauer, J. E. Modulation of cell-fibronectin matrix interactions during tissue repair. *J. Investig.*

Dermatology Symp. Proc. **11,** 73–78 (2006).

32. Sechler, J. L. & Schwarzbauer, J. E. Control of cell cycle progression by fibronectin matrix architecture. *J Biol Chem* **273,** 25533–25536 (1998).

33. Sakai, T. *et al.* Plasma fibronectin supports neuronal survival and reduces brain injury following transient focal cerebral ischemia but is not essential for skin-wound healing and hemostasis. *Nat. Med.* **7,** 324–330 (2001).

34. Brito, T. N. de S., Rocha, L. R. M. da, Jatobá, C. A. N., Sales, M. P. & Medeiros, A. da C. Effect of topical application of fibronectin in duodenal wound healing in rats. *Acta Cir. Bras.* **18,** 97–101 (2003).

35. Zhu, Q. L., Denefle, J. P. & Lechaire, J. P. Fibronectin (FN) localizations in early wound healing of cultured frog skins. *Biol. cell* **57,** 161–7 (1986).

36. Bachman, H., Nicosia, J., Dysart, M. & Barker, T. H. Utilizing Fibronectin Integrin-Binding Specificity to Control Cellular Responses. *Adv. wound care* **4,** 501–511 (2015).

37. Wierzbicka-Patynowski, I. & Schwarzbauer, J. E. The ins and outs of fibronectin matrix assembly. *J Cell Sci.* **116,** 3269–76. (2003).

38. Romberger, D. J. Fibronectin. *Int. J. Biochem. Cell Biol.* **29,** 939–943 (1997).

39. Antia, M., Islas, L. D., Boness, D. A., Baneyx, G. & Vogel, V. Single molecule fluorescence studies of surface-adsorbed fibronectin. *Biomaterials* **27,** 679–690 (2006).

40. Smith, M. L. *et al.* Force-induced unfolding of fibronectin in the extracellular matrix of living cells. *PLoS Biol.* **5,** 2243–2254 (2007).

41. Chen, L. B., Murray, A., Segal, R. A., Bushnell, A. & Walsh, M. L. Studies on intercellular LETS glycoprotein matrices. *Cell* **14,** 377–391 (1978).

42. Dzamba, B. J. & Peters, D. M. Arrangement of cellular fibronectin in noncollagenous fibrils in human fibroblast cultures. *J. Cell Sci.* **100,** (1991).

43. Singer, I. I. The fibronexus: a transmembrane association of fibronectin-containing fibers and bundles of 5 nm microfilaments in hamster and human fibroblasts. *Cell* **16,** 675–685 (1979).

44. Briknarová, K., Åkerman, M. E., Hoyt, D. W., Ruoslahti, E. & Ely, K. R. Anastellin, an FN3 Fragment with Fibronectin Polymerization Activity, Resembles Amyloid Fibril Precursors. *J. Mol. Biol.* **332,** 205–215 (2003).

45. Litvinovich, S. V *et al.* Formation of amyloid-like fibrils by self-association of a partially unfolded fibronectin type III module. *J. Mol. Biol.* **280,** 245–258 (1998).

46. Langenbach, K. J. & Sottile, J. Identification of protein-disulfide isomerase activity in fibronectin. *J. Biol. Chem.* **274,** 7032–8 (1999).

47. Chen, H., Strickland, D. K. & Mosher, D. F. Metabolism of thrombospondin 2. Binding and degradation by 3t3 cells and glycosaminoglycan-variant Chinese hamster ovary cells. *J. Biol. Chem.* **271,** 15993–9 (1996).

48. Morla, A., Zhang, Z. & Ruoslahti, E. Superfibronectin is a functionally distinct form of fibronectin. *Nature* **367,** 193–196 (1994).

49. Aguirre, K. M., McCormick, R. J. & Schwarzbauer, J. E. Fibronectin self-association is mediated by complementary sites within the amino-terminal one-third of the molecule. *J. Biol. Chem.* **269,** 27863–8 (1994).

50. Hocking, D. C., Sottile, J. & McKeown-Longo, P. J. Fibronectin's III-1 module contains a conformation-dependent binding site for the amino-terminal region of fibronectin. *J. Biol. Chem.* **269,** 19183–7 (1994).

51. Zhong, C. *et al.* Rho-mediated contractility exposes a cryptic site in fibronectin and induces fibronectin matrix assembly. *J. Cell Biol.* **141,** 539–51 (1998).

Chapter 5

3D Fibrillar Warm/Cold Casted Collagen Scaffold with Tunable Microarchitecture and Mechanical Properties

Contributor: Junhui Ye, Yifan Li and Delphine Gourdon

Abstract

In this study, three-dimensional (3D) fibrillar collagen scaffolds with tunable microarchitecture were fabricated using the warm/cold casting technique. The assembly of collagen fibers is a temperature and pH mediated process. By controlling the casting temperature, which in turn monitored the nucleation of collagen, the fibrillar collagen network could be generated in different topography/morphology with various mechanical properties. The properties of the extracellular matrix (ECM) play a key role on regulating cell behaviors while the effect of ECM architecture on cell-ECM interactions remains unclear. Specifically, collagen is one of the most abundant ECM proteins, and provides structural support to the resident cells. Here, these fibrillar collagen scaffold, whose fibers thickness could be increased by slow gelation in cold casting, offers a platform to investigate the impact of collagen fiber morphology/structure as well as mechanical properties on the cell functions. Further, cells were directly embedded in the scaffolds during the formation of the warm/cold casting collagen samples, which enabled better cell distribution and large volume cell cultures.

Introduction

Extracellular matrix (ECM) properties have been known as essential on regulating cellular behaviors such as proliferation, migration, and differentiation by modulation through cytoskeletal structure and contractility. [1–3]ECM-derived biological modulation on cells is affected by the composition, fibrils density, protein conformation, and structure of the matrix components. [4] Type I collagen (COL I), a major fibrillar ECM component, which plays an important role in regulating the ECM property together with fibronectin (Fn), have been the focus of research in recent decades. Fibrillogenesis of collagen is a spontaneous self-driven-assembly process, as studied by previous researchers. Based on such phenomenon, type I collagen has been fabricated into highly ordered matrices, and used to study the structure characteristics and mechanical properties of these entropy-driven assemble collagen fibrils.[2,3,5] The microstructure, including collagen density, cross-linking, and alignment of the type I collagen have been proved to be correlated with disease.[5–8] However, little is known in terms of how the microstructure of collagen fibers regulates the cellular behaviors due to the difficulty in decoupling individual effect from other physical properties of collagen matrix.[4] Engineered collagen scaffolds in different interior architectures or fibrillar structures with varying mechanical properties have been utilized for extensive *in vitro* biological studies. [9] The conditions of collagen polymerization such as pH, temperature, and ionic strength modulate the microarchitecture (pore size, density) of the matrix and microstructure of the fibers (diameter, length, and alignment), which collectively determine the biochemical and mechanical properties of the collagen matrix.[10] These matrix properties potentially regulate cells proliferation and migration.[11,12] The effects of cell traction *in vitro* could also cause the reorientation of the collagen matrix into a more complex process.[13] Furthermore, the Birk and Trelstad model of oriented collagen fibril bundles implies that cells lay down fibrils as they move in a particular direction. [14–16] As a result, the interaction between cell movement and

matrix orientation enables our study on understanding the role of cells in regulating the external collagen architecture using fibrillar collagen substrates with different microstructure.

In this study, we decided to use the temperature-mediated method to control the growth of the collagen fibers and fabricate the 3D fibrillar collagen scaffold with different micro-architectures. By precisely tuning the microstructure of the collagen fibers, we are able to investigate the cellular interaction with their extracellular environment, and understand how collagen fibers regulate the cell behaviors. Further, fibroblasts were added and co-culture within the 3D collagen system, which potentially aid and monitor the assembly of the collagen matrix. Also, this cell-embedded fibrillar collagen platform, which enables direct cell culture, provides an excellent platform for future cell study.

Materials and Methods

Cell culture

Cell adhesion was assessed with 3T3-L1 cells (ATCC #CL-173), an adipogenic subtype of mouse fibroblasts. These cells were incubated in αMEM (Sigma-Aldrich) containing 1 vol% fetal bovine serum (FBS, Tissue Culture Biologicals) and 1 vol% penicillin/streptomycin (pen/strep) (Life Technologies). The cells were then seeded in 10 μL suspensions (containing 30 thousand cells) into scaffolds and were allowed to adhere for 1 hour. Then, fresh media containing 1 vol% fetal bovine serum (FBS, Tissue Culture Biologicals) was added to the wells with the scaffolds, and they were cultured in the incubator at 37 °C (5% CO2) for 24 hours. Afterward, cell-seeded scaffolds were soaked in 3.7% ice-cold paraformaldehyde for chemical fixation and stained with 4′,6-diamidino-2-phenylindole (DAPI), calcein AM, and propidium iodide (PI) (all from Life Technologies), in order to evaluate cell infiltration into the scaffolds through fluorescence microscopy.

Fabrication of three-dimensional collagen scaffolds with varied microstructure

The suspension of an insoluble type I microfibrillar collagen derived from bovine Achilles tendon (Advanced BioMatrix), and the soluble type I collagen derived from rat tail tendon (Advanced BioMatrix) was used to fabricate the three-dimensional collagen scaffold, respectively. First, we used 3D printing (ObJet30 Pro 3D Printer with VeroClear) to micro-fabricate a mold for polydimethylsiloxane (PDMS) casting, with a dimension of 4-mm-diameter and 239-μm-thick in round shape. Then, the polydimethylsiloxane (PDMS) wells were fabricated with Sylgard® 184 silicone elastomer kit (Dow Corning). Afterward, the surface of the PDMS wells was treated by 1% [v/v] poly-ethylenimine (Aldrich) for 10 minutes and then 0.1% [v/v] glutaraldehyde (Fischer Scientific) for 30 minutes to improve the adhesion of collagen to the PDMS wells. The wells were then plasma treated for 5

minutes to sterilize. After the surface treatment, the PDMS wells were placed either under -20°C in the freezer or under 37°C in the incubator, and this difference in temperature could cause different velocities of collagen polymerization (fibrillogenesis), which modulates the thickness and density of the collagen fibrils as a result.

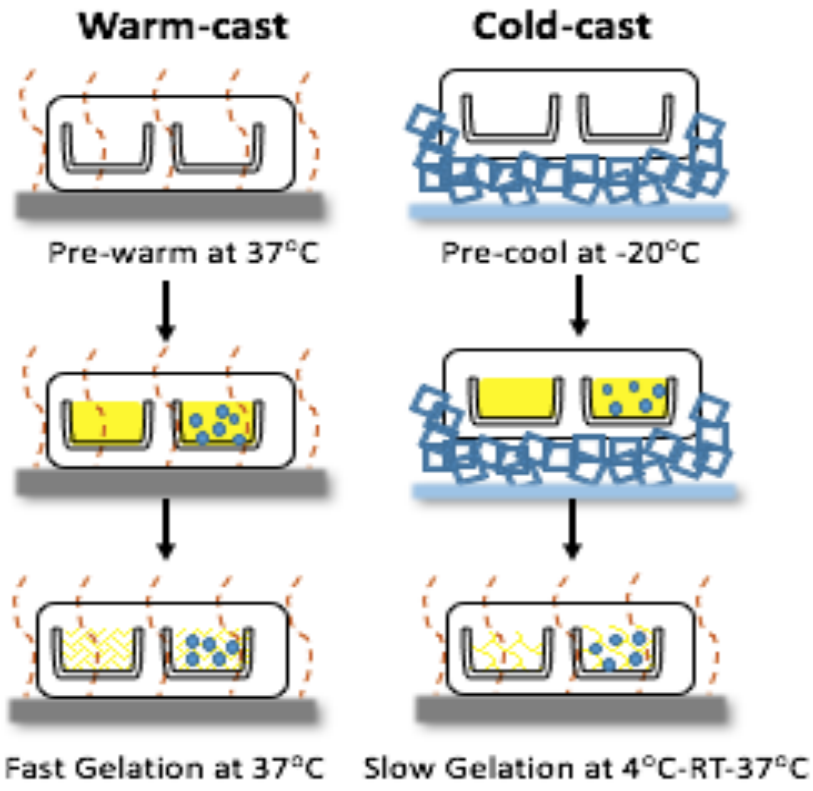

Fig. 5.1 The warm/cold casting technique for fibrillar collagen fabrication with/without cell content. The collagen in the warm-cast technique was quickly polymerized in high temperature, whereas the cold-cast collagen was slowly nuclei under a temperature gradient from 4°C to 37°C.

The bovine collagen suspension (Advanced BioMatrix), placing in ice, was neutralized to pH 7.2 by dropwise adding 1N and 0.1N NaOH, and diluted into 0.5% collagen suspension with αMEM (Sigma-Aldrich) containing 10 vol% fetal bovine serums (FBS, Tissue Culture Biologicals) and 1 vol% penicillin/streptomycin (Life Technologies). The rat tail collagen

solution (Advanced BioMatrix) was mixed with neutralizing solution (Advanced BioMatrix) in proportion of 9 to 1, and ultimately created a neutralized collagen suspension in a concentration of 3mg/ml. Subsequently, the suspended collagen was either injected on the pre-cooled PDMS wells and slowly polymerized under a gradual series of temperatures ranging from 4°C, room temperature to 37°C, which finally create thicker collagen fibrils, or was rapidly solidified in the pre-warmed PDMS wells under 37°C, which results in thinner collagen fibrils.

Cell-embedded collagen scaffold

The cell-embedded collagen scaffold was fabricated with a mixture of 3T3-L1 cells (ATCC #CL-173), mouse fibroblasts, and the soluble type I collagen derived from rat tail tendon (Advanced BioMatrix). The 3T3-L1 cells were incubated in αMEM (Sigma-Aldrich) containing 1 vol% fetal bovine serum (FBS, Tissue Culture Biologicals) and 1 vol% penicillin/streptomycin (Life Technologies) before blending. The rat tail collagen solution (Advanced BioMatrix) was mixed with neutralizing solution (Advanced BioMatrix) in a proportion of 9 to 1 and then 10μl 3T3-L1s cells solution containing 5 million cells/ml was added to produce a final cell-embedded collagen suspension with 50 thousand cells. Further, half of the 3T3-L1s suspended collagen was fabricated into thicker fibrils in the pre-cooled PDMS while the other was constructed into thinner fibrils in the pre-warmed PDMS wells. Later, the 96-well plate (ThermoFisher) was used to replace the PDMS wells in a revised protocol in order to get better cell culture environment and thermal effect.

Then, the completely polymerized cell-embedded collagen scaffolds were culture for 24 hours in the incubator at 37 °C (5% CO2) after adding fresh media containing 1 vol% fetal bovine serum (FBS, Tissue Culture Biologicals). Afterward, the collagen scaffolds containing

3T3-L1 cells were soaked in 3.7% ice-cold paraformaldehyde for chemical fixation. To evaluate cell infiltration and adhesion into the scaffolds, the cell-embedded collagen scaffolds were stained with 4′,6-diamidino-2-phenylindole (DAPI) (Life Technology), and observed through fluorescence microscopy.

Second harmonic generation (SHG) imaging

Second harmonic generation is an optical phenomenon where two photons of a certain wave length with a lower energy level from laser light illuminated to material like collagen are converted to a single photon of half the wavelength with a higher energy. This is related to the structure of the material, so non-centric-symmetric material like collagen can be imaged via SHG.[17]

Multiphoton SHG imaging was used to characterize three-dimension collagen scaffold structure. Imaging was performed with Zeiss 810 confocal multiphoton microscope using 940 nm illumination and an Olympus 40x/0.95W XLUMPlanFl objective. Z-stacks images were acquired in an 2μm interval for 50-100μm depth, as identified in transmitted light mode; 5 to 6 spots per sample were imaged. SHG channel images were extracted and analyzed through ImageJ and 3D reconstruction of the z-stacks was performed on Zen.

Confocal reflectance microscopy (CRM)

To visualize the microarchitecture of collagen scaffolds, confocal reflectance imaging of collagen fibrils was performed using Zeiss 710 confocal microscope on a Zeiss Axis Observer Z1 inverted stand with 40x water immersion objective. For cell-embedded collagen scaffolds, samples cultured for 24h were briefly washed with ice-cold PBS and then fixed with 3.7% paraformaldehyde (PFA). The samples were illuminated by a low intensity of

488nm laser split through an 80/20 dichroic beam splitter, and the backscatter light reflected from collagen fibrils were collected by a photomultiplier tube. Z-stack images were captured from 5-6 random spots per each sample with 2μm intervals. To assess fibril density and diameter, the z-stacks were analyzed using ImageJ; 30 to 50 fibrils per Z-stack were analyzed. The 3D reconstruction of the z-stacks was performed on Zen.

Scanning electron microscopy (SEM) imaging

The structure of collagen scaffolds was characterized by scanning electron microscopy (Mira3 FESEM, Tescan. For cell-embedded collagen scaffolds were cultured for 24 h, samples were briefly fixed by 2.5% glutaraldehyde in 0.05 M cacodylate buffer. The fixed scaffolds were sequentially dehydrated by a series of ethanol solution (25%, 50%, 75%, 95%, and 100%) and dried by a treatment with hexamethyldisilazane (Electron Microscopy Sciences) before imaging. The collagen scaffolds were adhered on the conductive carbon adhesive tab (Electron Microscopy Sciences), and then coated with gold/palladium alloy in sputter coater (Denton Vacuum, Desk II) for SEM imaging. Images were captured by scanning electron microscopy (Tescan, Mira3 LM) at 15kV.

Dynamic Mechanical Analysis

The compressive moduli of collagen scaffolds were measured by dynamic mechanical analysis (DMA Q800; TA Instruments). Collagen scaffolds were freshly prepared in PDMS micro-wells and kept submerged in PBS. For the test, gels were carefully taken out from the micro-well. Collagen scaffolds were placed under compressive loads before and after being soaked in room temperature cell culture medium (αMEM, Sigma-Aldrich) overnight. Measurements were comprised of a single loading cycle, with an initial contact force of 0.05N and a ramp rate of 0.005 N/min to 0.075N. The force F (force sensitivity of 0.001 N)

and thickness L (distance resolution of 0.05 μm) were measured simultaneously and converted into engineering stress-strain plots as follows: strain, ε=(Lo-L)/Lo (where Lo is the initial thickness and L the thickness of compressed sample) and stress, σ=F/Ao (where F is the applied force, and Ao the initial surface area). Elastic modulus was calculated as the slope of the stress-strain curve $\sigma = E \varepsilon$ over the 1-2% strain regime, and the mean was obtained from four different samples. (n = 4)

Fibronectin and FRET labeling

Fibronectin (Fn) was obtained from Life Technologies, NY. AlexaFluor 488 succinimidyl ester were used to obtain single-label Fn. AlexaFluor 488 succinimidyl ester and AlexaFluor 546 maleimide (Invitrogen, CA) were used to label Fn for intramolecular FRET as previously described by Smith et al.37 Labeling ratios and Fn concentrations were determined using a DU®730 UV/Vis spectrophotometer (Beckman, IN) at 280 nm, 495 nm, and 556 nm. Soluble calibration of FRET-labeled Fn was carried out in guanidine hydrochloride (GdnHCl) solution at concentrations of 0 M, 2 M, and 4 M to obtain FRET ratios, defined as acceptor/donor intensity ratios (IA/ID), as a function of protein denaturation.

FRET data acquisition and analysis

FRET-Fn adsorbed scaffolds were imaged with a Zeiss 710 confocal microscope (Zeiss, Munich, Germany). 16-bit z-stack images were acquired using the C-Apochromat water-immersion 40×/1.2 objective, a pinhole of 1 AU, 488 nm laser with 30% laser power, pixel dwell time of 6.3 μs, PMT1 and PMT2 gains of 500 V, and z step size of 0.5 μm. FRET-labeled Fn was excited with a 488 nm laser line; emissions from donor and acceptor fluorophores were simultaneously collected in the PMT1 channel (514–526 nm) and the PMT2 channel (566–578 nm), respectively. These z-stack images were analyzed with

customized Matlab code to generate FRET ratio (IA/ID) images as well as mean FRET ratios for all z-slices in a z-stack. 6 Z-stacks per sample, and three samples per condition were analyzed to determine the mean and standard deviation of the FRET intensities, and the histogram plots were generated to indicate FRET intensity at each representative location (n = 3).

Results and Discussions

The fabrication of collagen scaffolds with two different micro-architectures

To obtain fibrillar collagen scaffolds with two different microstructures, we used two different models for fabrication. First, both solubilized bovine collagen and rat tail collagen in acetic acid were neutralized to pH 7.2-7.4. Then, collagen was polymerized within the PDMS microwell (4mm diameter and 250μm in depth). The collagen fibrils were able to bind to the walls of the microwell during the fabrication so that avoided interior contraction. To get two different collagen fibrillar micro-structures, we controlled the temperature during collagen scaffold fabrication, which could regulate lateral growth of collagen micro-fibrils and consequently fibrillar thickness.[18,19] Half of the neutralized collagen solution was rapidly polymerized in the pre-warmed microwells at 37 °C for one hour, while rest of the collagen solution was slowly polymerized in pre-cooled microwells at initial temperature of 4°C for 15 minutes, and gradually increasing the temperature to 26°C for 15 minutes, and finally up to 37°C for an hour. Here we defined the collagen fibrillogenesis at 37 °C as the 'warm-cast' scaffold, and those casted in a gradually increasing temperature starting at 4°C as the 'cold-cast' scaffold. The three-dimension architectures of these two different collagen scaffolds were visualized by second harmonic generation (SHG) and confocal reflectance microscope (CRM) to determine whether altered the casting temperature changed the microstructure of the collagen scaffolds.

As we noticed in the experiment, the bovine collagen had a slower gelation and smaller scaffold thickness compared to the rat tail collagen, which indicates that the cells were more likely to sink down in the bovine collagen scaffold during the gelation. That means the bovine collagen is less suitable for future cellular behaviors studies. Therefore, in the following experiments, we concentrated in the rat tail collagen scaffold. One thing that need

to be emphasized is, even from the characteristic results of the bovine collagen scaffold (Fig.

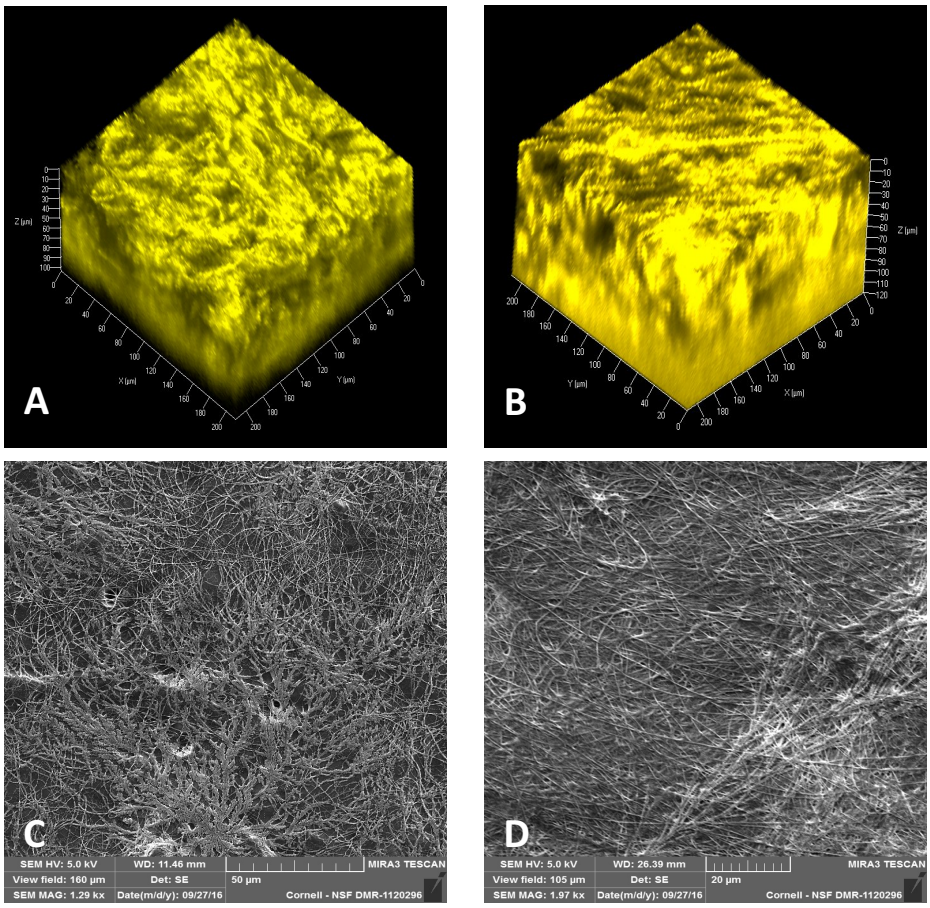

Fig. 5.2 Fabrication of bovine collagen scaffolds with two different micro-architectures. After the polymerization, the 3D microarchitecture of the warm-cast (A) and cold-cast (B) collagen fibrils were visualized by confocal reflectance microscope (CRM) and the structural characteristics of the warm-cast (C) and cold-cast. Scale bar = 50µm (D) collagen fibrils were visualized by scanning electron microscope (SEM). Scale bar = 20µm

5.2), we could still see that the cold-cast model (average fiber diameter = ~101nm) produced thicker fibrils than the warm-cast model (average fiber diameter = ~78nm) with tortuous collagen fibrils.

The 3D microstructure of the rat-tail collagen scaffolds (Fig. 5.3) were visualized by confocal reflectance mocroscope (CRM) and second harmonic generation (SHG). In agreement with

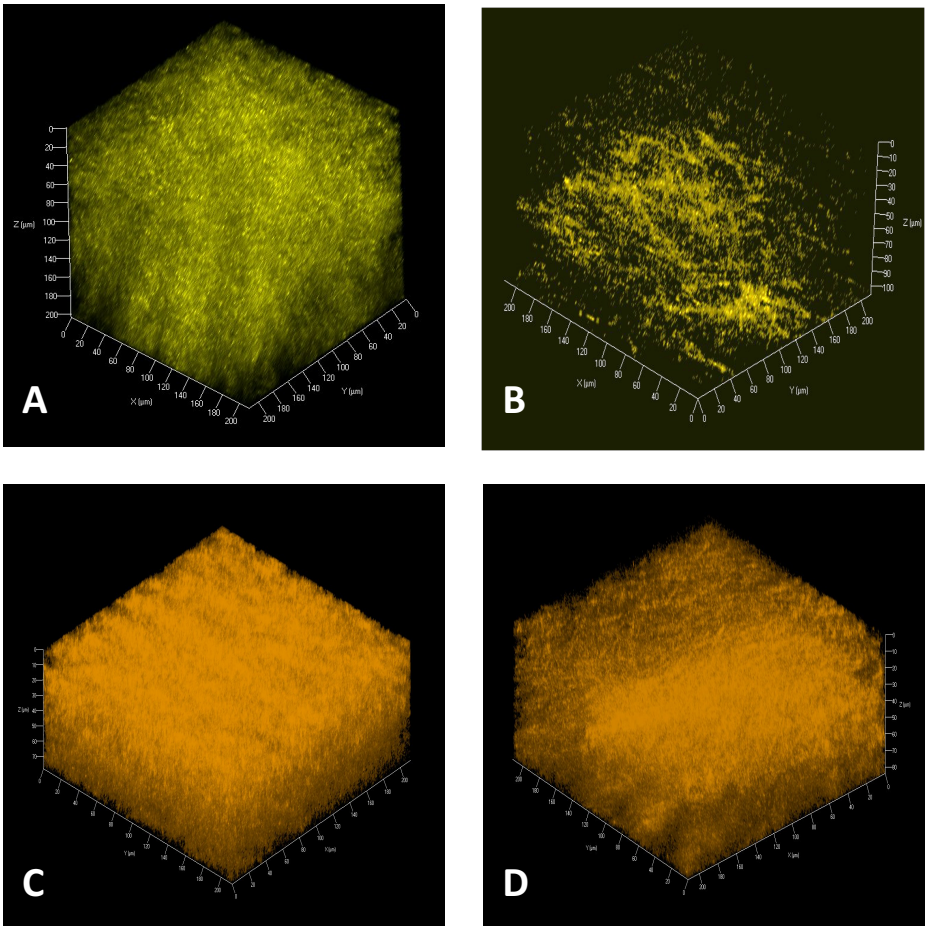

Fig. 5.3 Fabrication of rat tail collagen scaffolds with two different micro-architectures. After the polymerization, the three dimensional structure of the warm-cast (A) and cold-cast (B) collagen scaffold were characterized by confocal reflectance microscope. 3D reconstruction was based on z-stacks on Zeiss 710. And second harmonic generation(SHG) was also used to visualize the collagen structure of the warm-cast(C) and cold-cast (D) scaffolds. 3D reconstruction was based on z-stacks on Zeiss880.

the results of bovine collagen scaffolds discussed above, we could see that the warm-cast rat-tail collagen scaffold had denser collagen fibrils while the cold-cast scaffold showed more void space.

Characteristics of initial rat tail collagen scaffold microarchitectures

To assess structural property of the rat tail collagen scaffolds, we imaged the collagen scaffold by CRM (Fig. 5.4) and utilized the CRM images for fibers quantification,

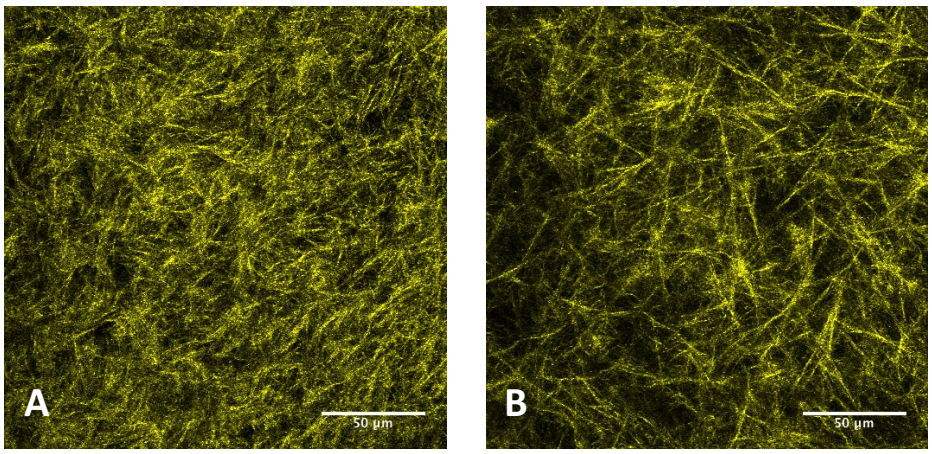

Fig. 5.4 Characteristics of initial rat tail collagen scaffold microarchitectures. The initial interior architecture of warm-cast (A) and cold-cast (B) scaffolds visualized by confocal reflectance microscope (CRM). Scale bars = 50 μm.

measurement of fibril thickness and pore size. We tried to utilize SEM for precise measurement due to their highest resolution at a nanometer scale as well as capacity to visualize collagen fibers at different angles, however, the scaffold tended to collapse under vacuum, which would result in unreliable measurements, and an promising substitute technique will be the AirSEM if available in the future.[9,20] For each sample 6 different spots were analyzed, and all these quantifications were performed on ImageJ. In accordance with CRM observations, collagen fibrils thickness changed as a function of cross-linking temperature.[19] The average fibrils density in the warm-cast scaffolds (16390/mm^2) was relatively higher than the one in the cold-cast scaffolds (8059/mm^2). The mean diameters of collagen fibrils in a cold-cast scaffold (236.9 ± 74.1 nm) were significantly higher than that

of a warm-cast scaffold (95.8 ± 17.1 nm). And we noticed that the collagen fiber thickness showed a wider range in the cold-cast scaffold, which might due to more collagen fibrils bundling up during the slow gelation in the cold casting. Also, the average pore size of cold-

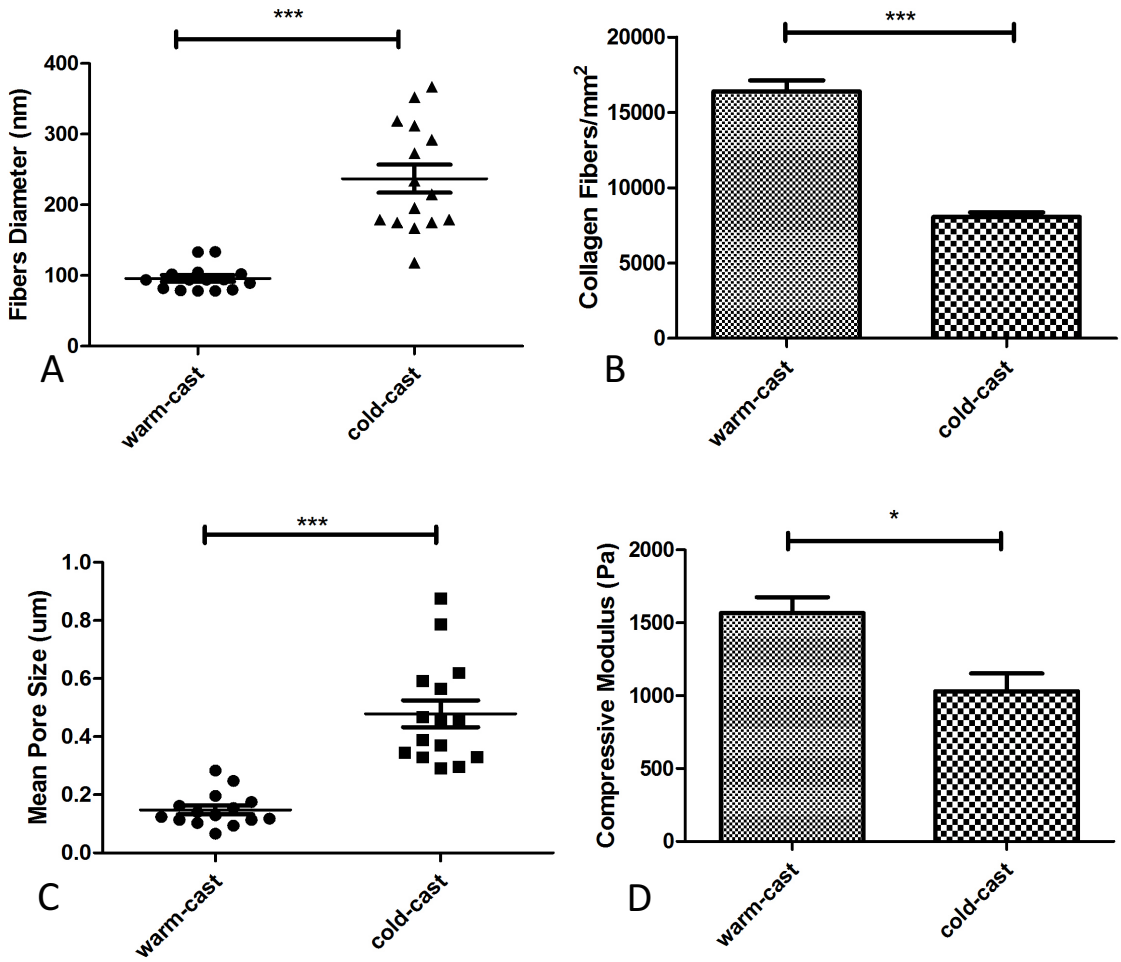

Fig. 5.5 CRM images and confocal stacks were used for calculating the collagen fiber thickness, density and average pore size of the collagen scaffold and analyzed by ImageJ. (A) Average fibers diameters of the warm-cast and cold-cast scaffolds. (B) Fibers densities of the warm-cast and cold-cast scaffolds. (C) Average pore sizes of the warm-cast and cold-cast scaffolds. (D) Dynamic mechanical analysis (DMA) indicated that the elastic module of the warm-cast scaffolds was higher than the cold-cast scaffold.

cast scaffolds was larger (489.3 ± 90.4 nm) than the warm-cast scaffolds (166.7± 9.0 nm). In brief, the cold-cast 3D collagen scaffolds were characterized to have thicker collagen fibers,

and lower fiber density with larger void spaces, compared to the warm-cast scaffolds, which exhibited denser and thinner fibrils with smaller pore sizes. The compressive modulus of the warm/cold casting scaffolds was measured in aqueous environment, and our result indicates that the warm-cast collagen scaffold showed a higher stiffness (1547 Pa) than the cold-cast scaffold (1094 Pa). This might be attributed to the higher collagen fiber density found in the warm-cast scaffold compared to its cold-cast counterpart, which provided higher rigidity.

The fabrication of cell-embedded collagen scaffolds

We utilized 3T3-L1 mouse fibroblasts mixing with the neutralized collagen solution to fabricate the cell-embedded collagen scaffolds. Briefly, rat tail collagen in acetic acid was neutralized to pH 7.2-7.4 then mixed with 3T3-L1s which formerly incubated in 10%FBS culture media. Afterward, the cell-collagen mixture was polymerized within the PDMS microwell (4mm diameter and 250μm in depth). Similar as described above, we controlled the temperature during collagen scaffold fabrication, in which half of the cell-collagen solution was rapidly polymerized in the pre-warmed microwells at 37 °C for one hour, while rest of them were slowly polymerized in pre-cooled microwells at initial temperature of 4°C for 15 minutes, and gradually increasing the temperature to 26°C for 15 minutes, and finally up to 37°C for 30 minutes. Subsequently, fresh media containing 1% FBS was added into the microwells, and incubated for 24h before imaging. A fluorescent assay was used to assess the distribution of the cells within the collagen scaffolds, and the three-dimensional architectures of these different collagen scaffolds were visualized by confocal reflectance microscope (CRM) to determine how casting temperature and cells coordinately affect the micro-structure of the collagen scaffolds.

Our results suggest that cells were able to adhere and distribute evenly in both warm-cast and

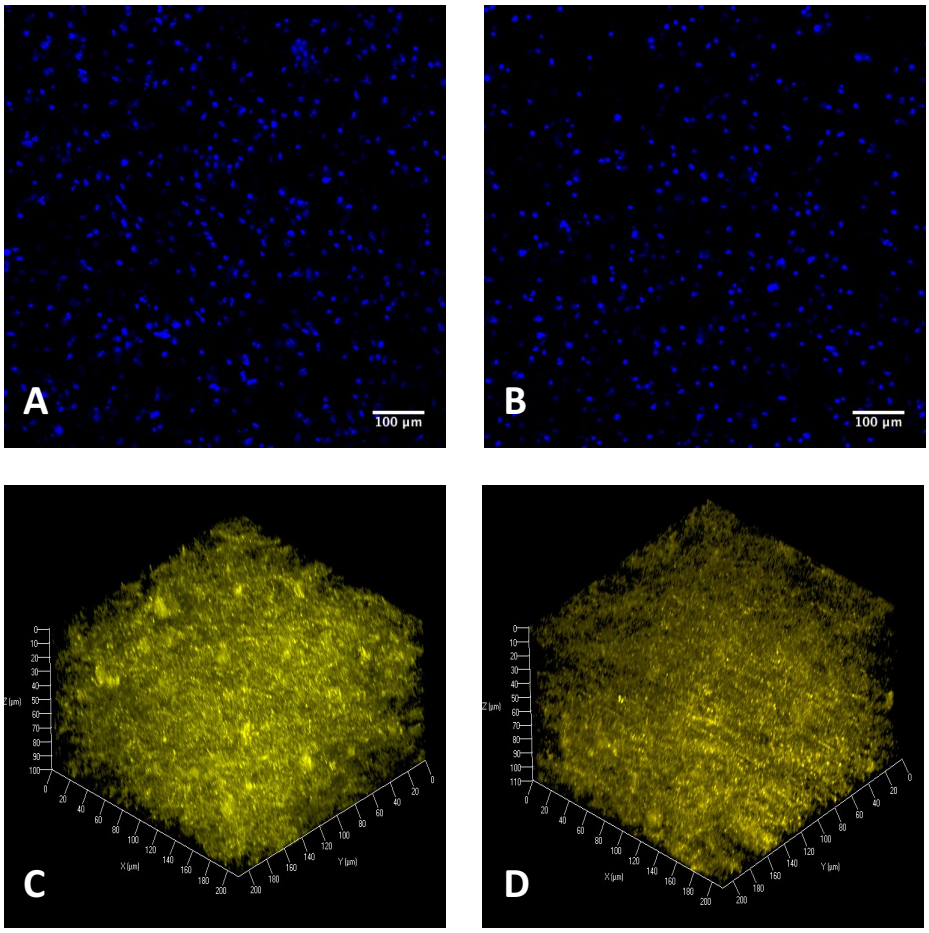

Fig. 5.6 Fluorescent images of cell-embedded warm-cast(A) and cold-cast (B) collagen scaffold. Cell nuclei was staining with DAPI (blue) after culture for 24h. Scale bars = 100µm. After the polymerization, the three dimensional structure of the warm-cast (C) and cold-cast (D) collagen scaffold were characterized by confocal reflectance microscope. 3D reconstruction was based on z-stacks on Zeiss 710.

cold-cast collagen scaffolds, as shown in the fluorescent images. (Fig. 5.6) Although the fibrils in the cell-embedded warm-cast collagen scaffold still appeared to be denser than the ones observed in the cold-cast cell-embedded collagen gel, the differences between these two models seemed to be mitigated by the effect of the presence of cells, as observed in the 3D reconstruction CRM images.

Characteristics of remodeled rat tail collagen scaffold microarchitectures

To evaluate the structure of those cell-embedded collagen templates fabricating by two different methods as described above. We used confocal reflectance microscope (CRM) (Fig. 5.6) to visualize the microstructures and quantify the results. Similar as above, CRM images were used to calculate the fiber density while SEM images were used to measure the fiber thickness and pore sizes of the architectures. For each sample 6 different spots were analyzed, and all these quantifications were performed on ImageJ. Interestingly, on the CRM images,

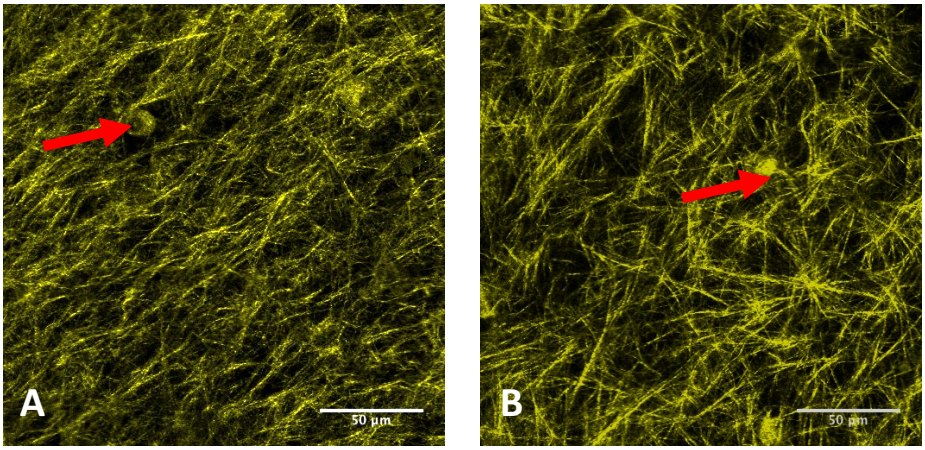

Fig. 5.7 Characteristics of cell-embedded rat tail collagen scaffold microarchitectures. The cell-mediated interior architecture of warm-cast (A) and cold-cast (B) scaffolds visualized by confocal reflectance microscope (CRM). Scale bars = 50 µm.

we could even see the cells that embedded in the collagen scaffold (indicated as red arrow in Fig. 5.7). The mean diameters of the collagen fibers in the cell-embedded scaffold still showed significant differences, in a similar trend as the collagen scaffolds without cell content. The collagen fibers in the cold-cast scaffold (188.6 ± 61.0 nm) remained greater than in the warm-cast scaffold (123.3 ± 24.3 nm) though the difference between two scaffolds was narrowed by the presence of embedded fibroblasts. The cell content helped the assembly of

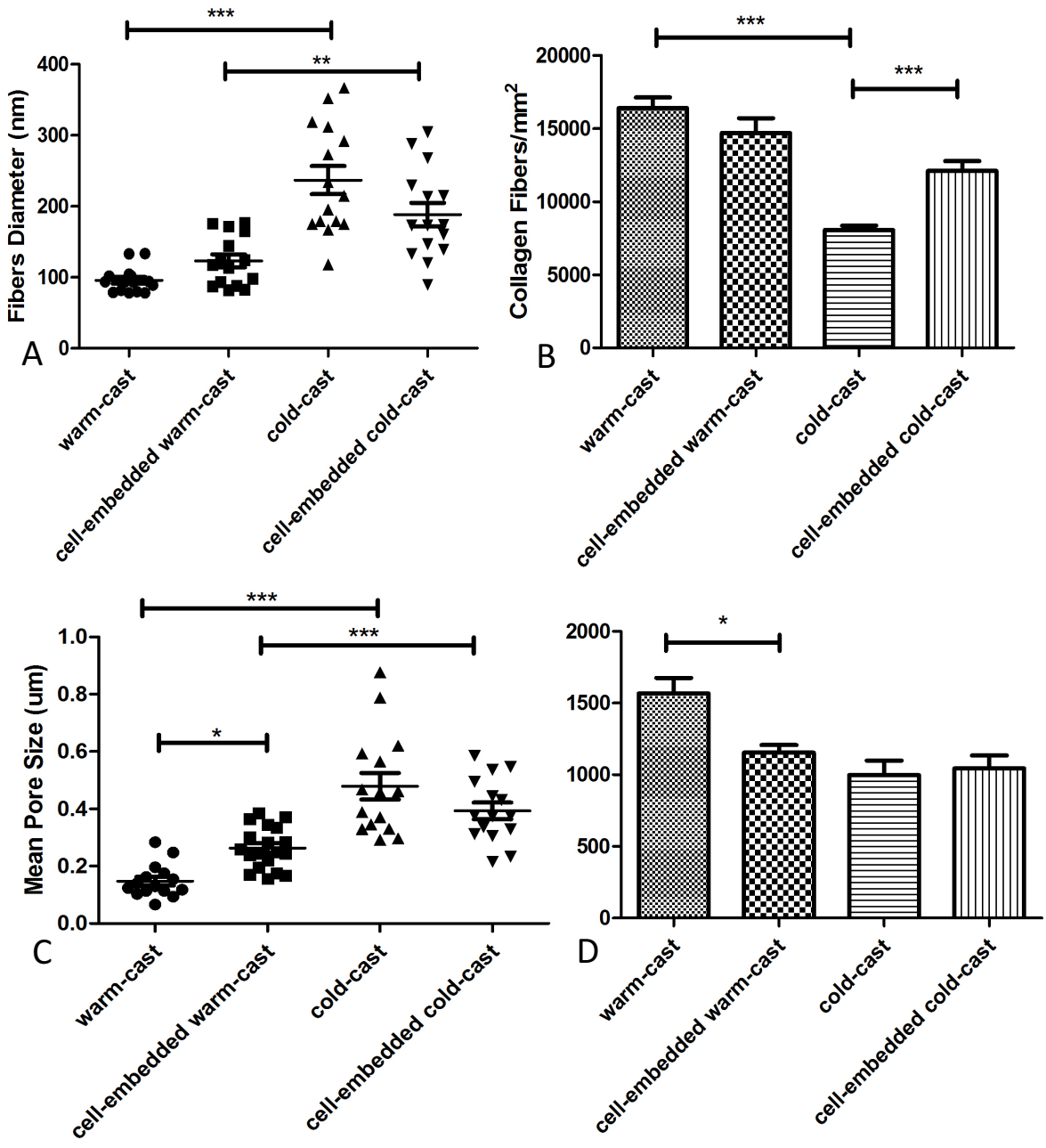

Fig. 5.8 CRM images were used for calculating the collagen fiber thickness, density and average pore size of the cell-embedded collagen scaffold and analyzed by ImageJ. (A) Average fibers diameters of the 3T3-L1 mouse fibroblast mediated warm-cast and cold-cast scaffolds. (B) Fibers densities of the 3T3-L1 mouse fibroblast mediated warm-cast and cold-cast scaffolds. (C) Average pore sizes of the 3T3-L1 mouse fibroblast mediated warm-cast and cold-cast scaffolds. (D) Dynamic mechanical analysis (DMA) indicated that the elastic modules were almost the same in both 3T3-L1 mouse fibroblast embedded collagen scaffold.

the collagen fibers during the fast gelation in the warm-cast scaffold, and seemed to limit the growth of the collagen fibers in the cold-cast scaffold. The average fibrils density in the warm-cast scaffolds was relatively higher than the one in the cold-cast scaffolds. The lower fiber density in the cold-cast scaffold (12716/mm^2) significantly increased in presence of cells, while the fiber density in the warm-cast scaffold (14786/mm^2) slightly decreased. The difference in pore sizes between the warm-cast (245.9 ± 16.6 nm) and cold-cast (378.3 ± 30.4 nm) scaffolds was mitigated by the remodeling of cells. The elastic modulus of the warm-cast and cold-cast scaffold had no significant difference, and the stiffness of the remodeled warm-cast scaffold was much lower, which might be due to the cells within the scaffold leaving larger void space in the structure.

The fabrication of collagen/ collagen-fibroblast scaffolds in 96-well plate

To improve the cell culture and staining process, we used the 96-well plates instead of the PDMS microwells, to fabricate the collagen scaffold. The 96-well plate also potentially improved the temperature gradient due to the larger contact surface to the collagen suspension, and enabled us to get a designed shape of the collagen scaffold. By altering the volume of the collagen solution, we could control the thickness of the scaffold, but we should note that thicker surface would affect the homogeneity of the system. In this case, we used 150 ml collagen solution in each well and obtained a 2 mm thick collagen scaffold. The fabrication process was the same as preciously described using rat tail collagen. Briefly, rat tail collagen in acetic acid was neutralized to pH 7.2-7.4 then was polymerized within the 96-well plate. Similar as described above, we controlled the temperature during collagen scaffold fabrication with half of the cell-collagen solution was rapidly polymerized in the pre-warmed 96-well plate at 37 °C for one hour, while rest of them were slowly polymerized in pre-cooled 96-well plate at initial temperature of 4°C for 15 minutes, and gradually

increasing the temperature to 26°C for 15 minutes, and finally in the incubator for 30 minutes. The microarchitecture of the resulting collagen system was observed by confocal reflectance microscope (CRM).

From our result (Fig. 5.9), we can see that the difference in microstructure of the warm-cast

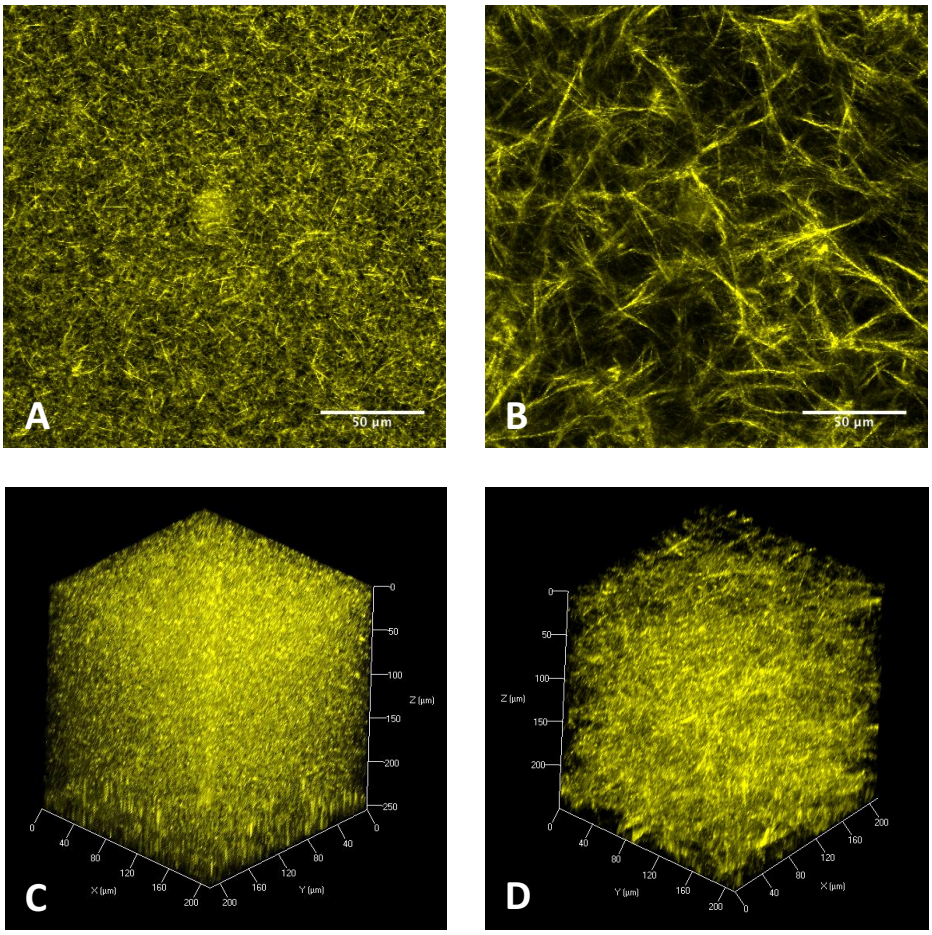

Fig. 5.9 The Fabrication of rat tail collagen scaffolds with two different micro-architectures within 96-well plate. After the polymerization, the three dimensional structure of the warm-cast (A) and cold-cast (B) collagen scaffold were characterized by confocal reflectance microscope. 3D reconstruction of the warm-cast (C) and cold-cast (D) collagen scaffold were based on z-stacks on Zeiss 710.

and cold-cast collagen scaffold is significant. The collagen fibers in the warm-cast scaffold were thinner and shorter with higher density, while the collagen fibers in the cold-cast system were thicker and longer, leaving larger void space. The microarchitecture of the warm/cold-cast collagen scaffold fabricated in 96-well plate was proved to be in agreement with the previous experiments using PDMS microwells. And we were able to obtain more collagen fibers in this system, which might be due to higher volume of the collagen suspension.

Afterward, we fabricated the collagen-fibroblast co-culture system within the 96-well plate. Briefly, 3T3-L1 mouse fibroblasts (30k) in 10%FBS culture media was mixed with rat tail collagen, which was formerly neutralized to pH 7.2-7.4. The cell-collagen mixture was polymerized within the 96-well plate similar as described above, with warm-cast scaffold was quickly polymerized in the pre-warmed 96-well plate at 37 °C for one hour, while the cold-cast scaffold was slowly polymerized in pre-cooled 96-well plate at 4°C for 15 minutes, gradually increased to 26°C for 15 minutes, and finally at 37 °C for 30 minutes. Subsequently, fresh media containing 1% FBS was added into the wells, and incubated for 24h before imaging. A fluorescent assay was used to assess the distribution of the cells, and the three-dimensional collagen structures were observed under confocal reflectance microscope (CRM) on Zeiss 710.

The fluorescent images (Fig. 5.10 A, B) suggest that the fibroblasts were able to adhere and distributed evenly in the warm/cold cast systems. Most importantly, within the 96-well plate, the different microarchitecture of the warm-cast and cold-cast collagen scaffold remained significant. The fibrils in the cell-embedded warm-cast collagen scaffold still appeared to be denser and thinner, whereas the fibrils observed in the cold-cast cell-embedded collagen gel were thicker and longer, which means the differences of these two models were no longer

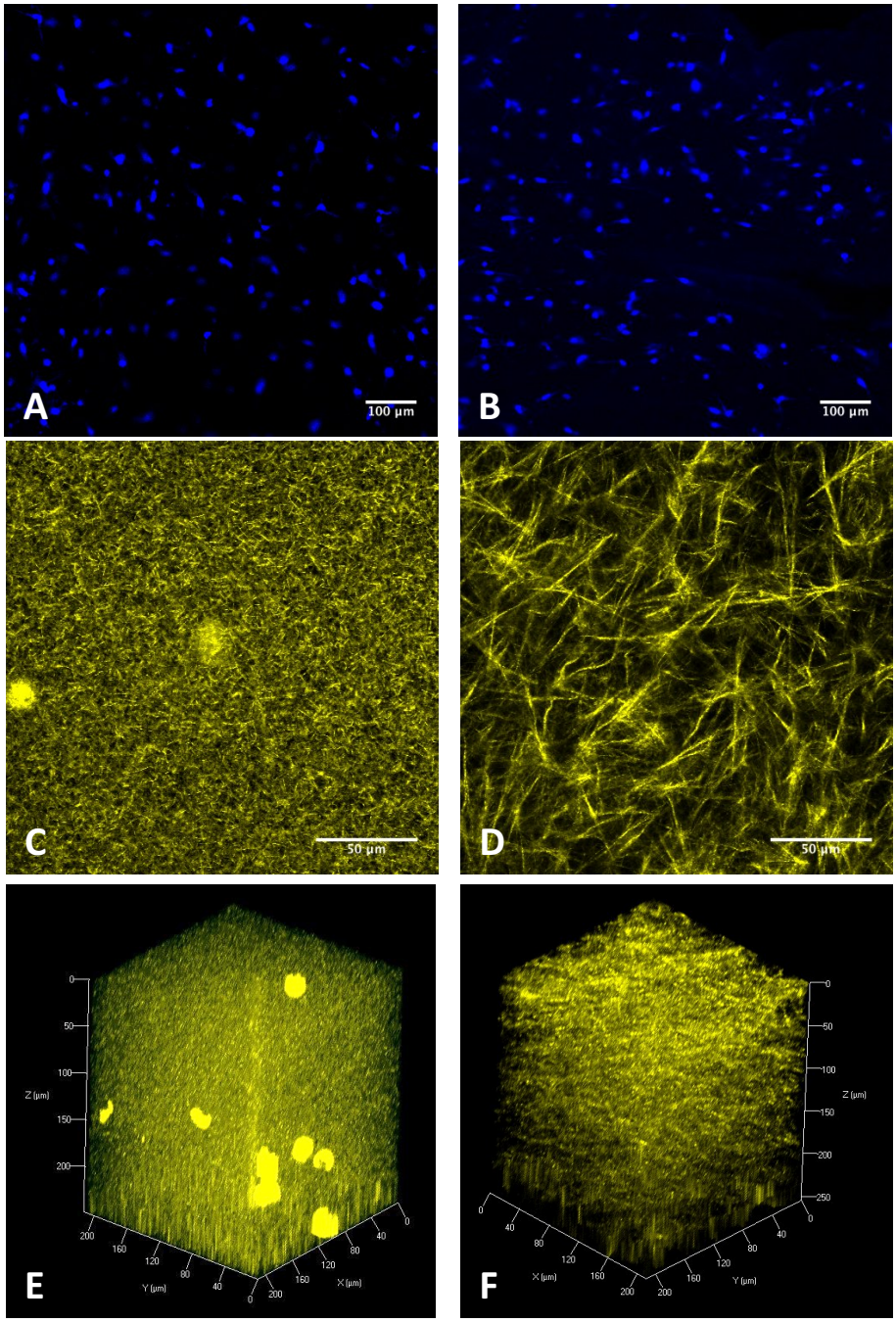

Fig. 5.10 Fluorescent images of cell-embedded warm-cast(A) and cold-cast (B) collagen scaffold. Cell nuclei was staining with DAPI (blue) after culture for 24h. Scale bars = 100µm. After the polymerization, the three dimensional structure of the warm-cast (C) and cold-cast (D) collagen scaffold were characterized by confocal reflectance microscope. 3D reconstruction of the warm-cast (E) and cold-cast (F) collagen scaffold were based on z-stacks on Zeiss 710.

largely affected by the existence cells as observed in the previous systems (Fig. 5.10). This might be due to, in these 96-well plate systems, the higher volume of collagen solution and larger surface contact area (which improved the temperature gradient within the system) improved the assembly of the collagen fibrils from which we could obtain higher quantity of the collagen fibers and maintain their temperature-mediated microarchitecture during the collagen fiber polymerization. And these results indicate that we were able to control the collagen structure even within the fibroblasts co-culture system, which in turn enable us to study the cell-ECM interactions using this cell-embedded system.

COL-Fn dual proteins fibrillar scaffold in 96-well plate

Further, we investigated if fibronectin (Fn) could simultaneously assemble into fibrils along with the collagen fibers via the same technique. Briefly, 15% fluorescent labeled Fn was

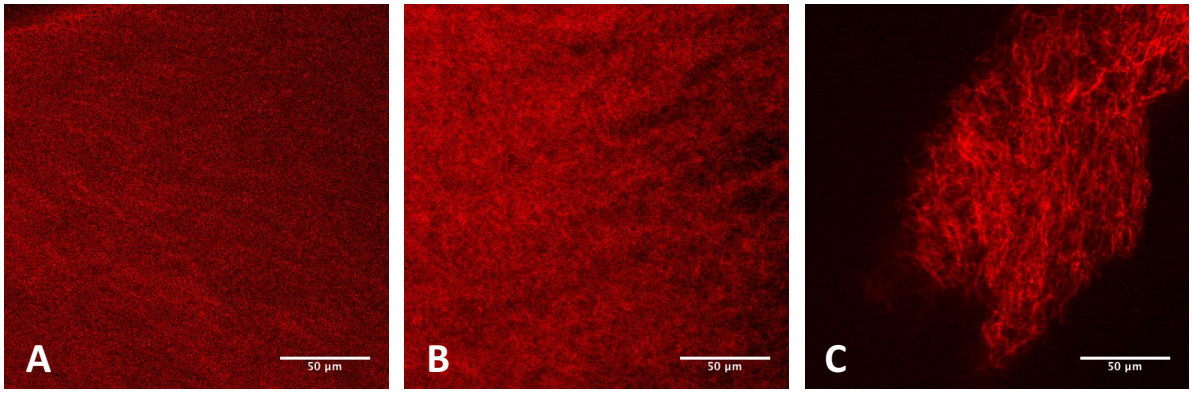

Fig 5.11 Flourescent images of the COL-Fn scaffold fabricated by warm/cold-cast technique with Fn in different concentrations. (A) warm-cast scaffold with Fn concentration of 300ug/ml. (B) cold-cast scaffold with Fn concentration of 300ug/ml. (C) cold-cast scaffold with Fn concentration of 500ug/ml.

diluted into a series of concentrations using the formerly neutralized rat tailed collagen solution as described above. Our result (Fig. 5.11) indicated that, at Fn concentration of 300ug/ml, both warm-cast and cold-cast scaffold showed initiation of Fn fibrillogenesis,

while the fluorescence in the cold-cast scaffold was much higher, which suggested higher tendency of Fn fiber assembly. When the Fn concentration increased, the collagen scaffold became more fragile due to the low available amount of collagen, which is essential in maintaining the mechanical properties and microstructure of the scaffold. As the Fn concentration reached 500ug/ml, the collagen in warm-cast technique could no longer polymerize into fibrillar scaffold. However, in the cold-cast technique, the collagen-Fn solution was still able to proceed gelation, even though the structure was fragile (In Fig. 5.11C, the scaffold broke apart when took out from the wells.). An exciting breakthrough is that we could obtain both Fn and collagen fibrils under this condition, and this COL-Fn dual proteins fibrillar scaffold enabled us to better mimic the ECM. In further experiment, if we could improve the technique, such as increasing the collagen/Fn concentration, or have more control on the process temperature, it would be very promising that we would be able to fabricate the COL-Fn dual proteins scaffold with different microarchitectures, and therefore being able to study how it regulates the cell functions.

Conclusion

In this study, we successfully fabricated 3D fibrillar collagen scaffolds with varying microarchitectures as well as mechanical properties. Miniaturized templates for cell culture and tissue engineering, such as our 3D micro-scaffolds, have promising applications in the future as they have high homogeneity within the system, and are able to control the cell-scale microenvironment.[21,22] The biggest challenge in altering the fibrillar collagen structure by temperature-controlled crosslinking is the efficiency of heat transfer within the systems, while temperature is critical for collagen fiber assembly rate and consequently its microstructure.[11,23,24] Utilizing this knowledge, we achieved thicker fibers in cold-cast scaffolds by slowing down fiber nucleation at lower temperatures, and quickly polymerized collagen into thinner fibers in a warm-cast scaffold. Collectively, compared to the cold-cast scaffold, the warm-cast collagen scaffold was confirmed to have higher fiber density, lower fiber thickness, smaller pore size and hence higher elastic modulus. This higher stiffness of the warm-cast scaffold might increase cell contractility in cell culture since the cells are able to physically respond to maintain the tensional balance in its microenvironment. [25,26]

Fibroblasts were then introduced to the warm/cold-casting system, and remodeled the microstructure of these collagen scaffolds. Under the cell mitigated effect, the average fiber density, pore size and Young's modulus of the cell-embedded scaffold showed no significant difference, while the collagen fibers in the cold-cast gel remains thicker than the ones in the warm-cast gel. Later, a revised protocol was used on the collagen-fibroblast system to improve the control on the collagen structures. Within this new remodeled system, the warm-cast cell-embedded collagen scaffold and cold-cast cell-embedded collagen scaffold were able to maintain significant differences in microarchitecture, while further characterizations need to be done. Fibronectin was also introduced into the system and formed a COL-Fn dual

proteins fibrillar scaffold by this 96-well plate protocol without cell involvement. Fn fibrils were able to polymerize along with the collagen fibers via the cold-cast technique at a Fn concentration of 500ug/ml.

By using this temperature-mediated method, we were able to control the collagen nucleation rate and the lateral growth of the collagen microfibrils.[27] Hence, 3D fibrillar collagen scaffolds were developed with tunable microarchitectures and mechanical properties. In addition, cells were successfully inserted during the direct formation of this 3D collagen template, which lays a groundwork for large volume cell culture and the study on tissue regeneration. Moreover, collagen-fibronectin fibrillar scaffold was fabricated via this technique, which enabled us to comprehensively understand the ECM-regulated cell behaviors in the future study.

Reference:

1. Mammoto, A. & Ingber, D. E. Cytoskeletal control of growth and cell fate switching. *Curr. Opin. Cell Biol.* **21,** 864–870 (2009).
2. Engler, A. J., Sen, S., Sweeney, H. L. & Discher, D. E. Matrix Elasticity Directs Stem Cell Lineage Specification. *Cell* **126,** 677–689 (2006).
3. Gardel, M. L. *et al.* Traction stress in focal adhesions correlates biphasically with actin retrograde flow speed. *J. Cell Biol.* **183,** (2008).
4. Wang, K. *et al.* Breast cancer cells alter the dynamics of stromal fibronectin-collagen interactions. *Matrix Biol.* 1–10 (2016). doi:10.1016/j.matbio.2016.08.001
5. Conklin, M. W. *et al.* Aligned Collagen Is a Prognostic Signature for Survival in Human Breast Carcinoma. *Am. J. Pathol.* **178,** 1221–1232 (2011).
6. Ganganna, K., Shroff, S. & Shetty, P. Collagen in histologic stages of oral submucous fibrosis: A polarizing microscopic study. *J. Oral Maxillofac. Pathol.* **16,** 162 (2012).
7. Levental, K. R. *et al.* Matrix Crosslinking Forces Tumor Progression by Enhancing Integrin Signaling. *Cell* **139,** 891–906 (2009).
8. Burke, R. M., Madden, K. S., Perry, S. W., Zettel, M. L. & Brown, E. B. Tumor-associated macrophages and stromal TNF-α regulate collagen structure in a breast tumor model as visualized by second harmonic generation. *J. Biomed. Opt.* **18,** 86003 (2013).
9. Cross, V. L. *et al.* Dense type I collagen matrices that support cellular remodeling and microfabrication for studies of tumor angiogenesis and vasculogenesis in vitro. *Biomaterials* **31,** 8596–8607 (2010).
10. Seo, B. R. *et al.* Obesity-dependent changes in interstitial ECM mechanics promote breast tumorigenesis. *Sci. Transl. Med.* **7,** (2015).
11. Hulmes, D. J. S. in *Collagen* 15–47 (Springer US, 2008). doi:10.1007/978-0-387-

73906-9_2

12. Xu, B., Chow, M.-J. & Zhang, Y. Experimental and modeling study of collagen scaffolds with the effects of crosslinking and fiber alignment. *Int. J. Biomater.* **2011,** 172389 (2011).

13. Gimble, J. M., Katz, A. J. & Bunnell, B. A. Adipose-Derived Stem Cells for Regenerative Medicine. *Circ. Res.* **100,** (2007).

14. Birk, D. E. & Trelstad, R. L. Extracellular compartments in tendon morphogenesis: collagen fibril, bundle, and macroaggregate formation. *J. Cell Biol.* **103,** 231–40 (1986).

15. Birk, D. E. & Trelstad, R. L. Extracellular compartments in matrix morphogenesis: collagen fibril, bundle, and lamellar formation by corneal fibroblasts. *J. Cell Biol.* **99,** 2024–33 (1984).

16. BIRK, D. E. & TRELSTAD, R. L. Fibroblasts Create Compartments in the Extracellular Space Where Collagen Polymerizes into Fibrils and Fibrils Associate into Bundles. *Ann. N. Y. Acad. Sci.* **460,** 258–266 (1985).

17. Williams, R. M., Zipfel, W. R. & Webb, W. W. Interpreting Second-Harmonic Generation Images of Collagen I Fibrils. *Biophys. J.* **88,** 1377–1386 (2005).

18. Raub, C. & Tromberg, B. Second-Harmonic Generation Imaging of Self-Assembled Collagen Gels. *Second Harmon.* (2013).

19. Collagen: Structure and Mechanics - Google Books. Available at: https://books.google.com/books?hl=en&lr=&id=dyWFTqEtXXwC&oi=fnd&pg=PR2&dq=D.+J.+S.+Humles,2008&ots=W-W7lsEcqS&sig=MroPCBT5p-8q58cJ6eCEmWFPQjA#v=onepage&q=D. J. S. Humles%2C2008&f=false. (Accessed: 3rd June 2017)

20. Franke, K., Sapudom, J., Kalbitzer, L., Anderegg, U. & Pompe, T. Topologically

defined composites of collagen types I and V as in vitro cell culture scaffolds. *Acta Biomater.* **10,** 2693–2702 (2014).

21. Håkanson, M., Cukierman, E. & Charnley, M. Miniaturized pre-clinical cancer models as research and diagnostic tools. *Adv. Drug Deliv. Rev.* **69–70,** 52–66 (2014).

22. Khetani, S. R. & Bhatia, S. N. Microscale culture of human liver cells for drug development. *Nat. Biotechnol.* **26,** 120–126 (2007).

23. Sung, K. E. *et al.* Control of 3-dimensional collagen matrix polymerization for reproducible human mammary fibroblast cell culture in microfluidic devices. *Biomaterials* **30,** 4833–4841 (2009).

24. Ghazanfarian, J. & Abbassi, A. Heat transfer and fluid flow in microchannels and nanochannels at high Knudsen number using thermal lattice-Boltzmann method. *Phys. Rev. E* **82,** 26307 (2010).

25. Parry, D. A. D. The molecular fibrillar structure of collagen and its relationship to the mechanical properties of connective tissue. *Biophys. Chem.* **29,** 195–209 (1988).

26. Voytik-Harbin, S. L., Roeder, B. A., Sturgis, J. E., Kokini, K. & Robinson, J. P. Simultaneous Mechanical Loading and Confocal Reflection Microscopy for Three-Dimensional Microbiomechanical Analysis of Biomaterials and Tissue Constructs. *Microsc. Microanal.* **9,** 74–85 (2003).

27. Achilli, M. & Mantovani, D. Tailoring Mechanical Properties of Collagen-Based Scaffolds for Vascular Tissue Engineering: The Effects of pH, Temperature and Ionic Strength on Gelation. *Polymers (Basel).* **2,** 664–680 (2010).

Chapter 6

Conclusions & Future Directions

The aim of this thesis was to develop 3D dual-protein (collagen-fibronectin) cell culture platforms, mimicking the physiological ECM environment and better understanding the ECM-cellular interactions with potential implications on wound healing. We first generated tunable 3D *porous* scaffolds and assessed cell invasion as a function of scaffold morphology and mechanical properties. Our results indicate that the 1.25 wt.% collagen scaffold with the smallest pore size and highest compressive modules showed best cell infiltration. This was attributed to its larger pore area providing more space for cell attachment, and its smaller pore size, which implied more interconnection within the structure, enabling the cells to migrate within the entire scaffold. Later experiments confirmed that the fibroblasts were able to migrate and adhere thoroughly in the scaffold, function normally, and remain viable after short-term (24h) as well as long-term (6 days) culture. We then coated this 1.25 wt.% collagen scaffold with a layer of fibronectin, and thermally controlled the fibronectin conformation. Collectively, our results showed that the presence of fibronectin improved the cell viability (>93%) and significantly enhanced the cell initial adhesion as well as proliferation (1 fold after 24h incubation). The conformational changes of the fibronectin were able to further regulate the cellular behavior. Fibroblasts showed preference on the low-temperature-coated scaffold with more compact Fn, as the results suggested a higher initial adhesion rate, viability and proliferation rate of cells in the collagen scaffold with more compact Fn. Future study should further investigate the wound healing effect of this 3D collagen-fibronectin system by studying the promotion of blast fibrocyte growth factor (bFGF) and vessel endothelium growth factor (VEGF). bFGF and VEGF may promote the production of vascular endothelial cell and blast figrocyte thus accelerating the growth of

blood vessels and connective tissue proliferation to achieve the effect of healing wounds. Studies can also be focus on how these thermally-controlled Fn-coated 3D collagen scaffolds potentially monitor more complex cell behaviors like cell differentiation, angiogenesis and cancer progression.

Next, the fibronectin was assembled into 3D fibrillar matrix within the porous collagen scaffolds to study and form a basis for tissue regeneration. Methods based on shear forces have been used to manually induce fibronectin fibrillogenesis in a cell-free process within a 3D collagen platform. Using a shaking technique with precise control on the fibronectin liquid volume as well as the shaking speed, short Fn fibrils were successfully introduced to the 3D collagen system. Longer and thicker fibronectin fibers could be produced by a combine technique of manually pulling and blowing with nitrogen air flow. These fibronectin fibers were evenly distributed in the 3D collagen scaffold in high quantity, whose conformation was varied among fibers, similar as in vivo ECM, while the longer fibers showed in a more unfolded form. This dual-protein 3D scaffold comprising porous collagen and fibrous Fn in different forms could be customized based on the need for future study by combining the proposed techniques to create proportional long/short Fn fibrils. It is known that Fn functions distinctly different in molecules and after assembly into fibers, therefore, future study would be focus on the control of the Fn fibers conformations within the 3D template and continue on its regulation of cell behaviors.

Finally, we developed 3D fibrillar collagen scaffolds with different microstructures, which were able to better mimic the *in vivo* ECM as well as the wound physiological environment. These fibrillar collagen scaffolds allowed for cell embedding during the direct formation of the scaffold due to the gentle fabrication process. Warm-cast and cold-cast techniques were

designed to fabricate the fibrillar collagen scaffold based on the sensitivity of temperature during the collagen fiber assembly process. Collectively, our results indicate that thicker and longer collagen fibers were produced in cold-cast scaffolds by slow down fiber nucleation at lower temperatures, whereas collagen was quickly polymerized into thinner and shorter fibers in a warm-cast scaffold. The existence of the co-culture fibroblasts aided the collagen fiber assembly and slightly mitigated the difference between the warm-cast and cold-cast collagen scaffold. These 3D fibrillar collagen scaffolds with varying microarchitectures as well as mechanical properties could provide templates for cell culture and tissue engineering. In addition, fibronectin fibrils were successfully produced in the fibrillar collagen system to develop a COL-Fn dual proteins fibrillar scaffold via the casing technique. Besides, compared to the porous collagen scaffold, the fibrillar collagen scaffold was crosslinked by tuning the pH and temperature instead of using chemicals, which enabled the scaffold to self-degraded after a specific period, i.e. 7-10 days (results not shown). Future study should focus on the cellular response towards these collagen scaffolds with different properties and the control of the degrading speed of the scaffold, which is essential in wound healing applications. Also, the techniques producing Fn monolayer/Fn fibers with controlled properties as described in Chapter 3, Chapter 4 and Chapter 5 could be applied on this 3D fibrillar collagen platform to enable the in-depth understanding of the role of collagen and fibronectin in cellular processes.

In conclusion, our study suggests that by tuning collagen (porous vs. fibrillar) structure and fibronectin molecular conformation, we were able to control cell behaviors including cell adhesion, migration and proliferation, and thus, potentially facilitate the wound healing process. These ECM structure mimicking 3D templates with precise control of protein

microarchitecture and conformation over large volumes, i.e., for long-term cell culture, and therefore have potential applications in tissue engineering as well as regenerative medicine.